

UNIVERSITY OF NAPLES FEDERICO II



DEPARTMENT OF PHARMACY

Ph.D. programme in “Nutraceuticals, Function Foods and Human Health”

*Thinned fruits as agro-food waste products with beneficial effects on
the control of glucose homeostasis*

Ph.D. student

Elisabetta Schiano

Coordinator

Prof.

ALBERTO RITIENI

Tutor

Prof.

GIAN CARLO TENORE

XXXV CYCLE (2020-2022)

PREFACE

This Ph.D. thesis is submitted as a requirement for obtaining the Ph.D. Degree at the University of Naples Federico II (Italy). It is written based on three-years research conducted by the author, Elisabetta Schiano, both at the Department of Pharmacy in Naples, under the supervision of Prof. Gian Carlo Tenore, and at the University of Westminster, Centre for Nutraceuticals, in London (United Kingdom), under the supervision of Prof. Mohammed Gulrez Zariwala.

Elisabetta Schiano
Naples, March 2023

ABSTRACT

Control of glucose homeostasis represents the main goal in both the prevention and management of diabetes and prediabetes. Although a wide range of pharmacological approaches is currently available for the treatment of diabetes and its related morbidities, these are often associated with side effects, leading to poor adherence and treatment failure. Therefore, there is growing interest in natural products with beneficial potential in the management of diabetic condition. In this context, particular attention has recently been paid to the investigation of abscisic acid (ABA), an endogenous hormone with hypoglycemic potential in humans. Additionally, the role of ABA as a terpenoid phytohormone mainly responsible for regulating plant growth and differentiation is extensively described in the scientific literature. Due to its involvement in plant developmental processes, ABA reaches its maximum concentration in immature fruits that are often subjected to fruit thinning, an agronomic practice carried out to improve fruit size and quality. In this scenario, the large number of unripe fruits discarded every year due to this process turns out to represent innovative and high-value resources of ABA, in line with the concepts of food waste valorization and environmental sustainability.

Based on these considerations, in the first part of this Ph.D. thesis, a screening of different extracts of unripe fruits derived from fruit thinning allowed us to identify thinned nectarines (*Prunus persica* L.) as the richest sources in terms of ABA content. In addition, the optimal extraction conditions to obtain the maximum ABA yield were explored, followed by the identification through HPLC-HESI-MS/MS analysis of three different ABA metabolites. Subsequently, we aimed to perform a qualitative and quantitative characterization of the polyphenolic profile of the thinned nectarine extract (TNE) through HPLC-HESI-MS/MS and HPLC-DAD-FLD analyses, which led to the detection of forty-eight polyphenolic compounds, nineteen of which were quantified. Overall, these results prompted us to test the

clinical potential of a TN nutraceutical formulation (TNnf) on glucose homeostasis. Sixty-one patients with type 2 diabetes mellitus (T2DM) were enrolled in a three-month, three-arm, parallel-group, randomized controlled trial (RCT). Specifically, two different doses of the nutraceutical formulation, i.e. a low dose (500 mg 3 times/day) and a high dose (750 mg 3 times/day) of TNnf, were tested. Although a significant reduction of glycemic parameters was observed in both treatment groups compared to baseline, the supplementation with TNnf low dose showed a greater insulin-sparing effect (fasting plasma insulin, FPI: -29.2%, $p < 0.05$ vs baseline), compared to TNnf higher dose (FPI: -16.5%, $p < 0.05$ vs baseline). Moreover, the quantification of ABA serum levels by using a previously validated LC-MS/MS method, allowed us to observe a significant correlation between glycemia and ABA levels in both intervention groups.

Finally, during my Ph.D. research period abroad, I had the opportunity to develop and optimize two nanoformulations (NF) containing a pure standard of ABA or TNE at the same ABA concentration, using ascorbyl palmitate/DSPE-PEG as nanocarrier delivery system. Overall, the results obtained demonstrated the high efficacy of the tested nanoformulated samples in terms of cell viability, antioxidant activity, and insulin secretion in a MIN6 pancreatic β -cell model. Moreover, the greater results obtained in cells treated with the NF-TNE sample compared to ABA alone, supported its additional potential to improve cellular antioxidant protection due to the synergistic combination of bioactive compounds contained in the TNE phytocomplex. Overall, the data obtained reasonably support TN as a source of innovative and promising nutraceutical products able to contribute to the management of glucose homeostasis. Undoubtedly, these data may pave the way for future in vitro and in vivo studies aimed at evaluating the beneficial potential of nutraceutical formulations based on TN in further experimental models.

LIST OF PUBLICATIONS

- Tenore GC., Caruso D., D'Avino M., Buonomo G., Caruso G., Ciampaglia R., **Schiano E.**, Maisto M., Annunziata G., Novellino E. A Pilot Screening of Agro-Food Waste Products as Sources of Nutraceutical Formulations to Improve Simulated Postprandial Glycaemia and Insulinaemia in Healthy Subjects. *Nutrients*. **2020**; 12(5), 1292.
- **Schiano, E.**, Annunziata, G., Ciampaglia, R., Iannuzzo, F., Maisto, M., Tenore, G.C., Novellino, E. Bioactive Compounds for the Management of Hypertriglyceridemia: Evidence From Clinical Trials and Putative Action Targets. *Frontiers in Nutrition*. **2020**; 7, 586178.
- Maisto, M., Annunziata, G., **Schiano, E.**, Piccolo, V., Iannuzzo, F., Santangelo, R., Ciampaglia, R., Tenore, G.C., Novellino, E., Grieco, P. Potential Functional Snacks: Date Fruit Bars Supplemented by Different Species of *Lactobacillus* spp. *Foods*. **2021**; 10(8), 1760.
- **Schiano, E.**, Piccolo, V., Novellino, E., Maisto, M., Iannuzzo, F., Summa, V., & Tenore, G. C. Thinned Nectarines, an Agro-Food Waste with Antidiabetic Potential: HPLC-HESI-MS/MS Phenolic Characterization and In Vitro Evaluation of Their Beneficial Activities. *Foods*. **2022**; 11(7), 1010.
- Maisto, M., **Schiano, E.**, Novellino, E., Piccolo, V., Iannuzzo, F., Salviati, E., Summa, V., Annunziata, G., Tenore, G.C. Application of a Rapid and Simple Technological Process to Increase Levels and Bioaccessibility of Free Phenolic Compounds in Annurca Apple Nutraceutical Product. *Foods*. **2022**; 11(10), 1453.

- **Schiano, E.**, Maisto, M., Piccolo, V., Novellino, E., Annunziata, G., Ciampaglia, R., Montesano, C., Croce, M., Caruso, G., Iannuzzo, F., Summa, V., Tenore, G.C. Beneficial Contribution to Glucose Homeostasis by an Agro-Food Waste Product Rich in Abscisic Acid: Results from a Randomized Controlled Trial. *Foods*. **2022**; 11(17), 2637.

- Maisto, M., Piccolo, V., Novellino, E., **Schiano, E.**, Iannuzzo, F., Ciampaglia, R., Summa, V., Tenore, G.C. Optimization of Phlorizin Extraction from Annurca Apple Tree Leaves Using Response Surface Methodology. *Antioxidants*. **2022**; 11(10), 1933.

- Maisto, M., Iannuzzo, F., **Schiano, E.**, Ciampaglia, R., Labanca, A., Montesano, D., Piccolo, V., Rossi, P., Tenore, G.C. Effects of Fortified Laying Hen Diet with Moringa oleifera Leaves and Goji Berries on Cholesterol and Carotenoid Egg Content. *Foods*. **2022**; 11(20), 3156.

- Iannuzzo, F., Piccolo, V., Novellino, E., **Schiano, E.**, Salviati, E., Summa, V., Campiglia P., Tenore G.C., Maisto, M. A Food-Grade Method for Enhancing the Levels of Low Molecular Weight Proanthocyanidins with Potentially High Intestinal Bioavailability. *International Journal of Molecular Sciences*. **2022**; 23(21), 13557.

- Maisto, M., Piccolo, V., Novellino, E., **Schiano, E.**, Iannuzzo, F., Ciampaglia, R., Summa, V., Tenore, G.C. Optimization of Ursolic Acid Extraction in Oil from Annurca Apple to Obtain Oleolytes with Potential Cosmeceutical Application. *Antioxidants*. **2023**; 12(2), 224.

- Maisto, M., Iannuzzo, F., Novellino, E., **Schiano, E.**, Di Lorenzo, R., Piccolo, V., Tenore, GC. Natural Polyphenols for Prevention and Treatment of Urinary Tract Infections. *International Journal of Molecular Sciences*. **2023**; 24(4), 3277.

- **Schiano, E.**, Cappello, E., Cecere, D., Pompeo, F., Novellino, E., Stornaiuolo, M., Izzo, M. Short communication: Increased Levels of Circulating Iron-Albumin Complexes in Peripheral Arterial Disease Patients. *Antioxidants*. **2023**; 12(2), 503.

- **Schiano, E.**, Neri, I., Maisto, M., Novellino, E., Iannuzzo, F., Piccolo, V., Summa, V., Grumetto, L., Tenore, GC. Validation of an LC-MS/MS Method for the Determination of Abscisic Acid Concentration in a Real-World Setting. *Foods*. **2023**; 12(5), 1077.

- Musto, G., **Schiano, E.**, Iannuzzo, F., Tenore, GC., Novellino, E., Stornaiuolo, M. Genotoxicity Assessment of Nutraceuticals Extracted from Thinned Nectarines (*Prunus persica* L.) and Grape Seeds (*Vitis Vinifera* L.) Waste Biomasses. *Foods*. **2023**; 12, 1171.

ABBREVIATIONS

ABA: Abscisic acid

ABTS: 2,20-azinobis(3-ethylbenzotiazoline-6-sulfonate)

AE: Anion exchanger

AGE: Advanced glycation end-product

ALT: Alanine aminotransferase

AMPK: Adenosine monophosphate-activated protein kinase

ANOVA: Analysis of variance

AST: Aspartate aminotransferase

AUC: Area under the curve

BCA: Bicinchoninic acid

BMI: Body mass index

BPD: Biliopancreatic diversion

BPS: Bis 4,4'-Sulfonyldiphenol

BSA: Bovine serum albumin

BW: Body weight

CAA: Cellular antioxidant activity

CaCl: Calcium chloride

cADPR: Cyclic ADP-ribose

cAMP: Cyclic adenosine monophosphate

CD38: Cluster of differentiation 38

CO₂: Carbon dioxide

CV: Coefficient of variation

CVD: Cardiovascular Disease

DCFH-DA: 2',7'-Dichlorofluorescein diacetate

DDA: Data-dependent acquisition

DL: Drug loading

DMEM: Dulbecco's Phosphate Modified Eagle Medium

DMSO: Dimethyl sulfoxide

DNS: 3,5-dinitrosalicylic acid

DPA: Dihydrophaseic acid

DPBS: Dulbecco's Phosphate Buffered Saline

DPPH: 2,2-diphenyl-1-picrylhydrazyl

DSPE-PEG: Polyethylene glycol grafted 1,2-distearoyl-sn-glycerol-3-phosphatidylethanolamine

EC₅₀: Half maximal effective concentration

EE: Encapsulation efficiency

ELISA: Enzyme-linked immunosorbent assay

ESI: Electrospray ionization

ESI-MS: Electrospray ionization mass spectrometry

FBS: Fetal bovine serum

FeCl₃: Ferric chloride

FLD: Fluorescence detector

FPG: Fasting plasma glucose

FPI: Fasting plasma insulin

FRAP: Ferric reducing/antioxidant power

FS: Full scanning

FTWPs: Fruit-thinning waste products

GDM: Gestational diabetes mellitus

GLP-1: Glucagon-like peptide 1

GLUT-4: Glucose transporter 4

GSIS: Glucose-stimulated insulin secretion

HbA_{1c}: glycated haemoglobin

HCOOH: Formic acid

HDL: High-density lipoprotein

HEPES: 4-(2-hydroxyethyl)-1-piperazineethanesulfonic acid
HG: High glucose
HMG-HOABA: Hydroxymethylglutaryl-hydroxy abscisic acid
HOABA: 8-Hydroxy abscisic acid
HPLC-DAD: High-Performance Liquid Chromatography with Diode-Array Detection
HRF: Heterocyclic ring fission
IC₅₀: Half-maximal inhibitory concentration
IS: Internal standard
KCl: Potassium chloride
KH₂PO₄: Potassium dihydrogen phosphate
KMnO₄: Potassium permanganate
LANCL2: Lanthionine Synthetase C-Like 2
LC-MS/MS: Liquid chromatography tandem-mass spectrometry
LDL: Low-density lipoprotein
LG: Low glucose
LLE: Liquid-liquid extraction
LOD: Limit of Detection
LOQ: Limit of Quantification
MAPK: Mitogen-activated protein kinase
MDA: Malondialdehyde
MEM: Minimum Essential Medium
MeOH: Methanol
MgSO₄: Magnesium sulfate
MIN6: Mouse insulinoma 6
MS: Mass spectrometry
MS/MS: Tandem mass spectrometry
MTT: 3-(4,5-Dimethylthiazol-2-yl)-2,5-diphenyltetrazolium bromide

MVD: Mean volume diameters
MW: Molecular weight
NaCl: Sodium chloride
NaHCO₃: Sodium bicarbonate
NaOH: Sodium hydroxide
NF: Nanoformulation
NGT: Normal glucose tolerant
NO: Nitric oxide
OGTT: Oral glucose tolerance test
[•]OH: Hydroxyl radical
PA: Phaseic acid
PDI: Polydispersity index
PEG: Polyethylene glycol
PGC-1 α : Peroxisome proliferator-activated receptor gamma coactivator 1-alpha
PIC: Protease inhibitor cocktail
PKA: Protein Kinase A
PMs: Polymeric micelles
PNPs: Polymeric nanoparticles
PPAR- γ : Peroxisome proliferator-activated receptor gamma
QCs: Quality control sample
QE: Quercetin equivalents
QM: Quinone methide cleavage
R²: Coefficient of determination
RDA: Retro Diels–Alder fission
RES: Reticuloendothelial system
ROS: Reactive oxygen species
RT: Retention time
SD: Standard deviation

SEM: Standard error of the mean
SGLT2: Sodium/glucose cotransporter 2
S/N: Signal-to-noise ratio
SNAP-25: Synaptosomal-associated protein of 25 kDa
SNARE: Soluble N-ethylmaleimide-sensitive factor attachment protein receptor
SRM: Selective reaction monitoring
STM: Standardized test meal
T2DM: Type 2 diabetes mellitus
TC: Total cholesterol
TE: Trolox equivalent
TNE: Thinned nectarine extract
TNnf: Thinned nectarine-based nutraceutical formulation
TPTZ: 2,4,6-Tri(2-pyridyl)-s-triazine
TROLOX: 6-hydroxy-2,5,7,8-tetramethylchroman-2-carboxylic acid
WC: Waist circumference

LIST OF TABLES

Table 1. Independent variables and their factor levels used for the optimization protocol	19
Table 2. Content of abscisic acid in different fruit thinning waste products	20
Table 3. Qualitative characterization of ABA derivatives in thinned nectarines extract determined by HPLC-HESI-MS/MS analysis	24
Table 4. Linearity range, limit of detection (LOD), and limit of quantification (LOQ) for polyphenols analysis	37
Table 5. Intra- and inter-day precision for polyphenols analysis	38
Table 6. Intra- and inter-day accuracy for polyphenols analysis	38
Table 7. Polyphenolic composition of thinned nectarines determined by HPLC-HESI-MS/MS analysis	40
Table 8. Quantitative analysis of thinned nectarines polyphenols determined by HPLC-DAD-FLD analysis	51
Table 9. Antioxidant activity of thinned nectarine extract evaluated by DPPH, ABTS, and FRAP assays	52
Table 10. Baseline anthropometric and glucometabolic parameters of study participants	66
Table 11. Summary of LC-MS/MS method validation parameters	70

Table 12. Baseline, and 3-month general data and anthropometric parameters of randomized subjects in placebo, high dose of TNnf group, and a low dose of TNnf group	78
Table 13. Baseline and 3-month biochemical parameters of patients of a placebo, high dose, and a low dose of TNnf groups	80
Table 14. Effects of low and high doses of thinned nectarine-based nutraceutical formulation on glycemic parameters at baseline and after 3 months	81
Table 15. Particle size and zeta potential of ABA and TNE-based nanoformulations	94
Table 16. List of samples at different glucose and iron concentrations.	100

LIST OF FIGURES

Figure 1. (-)-Abscisic acid chemical structure	4
Figure 2. Schematic representation of the proposed ABA effects in the regulation of blood glucose levels	7
Figure 3. Non-overlapping effects of ABA and insulin in muscle and adipose tissue	10
Figure 4. Immature nectarines derived from the agronomical practice of fruit thinning	13
Figure 5. Effects of different solvent mixtures on ABA extraction rates	22
Figure 6. Pareto chart of total parameters analyzed, i.e. matrix-to-solvent ratio (A), temperature (B), and incubation time (C)	23

Figure 7. Antioxidant activity of thinned nectarine extract expressed as (a) EC ₅₀ of DPPH assay and (b) EC ₅₀ of ABTS assay	53
Figure 8. Inhibition of α-amylase activity (%) by thinned nectarine extract and acarbose	54
Figure 9. Inhibition of Advances Glycation End-Product formation (%) by thinned nectarine extract and rutin	55
Figure 10. Change in postprandial plasma glucose and insulin concentration in healthy adults	688
Figure 11 ABA concentration change after the consumption of STM and TN-based product in healthy adults	68
Figure 12. Chromatogram of ABA in serum matrix	70
Figure 13. Study Consolidated Standards of Reporting Trials (CONSORT) flow diagram	75
Figure 14. Correlation analysis of serum ABA levels and glycemia	83
Figure 15. Representative image of DSPE-AP nanocarriers imaged at 13,500 magnification	95
Figure 16. Growth pattern of MIN6 cells into mature pseudoislets	957
Figure 17. Workflow of metabolic experiments at different glucose and iron concentrations	101
Figure 18. MTT analysis on MIN6 cell viability at 24, 48, and 72 hours	105

Figure 19. MTT results of 24-, 48- and 72-hours pre-treatment with (A) DSPE-PEG/Ascorbyl palmitate nanoformulated ABA and Free ABA, (B) DSPE-PEG/Ascorbyl palmitate nanoformulated TNE and Free TNE on MIN6 cells	107
Figure 20. Cellular antioxidant activity of the positive control Quercetin at different concentrations (0-2000 μ M)	1088
Figure 21. Cellular antioxidant activity (CAA) assay results of nanoformulated and unencapsulated TNE	109
Figure 22 and 23. Effects of iron (100 μ M) preincubation on MIN6 cells	110
Figure 24. The effect of treatment with two different concentrations of glucose (5 mM and 20 mM) w/wo iron (100 μ M) on MIN6 cells insulin secretion	112
Figure 25. The effect on MIN6 cells insulin secretion after incubation with two different glucose concentrations (5.5 mM and 20 mM)	113
Figure 26. The effect on MIN6 cells insulin secretion after incubation with glucose 5.5 mM (upper graph) and glucose 20 mM (lower graph)	115
Figure 27. The effect on MIN6 cell's insulin secretion after incubation with two different glucose concentrations (5.5 mM and 20 mM) and high iron levels (100 μ M)	116
Figure 28. The effect on MIN6 cell's insulin secretion after incubation with a combination of glucose 5.5 mM (upper graph) and glucose 20 mM (lower graph) with high iron levels (100 μ M)	118

TABLE OF CONTENTS

PREFACE	I
ABSTRACT	II
LIST OF PUBLICATIONS	IV
ABBREVIATIONS	VII
LIST OF TABLES AND FIGURES	XII

Introduction	1
▪ <i>Type 2 diabetes mellitus</i>	1
▪ <i>ABA in the vegetal world</i>	3
▪ <i>ABA in the animal world</i>	4
▪ <i>ABA as a regulator of glycemic homeostasis in mammals</i>	5
▪ <i>Agro-food waste products as sources of ABA</i>	11

Chapter 1

Thinned nectarines as sources of ABA and its derivatives

1.1. Introduction	15
1.2. Materials and Methods	16
1.2.1. <i>Chemicals and reagents</i>	16
1.2.2. <i>FTWPs collection and preparation for HPLC analysis</i>	17
1.2.3. <i>HPLC-DAD analysis of FTWPs samples</i>	17
1.2.4. <i>Optimization of ABA extraction conditions</i>	18
1.2.5. <i>HPLC-HESI-MS/MS analysis of ABA and its derivatives</i>	19
1.2.6. <i>Statistical analysis</i>	20
1.3. Results	20
1.3.1. <i>Selection of TN as the richest source of ABA</i>	20
1.3.2. <i>Effect of different extraction conditions on ABA yield</i>	21

1.3.3. <i>Identification of ABA metabolites in the TN sample</i>	23
1.4. Discussion	24
1.5. Conclusions	26

Chapter 2

Phenolic characterization and in vitro antioxidant and antidiabetic potential of TNE

2.1. Introduction	28
2.2. Materials and Methods	29
2.2.1. <i>Chemicals and reagents</i>	29
2.2.2. <i>Sample collection and preparation for HPLC analyses</i>	29
2.2.3. <i>HPLC analyses of samples</i>	30
2.2.3.1. <i>Qualitative polyphenols analysis by HPLC-HESI-MS/MS</i>	30
2.2.3.2. <i>Quantitative polyphenols analysis by HPLC-DAD-FLD</i>	31
2.2.4. <i>HPLC-DAD-FLD method validation</i>	31
2.2.5. <i>Evaluation of Total Phenol Content (TPC)</i>	32
2.2.6. <i>Antioxidant activity</i>	32
2.2.6.1. <i>DPPH[•] radical scavenging assay</i>	32
2.2.6.2. <i>TEAC (Trolox Equivalent Antioxidant Capacity) assay</i>	33
2.2.6.3. <i>Ferric Reducing /Antioxidant Power (FRAP) assay</i>	34
2.2.7. <i>Antidiabetic activity</i>	35
2.2.7.1. <i>α-amylase inhibitory assay</i>	35
2.2.7.2. <i>Advanced Glycation End-Product (AGE) inhibition</i>	36
2.2.8. <i>Statistics</i>	37
2.3. Results	37
2.3.1. <i>Validation of HPLC-DAD-FLD method</i>	37
2.3.2. <i>Qualitative polyphenols characterization by HPLC-HESI-MS/MS</i>	39

2.3.3. <i>Phenolic acid identification</i>	44
2.3.3.1. <i>Flavans identification</i>	47
2.3.3.2. <i>Flavonols identification</i>	49
2.3.4. <i>Quantitative polyphenols characterization by HPLC-DAD-FLD</i>	51
2.3.5. <i>Total polyphenols and in vitro antioxidant activity of TNE</i>	52
2.3.6. <i>In vitro antidiabetic activity</i>	53
2.3.6.1. <i>α-amylase inhibitory activity</i>	53
2.3.6.2. <i>Advanced Glycation End-Product (AGE) inhibitory activity</i>	54
2.4. Discussion	55
2.5. Conclusions	58

Chapter 3

Validation of an LC-MS/MS method to determine the ABA serum concentration

3.1. Introduction	59
3.2. Materials and Methods	60
3.2.1. <i>Study design</i>	60
3.2.1.1. <i>Participants and standardized test meal composition</i>	60
3.2.1.2. <i>Experimental procedures</i>	61
3.2.2. <i>Analytical method</i>	62
3.2.2.1. <i>Chemicals and reagents</i>	62
3.2.2.2. <i>Real sample preparation and extraction</i>	62
3.2.2.3. <i>Equipment</i>	63
3.2.2.4. <i>LC-MS/MS conditions</i>	63
3.2.2.5. <i>Calibration curve and linearity</i>	64
3.2.2.6. <i>Limits of Detection (LOD) and Quantification (LOQ)</i>	64
3.2.2.7. <i>Precision and accuracy</i>	64
3.2.2.8. <i>Selectivity</i>	65

3.2.2.9. <i>Carry-over</i>	65
3.2.2.10. <i>Matrix effect</i>	65
3.2.2.11. <i>Recovery</i>	66
3.3. Results	66
3.3.1. <i>Anthropometric and glucometabolic parameters</i>	66
3.3.2. <i>Two-hour glycemic and insulinemic responses to standardized test meal</i>	67
3.3.3. <i>Optimization of chromatographic method</i>	68
3.4. Discussion	70
3.5. Conclusions	72

Chapter 4

Clinical efficacy of a TN-based nutraceutical formulation (TNnf) on glucose homeostasis

4.1. Introduction	73
4.2. Materials and Methods	74
4.2.1. <i>Study population and design</i>	74
4.2.2. <i>Assessments</i>	76
4.2.3. <i>Quantification of serum ABA levels by LC-MS/MS analysis</i>	77
4.2.4. <i>Statistics</i>	77
4.3. Results	78
4.3.1. <i>Study sample</i>	78
4.3.2. <i>Glucometabolic parameters</i>	79
4.3.3. <i>Correlation analysis of serum ABA and glycemia</i>	81
4.4. Discussion	83
4.5. Conclusions	87

Chapter 5

In vitro antioxidant and antidiabetic properties of a TNE-based nanoformulation in a pancreatic β -cell line

5.1. Introduction	88
5.2. Materials and Methods	92
5.2.1. Reagents and materials	92
5.2.2. Preparation of thinned nectarine extract (TNE)	92
5.2.3. Preparation of ABA and TNE-based nanoformulations	93
5.2.4. Size and surface charge of the nanoformulations	94
5.2.5. Nanoformulation morphology	95
5.2.6. Determination of nanoformulation loading and encapsulation efficiency	95
5.2.7. MIN6 cell culture	96
5.2.8. Determination of cell viability by MTT assay	97
5.2.9. Cellular antioxidant activity (CAA) assay	98
5.2.10. MIN6 cells exposure to glucose and iron at different concentrations	99
5.2.11. Cell harvesting	101
5.2.12. Intracellular total iron quantification	102
5.2.13. Evaluation of insulin secretion	102
5.2.14. Statistical analysis	103
5.3. Results	103
5.3.1. Size, charge, and loading efficiency	103
5.3.2. Assessment of cellular viability	104
5.3.3. Determination of cellular antioxidant activity	107
5.3.4. Evaluation of total cellular iron content	109
5.3.5. Effects of glucose and iron on MIN6 cells insulin secretion	111
5.3.6. Assessment of insulin secretion in GSIS experiment	112
5.3.7. Assessment of insulin secretion in the iron-challenge assay	115

5.4. Discussion	118
5.4. Conclusions	124
Conclusions	126
References	127

Introduction

- *Type 2 diabetes mellitus*

Type 2 diabetes mellitus (T2DM) is a metabolic disease characterized by decreased β -cells insulin secretion and/or insulin resistance, resulting in chronic hyperglycemia (elevated blood glucose levels) [1]. This metabolic disease has reached epidemic proportions: the latest edition of the IDF Diabetes Atlas shows that 10.5% of adults aged 20–79 years are currently affected by diabetes, and this percentage is set to rise even further [1]. Accordingly, the number of people with diabetes mellitus has quadrupled in the past three decades, and this pathology currently represents the worldwide ninth major cause of death [2]. Although the aetiology of T2DM is still unknown, numerous risk factors have been recognized associated with the T2DM onset. These include genetic predisposition, older age, non-white ancestry, overweight or obesity, and sedentary lifestyle [2]. Regarding familiarity, about 40% of type 2 diabetic patients reported first-degree relatives (parents or siblings) affected by the same disease, suggesting a strong hereditary component for this type of diabetes [3]. Due to the significant individual, social and economic impact of this pathology, the correct management of diabetes represents a primary need, especially in order to avoid microvascular and macrovascular complications related to this condition [4]. The management of T2DM involves a wide range of approaches, such as changes in lifestyle, including diet and physical activity, and pharmacological treatment to achieve metabolic control [5].

The pharmacological treatment of T2DM involves therapies based on oral hypoglycaemic drugs, a large class of molecules able to reduce blood sugar through different mechanisms of action, mainly represented by the stimulation of insulin release, improvement of insulin sensibility, inhibition of gastrointestinal enzymes, or reduction of renal tubular glucose reabsorption. Oral anti-diabetics drugs currently

available on the market are as follows: biguanides, sulfonylureas, glinides, glitazones, dipeptidyl peptidase-4 inhibitors, intestinal α -glucosidase inhibitors and renal sodium-glucose transport protein 2 (SGLT-2) inhibitors [6]. Although these approaches can substantially reduce diabetes-related morbidity and mortality, conventional medications in diabetes treatment can cause unwanted side effects to patients, leading to incompliance and treatment failure [7]. In general, therapy with oral antidiabetic therapies results to be associated with an increased risk of hypoglycemia, gastrointestinal and skin disorders, skin, asthenia, and weight gain [8]. More specifically, other side effects are dependent on the drug category. As example, thiazolidinediones can cause liver toxicity; metformin, a widespread biguanide, can enhance the effect of anticoagulants and limit the absorption of vitamin B12, while the therapy with sulfonylureas can be associated with a higher risk of photosensitivity, cholestatic jaundice, and hematologic disorders [9].

Based on such considerations, the interest towards plants and plant products as sources of antioxidant and antidiabetic agents is increasing over time [9–11]. In this regard, bioactive molecules of natural origin have played and continue to play a valuable role in the prevention and management of various diseases and drug discovery processes. The most convincing example of antidiabetic drugs developed from natural sources is represented by metformin, the current drug of choice for the treatment of T2DM, which is derived from the guanidines firstly obtained from *Galegine officinalis* [12]. Nonetheless, the consumption of natural products is commonly considered to be cheaper, easily available, and safer than synthetic drugs [9]. Additionally, despite thousands of years of traditional use of some natural products, great efforts have been made to scientifically assess the efficacy and safety of many natural products by conducting in vitro and in vivo studies [13]. It has been estimated that about 80% of the population both from developed and developing countries rely on natural products for their health management, most of them represented by plant extracts or the derived active principles [9,12]. Among bioactive

molecules of plant origin with beneficial potential for the management of diabetes, a specific interest has recently been placed on the investigation of abscisic acid (ABA).

- *ABA in the vegetal world*

2-*cis*, 4-*trans*-Abscisic acid (ABA) is a sesquiterpenoid phytohormone naturally present in fruits and vegetables [14]. Two pathways are involved in the ABA biosynthesis in plants: the terpenoid pathway, which synthesizes ABA directly from mevalonic acid, and the carotenoid pathway, which synthesizes ABA indirectly via the all-*trans* C40 carotenoid precursors followed by oxidative cleavage [14,15]. ABA was first identified in plants in the late 1960s, in relation to the wilting and nitric oxide (NO)-mediated closure of stomata [16]. The ABA chemical structure is simple compared to other hormones (an isoprenoid structure with a molecular weight of 264, Figure 1), although the signaling pathways activated by this molecule are quite complex and may vary in different organisms, such as plants and mammals [17]. Nowadays, ABA is recognized as a phytohormone involved in the adaptive response to a wide variety of environmental stresses, such as drought, high temperatures, cold stresses, and salinity [18]. Additionally, this phytohormone is majorly responsible for the regulation of plant growth and differentiation [18–20]. In this regard, the influence of ABA on fruit ripening has been well documented, although its mechanism of action is still unclear. Studies have revealed that there is a progressive accumulation of ABA during fruit ripening, reaching its maximum concentration at a specific stage after full bloom and then decreasing to its minimum level at the fruit fully ripe/harvest stage [21–23]. Therefore, ABA is considered a suppressive plant growth regulator, inducing the expression of cell cycle inhibitors that act on DNA [24] and protein synthesis [25], thereby arresting cell division [26] and blocking the progression of the cell cycle in its initial stages [27]. Probably, this effect would be

highly requested by the fruit at an immature stage when cell cycle progression can be disturbed by several environmental factors such as oxidative stress [27]. Later, the production of increasing levels of protective compounds, such as antioxidants, would make possible the completion of fruit development, so that the action of ABA is no longer required [27].

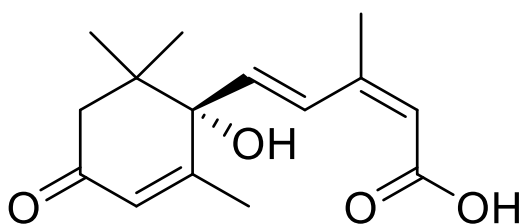


Figure 1. (-)-Abscisic acid chemical structure

- *ABA in the animal world*

Although ABA has long been known as an ancient signal molecule in plants, the discovery of its role as an endogenous hormone in mammals dates back to the last decades. A study conducted in the late 1980s on pigs and rats has indeed identified the presence of this molecule within the tissues of these animals, with specific high levels in the brain [28]. Specifically, the observation of higher ABA levels in the brain of rats fed with low exogenous ABA, compared with rats fed with a diet higher in ABA content, provided the first indication of the endogenous synthesis of ABA in mammals [28]. Nowadays, numerous studies carried out on in vitro models have confirmed the contribution of this molecule as an endogenous hormone, as its synthesis and release were observed from granulocytes [29], monocytes [30], macrophages [31], pancreatic β -cells [32], mesenchymal stem cells [33], and adipocytes [34]. Evidence from scientific literature has highlighted the beneficial potential of this molecule in the management of various pathological conditions in animals, including atherosclerosis [35], ischemic retinopathies [36], inflammatory

[37], and neurodegenerative diseases [15], therefore attracting enormous attention from researchers.

Moreover, the effects attributed to the activity of ABA at the cellular level lead to the hypothesis of the conservatory role of this hormone in the adaptive response to stressful stimuli at an early stage of evolution, both in plants and animals [38]. A first observation that warranted this hypothesis derives from the similarity of the ABA signal transduction pathway in plants and animals which involves the increase in the concentration of intracellular calcium levels after stimulation by cyclic adenosine diphosphate (ADP) ribose. This evidence is supported by ABA-mediated effects exerted by granulocytes, well-recognized examples of mammalian cells highly exposed to environmental stimuli. The phagocytic activity, oxygen species (ROS), and nitric oxide (NO) production triggered by these cells as a defense against pathogens are mediated by a metabolic pathway that involves the phosphorylation of cyclic ADP-ribose and the consequent increase in the intracellular calcium levels [29]. Therefore, ABA has been recognized as an endogenous pro-inflammatory cytokine in mammals [29] and, similarly to plants, it seems to contribute to the response to stressful conditions such as trauma, fever, or infections. Considering that all these conditions can lead to hyperglycemia, which in turn is a stress stimulus for the organism, and considering that the messengers of the ABA signaling pathway in granulocytes are also known mediators of glucose-induced insulin secretion [32], a role for ABA as a main regulator of glucose homeostasis has been proposed.

- *ABA as a regulator of glycemic homeostasis in mammals*

The first evidence concerning the involvement of ABA in the management of glucose homeostasis in mammals has been elaborated based on the structural similarity of this hormone with thiazolidinediones, a class of insulin-sensitizing antidiabetic drugs [39]. The ABA-related beneficial effects on the control of

glycemic homeostasis are exerted through different mechanisms of action, all mediated by interaction with its specific receptor LANCL2 (Lanthionine Synthetase C-like 2). This receptor belongs to the mammalian LANCL family which also includes LANCL1, the most highly expressed receptor (especially in the brain), and LANCL3, currently considered a pseudogene [40]. In vitro studies have demonstrated the ability of ABA to bind with high affinity to human recombinant LANCL2 (Kd 2.6 nM). Indeed, the presence of this receptor is required for ABA to exert its effects in various cell types [41]. LANCL2 is coupled to a G protein when bound to the membrane but is then demyristoylated after binding to ABA. This interaction leads to the detachment of LANCL2 from the membrane and its accumulation in the cell nucleus [42]. The binding of ABA to its receptor requires influx through transporters of the anion exchanger (AE) superfamily [43]. Protonated ABA may instead diffuse through the lipid bilayer, although a very small percentage of this molecule is protonated at the near-neutral pH of plasma and interstitial fluids. Therefore, the exchange of ABA between the external and internal cellular environment requires a transport system. On the other hand, the strongly acidic pH at the stomach levels favors the protonated, membrane-permeable form of ABA and allows its diffusion through the lipid bilayer of the stomach [17]. This situation likely explains the rapid absorption of the hormone after oral administration.

As shown in Figure 2, the major activities of this endogenous hormone in relation to hypoglycemic potential include the i) stimulation of insulin release by pancreatic β -cells, ii) increase in GLP-1 (glucagon-like peptide 1) production by enteroendocrine cells, and iii) upregulation of GLUT-4 (glucose transporter 4) expression and translocation in muscle and adipose tissue [34,44].

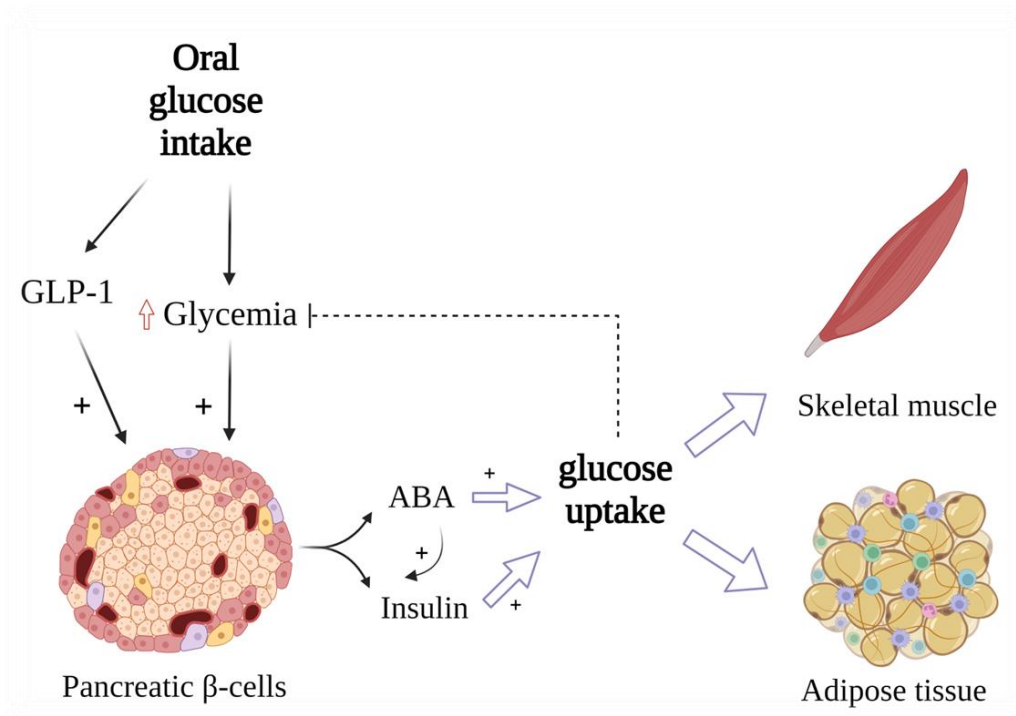


Figure 2. Schematic representation of the proposed ABA effects in the regulation of blood glucose levels.

As regards the effects observed on insulin secretion, Bruzzone et al. demonstrated that the high glucose concentration may stimulate ABA production and release from RIN-m and INS-1 cells and human pancreatic β -cells. Nanomolar ABA in turn showed to stimulate glucose-independent (i.e., in the absence of glucose) and potentiate glucose-dependent (i.e., in the presence of either low or high glucose) insulin release [32]. The main stages of the cellular signaling pathway of ABA are the following: i) interaction of ABA in β -cells with its receptor LANCL2, which is functionally coupled to a PTX-sensitive G_i protein; ii) this interaction stimulates Adenylate cyclase (AC) with overproduction of the ABA upstream second messenger Cyclic AMP; iii) activation of PKA (Protein Kinase A); iv) PKA-mediated phosphorylation and stimulation of CD38 (cluster of differentiation 38). Accordingly, NAD^+ is converted to Cyclic ADP-ribose (cADPR), which acts as a

downstream second messenger of ABA; v) cADPR enhances the $[Ca^{2+}]_i$ through a cell-specific combination of increased Ca^{2+} influx and intracellular Ca^{2+} mobilization from the endoplasmic reticulum; vi) the increased $[Ca^{2+}]_i$ levels stimulate functional responses (e.g. release of insulin in pancreatic β -cells). It is now known that these cADPR and $[Ca^{2+}]_i$ -upregulated functional responses include in some types of cells the autocrine generation of ABA to amplify the above-mentioned signal transduction pathway [32]. Additionally, a very recent study conducted on type 1 diabetic mice showed that the coadministration with oral ABA and low-dose subcutaneous insulin led to a significantly greater improvement in the glycemic profile and an increased transcription and protein expression of PGC-1 α (peroxisome proliferator-activated receptor gamma coactivator 1-alpha), AMPK (adenosine monophosphate-activated protein kinase), and GLUT4 compared with controls treated with insulin alone [45]. These findings may therefore pave the way for a combination of ABA-based nutraceutical products with insulin to eventually reduce the insulin dose required in T1DM, thereby reducing the risk of hypoglycemia and improving muscle insulin sensitivity.

As mentioned above, a second mechanism of action that further supports the blood glucose-lowering potential of ABA is the stimulation of the release of the incretin hormone GLP-1. Incretins are known intestinal hormones secreted by enteroendocrine cells after meals. As a result, these hormones promote the reduction of blood glucose levels by stimulating insulin secretion and inhibiting glucagon secretion [46]. A study conducted by Bruzzone and colleagues demonstrated the increase in plasmatic ABA following glucose uptake in healthy individuals [34]. Specifically, the increase in ABA levels above basal levels was reported from 15 to 60 min in all participants undergoing the oral glucose tolerance test (OGTT). Since the administration of intravenous glucose did not cause a similar increase in the same group of subjects, the authors assumed a stimulating effect of incretins on the ABA release [34]. Moreover, *in vivo* studies have better clarified the positive feedback

between ABA and GLP-1 activated by hyperglycemia: GLP-1 stimulates the endogenous release of ABA from β -cells, while ABA in turn induces the release of GLP-1 through a cAMP/PKA-dependent mechanism of action and GLP-1 transcription factor activation [47].

The third hypoglycemic mechanism of action associated with ABA is the upregulation of GLUT-4 expression and translocation in muscle and adipose tissue. In this regard, scientific evidence have reported the ability of ABA at nanomolar concentrations to stimulate the peripheral glucose uptake, similarly to insulin, in rat L6 myoblasts and murine 3T3-L1 cells differentiated to adipocytes, by upregulation of GLUT-4 translocation to the plasma membrane [34]. Specifically, the insulin-independent hypoglycemic activity of ABA has been proposed by recent *ex vivo* experiments, in which this molecule was demonstrated to stimulate the uptake of a fluorescent glucose analog by mouse skeletal muscle in the absence of insulin, and the LNC2 silencing reduced all the observed effects [48]. These results were also confirmed *in vivo* on rats undergoing an oral glucose load, as the ABA-induced glucose and storage in skeletal muscle were detected by micro-PET [48].

From a mechanistic point of view, the activation of AMPK would be responsible for these effects. More specifically, incubation with ABA has been shown to increase phosphorylation of AMPK, leading to phosphorylation and activation of PGC-1 α in skeletal muscle. Therefore, the main consequence of this process is represented by the increase in GLUT4 expression and glycogen accumulation [48,49]. AMPK is also an upstream positive regulator of p38 mitogen-activated protein kinase (MAPK) [50], which has the ability to promote PPAR- γ (peroxisome proliferator-activated receptor gamma) phosphorylation on Ser122, thus preventing PPAR- γ -induced inhibition of GLUT4 expression [48,51,52]. As indeed reviewed by previous authors, under conditions of high blood glucose (HG), insulin acts as an anabolic hormone by stimulating muscle glycogen and white adipocyte triglycerides synthesis through its key mediator Akt. This latter is also responsible for the inhibition of AMPK, the

main enzyme involved in the ABA signaling pathway. On the other hand, both under conditions of low (LG) and high glucose (HG), ABA is responsible for the stimulation of energy production via increased mitochondrial activity and biogenesis in muscle and adipose cells, thermogenesis, and browning of the white adipose tissue [17] (Figure 3).

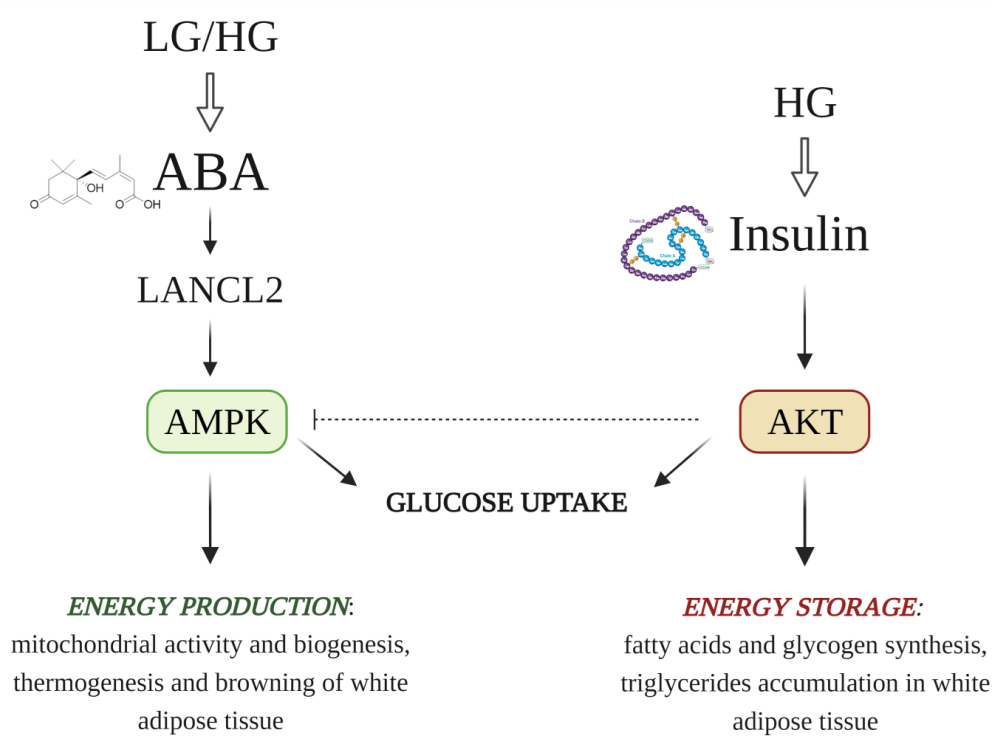


Figure 3. Non-overlapping effects of ABA and insulin in muscle and adipose tissue.

Overall, the observations on the AMPK-mediated signaling pathways of ABA and the non-overlapping metabolic effects with insulin highlight a role of ABA as an upstream regulator of glucose homeostasis and strongly support supplementation with exogenous ABA to prevent the excessive insulin release associated with fatty acid accumulation in the adipose tissue and eventual β -cell failure. Despite the evidence observed in vitro, recent studies have shown that the mechanism behind the

hypoglycemic effect of ABA *in vivo*, when administered at low doses (few micrograms/kg body weight), would depend on its ability to upregulate the peripheral glucose transport, rather than its stimulatory activity on insulin release [53]. Although the reasons for this unexpected effect have not yet been fully elucidated, various hypotheses have been proposed. Based on these assumptions, the stimulation of glucose uptake in GLUT4-expressing cells induced by ABA could precede in time and/or exceed in extent the stimulation of insulin release or, in a not necessarily exclusive manner, these cells may be more sensitive to the effect of ABA than pancreatic β -cells *in vivo* [44]. Therefore, the administration of ABA at low doses may be suggested as a useful tool for the improvement of glucose tolerance in subjects with a deficiency of/or insulin resistance. In this regard, there is a growing consensus within the scientific community that the protracted stimulation of insulin release from pancreatic β -cells under conditions of chronic hyperglycemia may eventually contribute to their exhaustion [54]. In view of this evidence, hypoglycemic molecules able to decrease glycemia without increasing insulinemia are highly desirable, as they could improve the survival and function of pancreatic β -cells.

- *Agro-food waste products as sources of ABA*

During food processing, about 70% of the biological feedstock becomes waste. Every year, one billion tons of food by-products are discarded worldwide, and this amount is set to rise even further within the next decades [55]. Food waste is a pollutant with a huge environmental impact and, considering the cost of its disposal, it represents a considerable global emergency [56]. Recently, the recycling of food by-products has proven to be an attractive area of research for nutraceutical applications due to the high content of bioactive compounds [57]. Several pharmaceutical companies are nowadays using agro-food by-products as alternative

raw materials for the extraction of bioactive compounds (mostly antioxidants) to include in nutraceuticals and food supplements. This recycling activity is encountering the support of authorities, which are alarmed by air, soil, and water pollution generated by agricultural waste disposal. Waste reuse has several economic advantages: (i) its low cost; (ii) its abundance; (iii) the high content of bioactive molecules; as well as (iv) the financial support received by governments eager to promote eco-compatible and pollution-reducing practices. A significant portion of waste biomass is represented by agricultural by-products (e.g. leaves, bark, roots, seeds, and wood), while another significant portion consists of food products (mainly fruits and vegetables) whose morphological and esthetic characteristics do not meet the requirements of the modern world market [55].

Nonetheless, agro-food waste products are also increasingly attracting great interest from the nutraceutical industry as sources of bioactive compounds useful for the formulation of food supplements indicated for the control of glycemia [58]. These biowaste matrices might include immature fruits deriving from fruit thinning, which is a widespread agronomical practice that involves removing excess unripe fruits, measuring 1–2 centimeters in diameter, to produce better-sized, ripe, and healthy fruits, albeit in smaller numbers. This procedure is generally applied to a specific range of tree fruits, including apples, pears, plums, peaches, and nectarines, and consists of leaving a minimum of one fruit every 5–8 cm (plums and apricots) to a maximum of one fruit every 10–15 cm (apples and pears) and 20–25 cm (peaches and nectarines) on tree branches [59]. The very high load of fruits can in fact lead the fruit production to be small and of poor quality, but this condition significantly improves after the thinning process. Among other benefits, this practice ensures that sunlight and air can penetrate the branches, thus enhancing the uniformity of ripening and limiting the breaking of the branches themselves and the spread of diseases [60]. Since fruit thinning may interest up to 40% of the entire tree fruit load, it can lead to a massive agricultural waste product which is generally destined for fertilizing or

feeding. Interestingly, as reported above, it is well known the role of ABA as a terpenoid phytohormone majorly responsible for the regulation of plant growth and differentiation, whose content results to be at its maximum level at a specific stage after full bloom [18]. From this point of view, thinned fruits represent rich sources of this phytohormone, and their exogenous supplementation in the form of nutraceutical formulations would promote the exogenous intake of ABA in humans, favoring its physiological potential in the regulation of glucose homeostasis.



Figure 4. Immature nectarines derived from the agronomical practice of fruit thinning. (Source: Campania Region, Agriculture Department).

Nonetheless, immature fruits have long been underestimated as potential high-value-added plant resources, and their physiochemical profile and bioactive capacity remain poorly studied. In this scenario, these waste-food products may represent not only precious sources of ABA, but also other bioactive molecules with potential health benefits, such as polyphenols [61]. It is widely described that these compounds possess crucial antioxidant activity, thus preventing cellular oxidative stress caused by free radicals [62]. In this regard, growing scientific evidence suggest that an excess of highly reactive species, largely due to hyperglycemia, may lead to oxidative stress, which further supports the development and progression of diabetic complications [63,64]. In this context, scientific evidence reported a different

qualitative and quantitative composition of active molecules, especially polyphenols, in unripe nectarines, compared to full-harvest fruits [61]. Generally, TN at the early stage of fruit development have notably higher polyphenol content than ripe fruits, thus determining a higher antioxidant potential [61]. Polyphenolic compounds are indeed crucial for fruit quality, as they determine properties such as colour, astringency, and bitterness [65]. Therefore, the observed difference in the polyphenolic profile compared to ripe fruits makes this natural product of great interest for the development of innovative nutraceutical formulations.

Chapter 1

Thinned nectarines as sources of ABA and its derivatives

1.1. Introduction

As previously discussed in the Introduction section, thinned fruits at the early stages of their development have aroused particular interest in the scientific literature as a consequence of their high content of ABA [58], a plant phytohormone majorly involved in suppressing fruit ripening [18]. From this point of view, unripe fruits may promote the intake of this endogenous hormone in humans, contributing to its beneficial activity in modulating glycaemic levels. ABA is a key mediator in plants, being involved in various physiological processes such as plant growth, seed maturation, germination, development, or dormancy [20,66] as well as in regulating the response to abiotic stresses (e.g., low temperature, UV radiation, water deficiency, etc.). Nevertheless, scientific literature has also clarified the metabolism of this phytohormone in plants. Specifically, the first step involves its conversion to 8-hydroxy ABA (HOABA) and its further metabolization into other inactive structures, such as hydroxymethylglutaryl (HMG)-HOABA, methyl ester (Me)HMG-HOABA, phaseic acid (PA), dihydrophaseic acid (DPA), etc. The latter compounds derive from the ABA conjugation process with ABA-glucosyl ester (-GE) or ABA glucosyl ether (-GS). ABA-GE and ABA-GS have been isolated from many plant species, although the physiological significance of ABA conjugations in plants, and especially ABA glycosylation, remains unclear [67].

ABA-derived molecules are usually regarded as inactive forms of this molecule. However, this perspective has been challenged by the finding that some metabolites produced by ABA catabolism still exhibit biological activities [68–71]. Therefore, the putative biological effects of these metabolites in animals cannot be excluded,

and conversely, the investigation of their beneficial potential would be of great interest. Extraction protocols for plant-based secondary metabolites are mainly influenced by the selection of temperature, incubation time, solvent, and solvent-to-feed ratio [72,73]. Water, aqueous mixtures of ethanol, methanol, and acetone are commonly used as extraction mixtures. In this context, it is well recognized that the choice of extraction conditions can strongly influence the recovery of bioactive compounds of interest from a complex origin matrix [74]. Based on these considerations, the first aims of the present thesis work were:

- To perform a screening of different extracts of unripe fruits derived from fruit thinning (fruit thinning waste products, FTWPs) in terms of ABA content.
- To optimize the ABA extraction conditions to reach the highest yield of this molecule from the previously selected FTPW.
- Finally, to qualitatively determine the presence of other ABA-derivates in the extract obtained under optimized conditions, through an HPLC-HESI-MS/MS analysis.

1.2. Materials and Methods

1.2.1. Chemicals and reagents

All chemicals and reagents used were either analytical-reagent or high-performance liquid chromatography (HPLC) grade. The water was treated in a Milli-Q water purification system (Millipore, Bedford, MA) before use. (±)-2-Cis-4-trans-Abscisic acid (ABA), methanol, acetonitrile, and formic acid were all purchased from Sigma–Aldrich (Milano, Italy).

1.2.2. FTWPs collection and preparation for HPLC analysis

FTWPs (apples, pears, plums, peaches, and nectarines) were collected in June 2018 at the orchards of “Giaccio Frutta” society (Vitulazio, Caserta, Italy, 41°10'N - 14°13'E), at 20-25 days after full bloom, coinciding with fruit thinning stage. Samples were immersed in liquid nitrogen (N₂) and maintained at -80 °C until analysis. Then, samples were weighed and ground in liquid N₂, and 1.5 g of each homogenized sample was suspended in 15 mL of 80% methanol (methanol:water, 80:20 v/v) containing 1% formic acid for 16 h at 4 °C in darkness under magnetic stirring. The extract was then centrifuged for 10 min at 9000 × g and the supernatants were filtered and stored at -20 °C until analysis.

1.2.3. HPLC-DAD analysis of FTWPs samples

The chromatographic apparatus consisted of a Jasco Extrema LC-4000 system (Jasco Inc., Easton, MD) provided with the following modular components: a vacuum degassing unit, a quaternary pump, an autoinjector, a column oven, a diode array detector photodiode array detector (DAD). The chromatographic analyses to determine the ABA content in FTWPs samples were performed according to previous authors, with slight modifications [75]. The column selected was a Kinetex[®] C₁₈ column 100A (250 mm x 4.6 mm i.d., 5 μm) (Phenomenex, Torrance, CA). The mobile phases were water at 1% formic acid (A) and acetonitrile (B). After 3 min hold at 5% solvent B, elution was performed according to the following conditions: from 5% (B) to 75% (B) in 20 min, followed by 1 min of maintenance; then the column was equilibrated to the initial conditions for another minute. The separation conditions were as follows: column temperature was set at 30°C, inject volume was 20 μl, the flow rate was set at 1 ml/min. Abscisic acid analysis was monitored at 265 nm. Peak identifications were based on retention times and

standard addition to the samples. Compounds were quantified according to a calibration curve made with six different concentrations over a concentration range of 0.1–100 ppm and triplicate injections at each level.

1.2.4. Optimization of ABA extraction conditions

As first, the optimization of the most efficient solvent mixture, in terms of ABA recovery, was performed. Briefly, 0.5 g of the freeze-dried sample was ground before adding 20 ml of one of the selected extraction solvents (from 100% methanol solution to 100% water solution containing 0.1, 1, or 10% formic acid). The mixture was then shaken at 25°C for 2 hours, centrifuged at 14000 g for 10 minutes, and the supernatant was stored at -20° until analysis. Each sample was extracted in triplicate. Afterwards, as indicated in Table 1, different incubation times (1, 2, and 4 hours), matrix-to-solvent ratios (1:10, 1:20, 1:40, and 1:60), and incubation temperatures (25, 40, and 60 °C) were opportunely combined for the optimization of ABA extraction conditions. A total of forty-eight combinations of different parameter conditions were tested. According to the generally applied extraction protocol, the mixture was incubated at a selected temperature and time on an orbital shaker. At the end of each extraction time, samples were centrifuged at 14000 × g for 10 min. Supernatants were filtered using a 0.22 µm nylon filter (Cell Treat, Shirley, MA, USA) and stored at -20 °C until analysis. All the extractions were performed in triplicate. The ABA content of the samples was finally evaluated by following the above-mentioned protocol.

Table 1. Independent variables and their factor levels used for the optimization protocol.

Independent Variable	Factor levels			
Matrix-to-solvent ratio	1:10	1:20	1:40	1:60
Incubation time (hours)	1	2	4	6
Temperature (°C)	25	40	60	
Total runs	144			

1.2.5. HPLC-HESI-MS/MS analysis of ABA and its derivatives

The protocol described in the previous section, using 80% methanol with 1% formic acid as the solvent mixture, was used to extract the FTWP sample for the HPLC-HESI-MS/MS analysis of ABA metabolites. An HPLC DIONEX UltiMate 3000 (Thermo Fisher Scientific, San Jose, CA, USA) equipment, coupled with an autosampler, a binary solvent pump, a diode-array detector (DAD), and an LTQ XL mass spectrometer (Thermo Fisher Scientific, San Jose, CA, USA), were used for the analysis. The separation conditions were as follows: column temperature was set at 35 °C, the injection volume was 5 μ L, and the flow rate was set at 1 mL/min. The selected column was the Kinetex[®] C18 column (75 mm \times 2.1 mm, 2.6 μ m; Phenomenex, Torrance, CA, USA). The mobile phases were water at 0.1% formic acid (A) and acetonitrile at 0.1% formic acid (B). Elution was performed according to the following conditions: 0–1.5 min hold at 5% solvent B, from 5% (B) to 95% (B); for the remaining 3 min, the column was equilibrated to the initial conditions. Regarding the mass parameters, the source was a heated electrospray interface (HESI), operated in negative ionization with full scanning (FS) and product ion acquisition (MS/MS). Collision-induced fragmentation was made using argon, with a collision energy of 32.0 eV. The ion source was set using the following parameters: sheath gas flow rate: 30; auxiliary gas flow rate: 10; capillary temperature: 320 °C;

source heated temperature: 150 °C; source voltage: 3.5 kV; source current: 100 µA; capillary voltage: 31 V; and tube lens: 90 V.

1.2.6. Statistical analysis

Unless otherwise stated, all the experimental results were expressed as mean \pm standard deviation (SD) of at least three replicates. Statistical analysis of data was performed by two-way ANOVA followed by Tukey-Kramer multiple comparison test or Dunnett's multiple comparison test using GraphPad Prism 8.4.3 software. *P*-values less than 0.05 were regarded as statistically significant. The Pareto Chart was created using Minitab software version 21.1.0.

1.3. Results

1.3.1. Selection of TN as richest sources of ABA

As a first result of this Ph.D. thesis, thinned nectarines (TN) (*Prunus Persica* L.) were found to be the richest in ABA content among all FTWPs (Table 2) [58]. Thus, these by-product matrices were chosen as ideal candidates for future investigation about their beneficial potential role for nutraceutical applications.

Table 2. Content of abscisic acid in different fruit thinning waste products.

	Peaches	Nectarines	Apples	Plums	Pears
µg/g FW	0.9 \pm 0.5 ^a	4.5 \pm 1.5 ^c	0.8 \pm 0.3 ^a	0.4 \pm 0.2 ^b	0.3 \pm 0.1 ^b
µg/g DW	9.5 \pm 1.6 ^a	15.0 \pm 3.0 ^c	8.1 \pm 1.1 ^a	6.5 \pm 0.9 ^b	5.5 \pm 0.8 ^b

Values are the means \pm SD ($n = 5$; $p < 0.01$). ^{abc}Mean values in rows with different superscript letters are significantly different by the Tukey-Kramer multiple comparison test. Abbreviations: DW, dry weight; FW, fresh weight.

1.3.2. Effect of different extraction conditions on ABA yield

As can be seen in Figure 5, optimization of the most efficient solvent mixture showed that 80% methanol (methanol:water, 80:20 v/v) containing 1% formic acid was the most efficient solvent in terms of ABA recovery from the freeze-dried TN product ($p < 0.0001$, compared with other solvent mixtures). In this regard, experimental data obtained with different extraction solvents showed that the lowest percentage of ABA yield was obtained using 100% water containing 10% formic acid as extraction solvent.

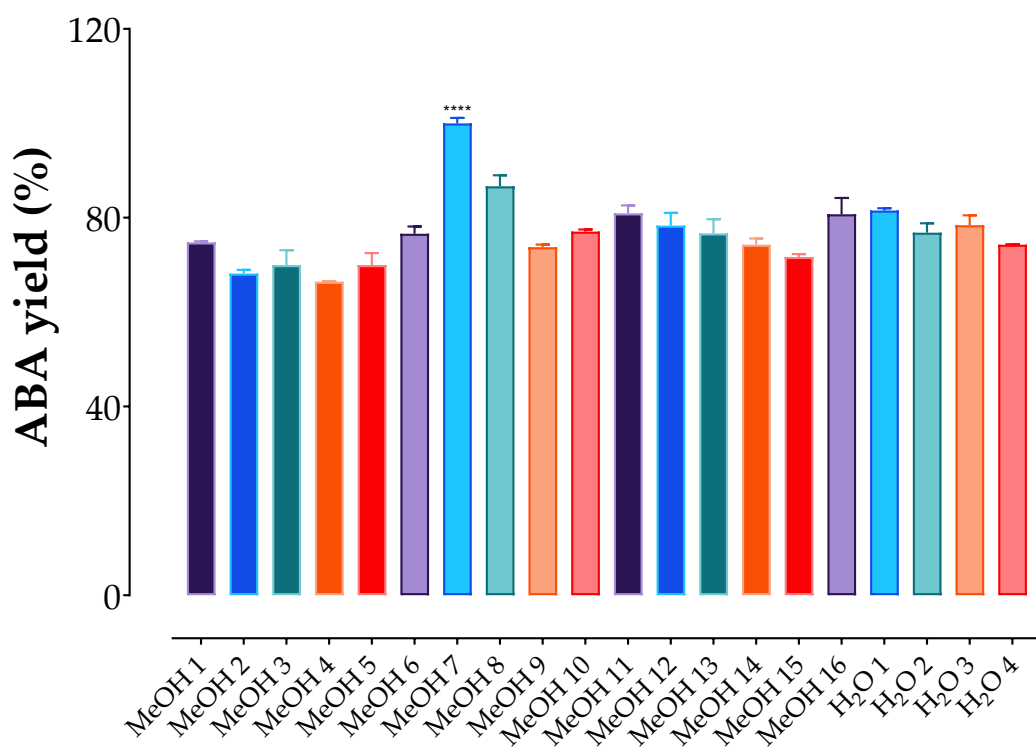


Figure 5. Effects of different solvent mixtures on ABA extraction rates. Abbreviations: ABA, abscisic acid; MeOH 1, 100% methanol; MeOH 2, 100% methanol with 0.1% formic acid; MeOH 3, 100% methanol with 1% formic acid; MeOH 4, 100% methanol with 10% formic acid; MeOH 5, methanol/water (80/20, v/v); MeOH 6, methanol/water (80/20, v/v) with 0.1% formic acid; MeOH 7, methanol/water (80/20, v/v) with 1% formic acid; MeOH 8, methanol/water (80/20, v/v) with 10% formic acid; MeOH 9, methanol/water (50/50, v/v); MeOH 10, methanol/water (50/50, v/v) with 0.1% formic acid; MeOH 11, methanol/water (50/50, v/v) with 1% formic acid; MeOH 12, methanol/water (50/50, v/v) with 10% formic acid; MeOH 13, methanol/water (20/80, v/v); MeOH 14, methanol/water (20/80, v/v) with 0.1% formic acid; MeOH 15, methanol/water (20/80, v/v) with 1% formic acid; MeOH 16, methanol/water (20/80, v/v) with 10% formic acid; H2O 1, 100% water; H2O 2, 100% water with 0.1% formic acid; H2O 3, 100% water with 1% formic acid; H2O 4, 100% water with 10% formic acid. All extractions were performed at 25 °C for 2 hours with a matrix-to-solvent ratio of 1:40. Values are mean \pm standard deviation (SD) of three repetitions. Statistical significance was calculated by two-way ANOVA followed by Dunnett's multiple comparison test; **** $p < 0.0001$ vs all other conditions. Results are normalized to the highest yield of ABA.

In addition to the solvent mixture, other three independent commonly modified factors, i.e., extraction time (1, 2, and 4 hours), temperature (25, 40, and 60 °C), and matrix-to-solvent ratio (1:10, 1:20, 1:40, and 1:60) were considered for optimization of the ABA recovery in the hydroalcoholic solvent. As reported in the Pareto-chart graph (Figure 6), preliminary ANOVA analysis showed that only the matrix-to-solvent ratio (A) was found to be significantly correlated with the ABA extraction rate, with $\alpha=0.05$. In this regard, longer extraction duration or higher incubation temperature didn't result in a significant increase in extraction efficiency. Instead, after reaching the highest extraction efficiency after 2 h incubation at 40 °C, the extraction efficiency showed a gradual decrease.

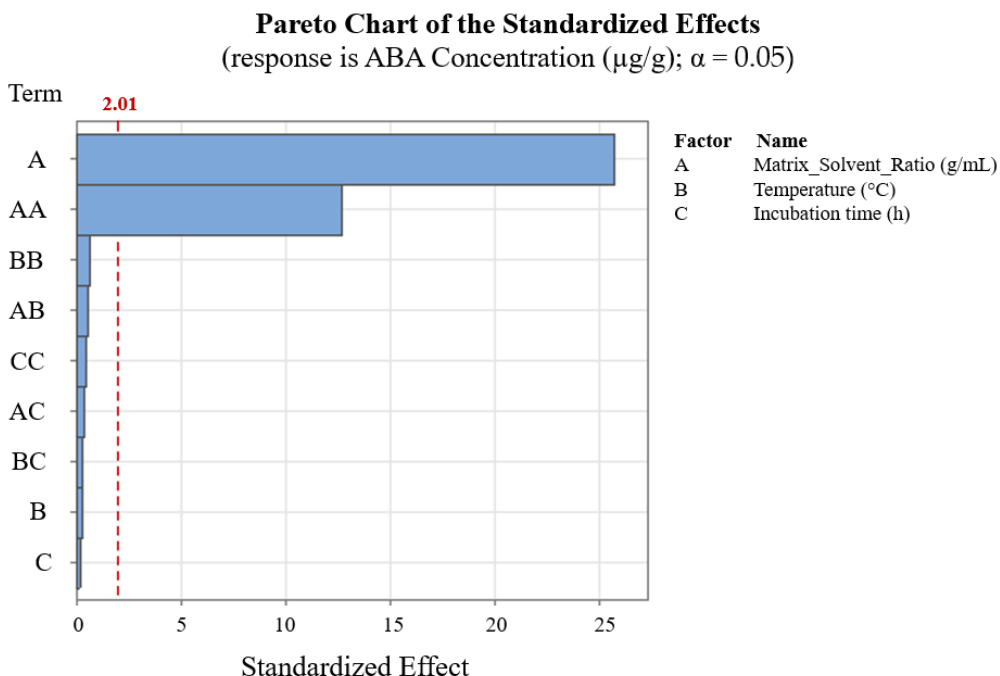


Figure 6. Pareto chart of total parameters analyzed, i.e. matrix-to-solvent ratio (A), temperature (B), and incubation time (C).

According to the statistical results of model fitting, the best model to maximize the ABA yield would be achieved by limiting the statistical analysis to the analysis of variance. The model was demonstrated to be significant ($p < 0.0001$), while the percentage predictivity of the model was 91.99 % (R-sq 94.13 %, R-sq(adj) 93.08 %; R-sq(pre) 91.99 %).

1.3.3. Identification of ABA metabolites in the TN sample

Based on the comparison with literature data [76,77], HPLC-HESI-MS/MS analysis performed on the TN polyphenolic extract led to the identification of three compounds derived from the ABA metabolism (Table 3).

Table 3. Qualitative characterization of ABA derivatives in thinned nectarine extract determined by HPLC-HESI-MS/MS analysis.

Compound	[M-H] ⁻ <i>m/z</i>	R _t	Fragmentation
Abscisic acid	263	8.41	245, 219, 201, 153
Phaseic acid	279	7.23	235, 205, 139
Neophaseic acid	279	7.91	235, 205 , 139
Abscisic acid glucoside ester	425	7.52	407, 381, 263 , 219, 201

Fragment ions' base peaks are shown in bold.

1.4. Discussion

An aspect of great interest of the present work is represented by the possibility of obtaining useful nutraceutical formulations from agricultural by-products. The management of solid wastes originating from agricultural processing is a serious emerging problem in both Western and developing countries. In particular, the costs of drying, storage, and shipment of by-products for their disposal are economically crucial factors [57]. As a result, agro-food wastes are often employed as fertilizer or feed and numerous attempts have been made by researchers and industries to recycle them. Specifically, several by-products which were first underexploited and disregarded are increasingly being converted into valuable ingredients. Some of these ingredients are commercialized and widely used by industries as food products or as nutraceutical ingredients in functional foods [78]. The present study is thus in line with the current worldwide trend to recover such agro-food wastes for environmental, economic, and health purposes.

Extraction protocols for plant-based secondary metabolites are strongly influenced by the selection of temperature, incubation time, solvent and solvent-to-feed ratios [73]. Water, aqueous mixtures of ethanol, methanol, and acetone are commonly used as extraction mixtures [74]. We herein chose to test twenty solvent mixtures with different polarities and acidic levels. Finally, the optimization performed allowed us to identify an 80% methanol solution with 1% formic acid as the most efficient solvent in terms of ABA recovery from the TN vegetable matrix. In this context, the extensive use of this solvent is frequently reported in the scientific literature to achieve the maximum extraction rate of various plant-derived molecules, especially polyphenols, is widely reported by [79,80]. Moreover, the differences observed for the different solvents tested in ABA recovery could be due to the different polarities of the extraction solvents, which might affect the solubility of the chemical constituents in a solution and the extraction yield [81]. In the present project, we decided to keep the temperature values constantly below 60 °C to avoid the temperature-dependent decomposition of bioactive compounds during the extraction process [82]. Among all conditions tested, the matrix-to-solvent ratio (g/ml), which in our study was related to the mass of freeze-dried TN and the volume of extraction solvent, was found to play a key role in extraction efficiency [72,83]. In particular, the results showed that the matrix-to-solvent ratio is the only condition that has a relevant and statistical significance for ABA recovery from our vegetable matrix. In agreement with our observations, a study conducted by Luck and colleagues showed that the accessibility of the polyphenol rutin, present in the plant matrix studies, was limited by side compounds depending on the solvent-to-feed ratio [72]. In the present project, the maximum extraction yield of ABA was reached using a matrix-to-solvent ratio of at least 1:60, which allowed us to determine a final ABA concentration of 21.71 µg/g freeze-dried TN. Based on scientific literature, three putative mechanisms could explain the limited yield of bioactive compounds at low matrix-to-solvent ratios: i) poor solubility of the target compound in the

solvent [84], ii) limited accessibility of the molecule due to the negative influence of side compounds [72], iii) adsorptive effect of the compound into the plant matrix. Generally, based on the principles of mass transfer and in accordance with available scientific evidence, the higher the matrix-to-solvent ratio, the higher the total plant compounds content obtained [85].

In the first part of this thesis project, a qualitative characterization of ABA derivatives contained in the TN by-product was also carried out. The HPLC-HESI-MS/MS analysis performed led to the identification of three compounds derived from the ABA metabolic pathway in plants, i.e. PA, DPA, and ABA-GS. Although the physiological relevance of these molecules in plants has not been fully elucidated, it has been speculated that biological activities commonly attributed to the role of ABA may also be exerted by its metabolites. In particular, PA has been reported to be able to interact with ABA-specific receptors [70], suggesting a putative synergistic effect associated with the combination of these bioactive compounds. Undoubtedly, the determination of ABA derivatives in our by-product matrix lets us envisage future investigations of their biological activities after isolating them from the complex plant matrix.

1.5. Conclusions

Control of glucose homeostasis represents the main goal in both the prevention and management of diabetes and prediabetes. Numerous drugs are available, despite their side effects. Currently, a great interest has been focused on the valorization of agricultural by-products as sources of bioactive compounds with health-promoting effects. In the first part of this project a screening of various unripe fruits derived from the thinning process led to the identification of thinned nectarines as the richest sources in terms of ABA content. Moreover, the combination of different extraction conditions was investigated to optimize ABA recovery, finally indicating that the

extraction of ABA from TN strongly depends on the matrix-to-solvent ratio parameter. Finally, HPLC- HESI-MS/MS analysis performed on the extract obtained under optimized conditions allowed us to qualitatively characterize the presence of ABA derivatives in our vegetable matrix. Therefore, the TN by-product was selected as the ideal candidate for future studies on its positive potential role for nutraceutical applications, especially in terms of glucose homeostasis control.

Chapter 2

Phenolic characterization and in vitro antioxidant and antidiabetic potential of TNE

2.1. Introduction

Thinned fruits have long been underestimated as potential high-value-added plant resources, and their physiochemical profile and bioactive capacity remain poorly studied. The previous screening performed on different fruit thinning waste products (i.e., peaches, nectarines, apples, pears, and plums) allowed us to identify nectarines as the richest matrices in terms of ABA content [58]. Thus, the TN plant matrix was chosen as the ideal candidate to be tested for its hypoglycemic potential. Noteworthy, thinned fruits represent not only precious sources of ABA but also other bioactive molecules with potential health benefits, such as polyphenols [61]. Accordingly, growing scientific evidence describes the potential role of polyphenolic compounds in the management of the diabetic condition, being able to act on the control of blood sugar on different levels [63,64]. In view of these considerations, natural products containing bioactive molecules with antioxidant potential would be highly desirable for more efficient control of glycemic levels. Therefore, in order to investigate high added-value components possibly contained in TN by-products, we aimed to perform a qualitative and quantitative characterization of the TN polyphenolic profile by HPLC-HESI-MS/MS analysis. Additionally, the in vitro antioxidant and antidiabetic potential of a thinned nectarine extract (TNE) was evaluated.

2.2. Materials and methods

2.2.1. Chemicals and reagents

All chemicals, reagents, and standards used were either analytical or LC-MS grade reagents. The water was treated in a Milli-Q water purification system (Millipore, Bedford, MA, USA) before use. Gallic acid (purity $\geq 98\%$ HPLC), procyanidin B1 (purity $\geq 90\%$ HPLC), procyanidin B2 (purity $\geq 90\%$ HPLC), procyanidin B3 (purity $\geq 95\%$ HPLC), procyanidin C1 (purity $\geq 90\%$ HPLC), catechin (purity $\geq 98\%$ HPLC), chlorogenic acid (purity $\geq 95\%$ HPLC), neochlorogenic acid (purity $\geq 98\%$ HPLC), caffeic acid (purity $\geq 98\%$ HPLC), vanillic acid (purity $\geq 97\%$ HPLC), syringic acid (purity $\geq 98\%$ HPLC), *p*-coumaric acid (purity $\geq 98\%$ HPLC), epicatechin (purity $\geq 98\%$ HPLC), ferulic acid (purity $\geq 99\%$ HPLC), rutin (purity $\geq 94\%$ HPLC), naringenin (purity $\geq 95\%$ HPLC), quercetin 3-*O*-glucoside (purity $\geq 98\%$ HPLC), kaempferol 3-*O*-glucoside (purity $\geq 90\%$ HPLC), quercetin (purity $\geq 98\%$ HPLC) and reagents for in vitro studies were purchased from Sigma-Aldrich (Milan, Italy).

2.2.2. Sample collection and sample preparation for HPLC analyses

TN were collected in June 2019 at the orchards of “Giaccio Frutta” society (Vitulazio, Caserta, Italy, 41°10' N–14°13' E), at 20–25 days after full bloom, coinciding with the fruit thinning stage. The whole fruits were frozen at $-80\text{ }^{\circ}\text{C}$, freeze-dried, and ground to obtain a uniform powder that represented the production batch used for the analysis. For TN polyphenols extraction, 1 g of homogenized sample was suspended in 5 mL of 80% aqueous methanol containing 1% formic acid for 10 min, mixed on a vortex mixer for 1 min, sonicated (Branson Fisher Scientific 150E Sonic Dismembrator) for 10 min, and centrifuged for 10 min at $9000\times g$. The

supernatant was decanted, and the pellet was re-extracted with 5 mL of the previous solution. Finally, the combined supernatants were filtered with a 0.22 μm nylon filter (CellTreat, Shirley, MA, USA) and stored at $-20\text{ }^{\circ}\text{C}$ until analysis [86].

2.2.3. HPLC analyses of samples

2.2.3.1. Qualitative polyphenols analysis by HPLC-HESI-MS/MS

An HPLC DIONEX UltiMate 3000 (Thermo Fisher Scientific, San Jose, CA, USA) equipment, coupled with an autosampler, a binary solvent pump, and an LTQ XL mass spectrometer (Thermo Fisher Scientific, San Jose, CA, USA), was used for the analysis. The chromatographic analysis was performed according to Maisto et al., with slight modifications [87]. Elution was performed on a Kinetex[®] C18 column (250 mm \times 4.6 mm, 5 μm ; Phenomenex, Torrance, CA, USA). The mobile phases were water at 2% formic acid (A) and 0.5% formic acid in acetonitrile and water at 50:50 (v/v). After 2 min hold at 10% solvent B, elution was performed according to the following conditions: from 10% (B) to 55% (B) in 50 min and to 95% (B) in 10 min, followed by 10 min of maintenance; then the column was equilibrated to the initial conditions for the remaining 10 min to recondition the column. The separation conditions were as follows: column temperature was set at $30\text{ }^{\circ}\text{C}$, inject volume was 10 μL , and the flow rate was set at 1 mL/min. The source was a heated electrospray interface (HESI), operated in negative ionization with full scanning (FS) and data-dependent acquisition (DDA). Collision-induced fragmentation was made using argon, with a collision energy of 35.0 eV. The ion source was set using the following parameters: sheath gas flow rate: 30; auxiliary gas flow rate: 10; capillary temperature: $320\text{ }^{\circ}\text{C}$; source heated temperature: $150\text{ }^{\circ}\text{C}$; source voltage: 3 kV; source current: 3.20 μA ; capillary voltage: -20 V ; tube lens: -106.40 V .

2.2.3.2. Quantitative polyphenols analysis by HPLC-DAD-FLD

An HPLC Jasco Extrema LC-4000 system (Jasco Inc., Easton, MD, USA), coupled with an autosampler, a binary solvent pump, a diode-array detector (DAD), and a fluorescence detector (FLD). The chromatographic analysis was performed according to Maisto et al., as previously described [88]. Phenolic acids, hydroxycinnamic acids, flavanols, and flavanones were monitored at 280 nm, while flavonols were monitored at 360 nm. Procyanidins were monitored by a fluorescence detector that was performed with an excitation wavelength of 272 nm and an emission wavelength of 312 nm. Peak identifications were based on retention times and standard addition to the samples. Compounds were quantified according to a calibration curve made with six different concentrations over a concentration range of 0.1–1000 ppm and triplicate injections at each level.

2.2.4. HPLC-DAD-FLD method validation

Method validation was performed according to the ICH validation guideline (ICH.Q2[R1], 1995), which included the evaluation of a set of parameters, such as linearity range, the limit of detection (LOD), the limit of quantification (LOQ), precision and accuracy [89]. As regards polyphenolic quantification, the construction of a six-point calibration curve using diluted standard solutions was performed. Eight polyphenols (gallic acid, catechin, epicatechin, chlorogenic acid, procyanidins B1 and B2, quercetin, and rutin) were selected for method development and validation. To assess these parameters, calibration curves were prepared in triplicate. The LOD and LOQ were calculated using the following equations: $LOD = 3.3 S_a/b$ and $LOQ = 10 S_a/b$, where S_a is the standard deviation of the intercept of the regression line and b is the slope of the calibration curve. The precision of the method was evaluated through the percentage coefficient of variation (CV%), while method accuracy was

evaluated through bias. The intra-day precision and accuracy were assessed with three concentration levels in one day. The inter-day precision and accuracy were assessed with three concentration levels over three consecutive days.

2.2.5. Evaluation of Total Phenol Content (TPC)

The total phenol content (TPC) was determined through Folin–Ciocalteu’s method, using gallic acid as standard (Sigma-Aldrich, St. Louis, MO, USA). Briefly, 0.125 mL of sample (properly diluted with water to obtain an absorbance value within the linear range of the spectrophotometer) underwent an addition of: 0.5 mL of distilled water, 0.125 mL of Folin–Ciocalteu’s (Sigma-Aldrich, St. Louis, MO, USA) reagent and 1.25 mL of an aqueous solution of Na₂CO₃ 7.5% (w/v %), bringing the final volume to 3 mL with water. After mixing, the samples were kept in the dark for 90 min. After the reaction period, the absorbance was measured at 760 nm using a V-730 UV-visible/NIR spectrophotometer operated by Spectra Manager™ Suite (Jasco Inc., Easton, MD, USA). Each sample was analyzed in triplicate, and the concentration of total polyphenols was calculated in terms of gallic acid equivalents (GAE) [86].

2.2.6. Antioxidant activity

2.2.6.1. DPPH• radical scavenging assay

The antioxidant activity of TN was measured with respect to the radical scavenging ability of the antioxidants present in the sample using the stable radical 2,2-diphenyl-1-picrylhydrazyl (DPPH) (Sigma-Aldrich St. Louis, MO, USA). Briefly, 200 µL of the sample was added to 1000 µL of a methanol solution of DPPH (0.05 mM). The antioxidant effect was evaluated by following the decrease in UV

absorption at 517 nm with a UV-visible spectrophotometer (Jasco Inc., Easton, MD). The absorbance of DPPH radical without antioxidant compounds, i.e., the control, was measured as blank. All determinations were in triplicate. Inhibition was calculated according to the formula:

$$[(A_i - A_f)/A_c] \times 100, \quad (1)$$

where A_i is the absorbance of the sample at $t = 0$, A_f is the absorbance after 9 min, and A_c is the absorbance of the control at time zero. The 6-hydroxy-2,5,7,8-tetramethylchroman-2-carboxylic acid (Trolox) was used as a standard antioxidant, and the results were expressed in μmol Trolox Equivalent (TE). Furthermore, the results were also reported as EC_{50} , which is the amount of antioxidant necessary to decrease the initial DPPH \cdot concentration by 50% [90].

2.2.6.2. TEAC (Trolox Equivalent Antioxidant Capacity) assay

The method is based on the ability of antioxidant molecules to quench ABTS $^{+\cdot}$ radical (2,20-azinobis(3-ethylbenzotiazoline-6-sulfonate)), a blue-green chromophore with characteristic absorption at 734 nm. The assay was performed according to the method described by Babbar et al. (2011) [91], with slight modifications. ABTS solution was prepared by dissolving 2.5 mL of ABTS 7.0 mM solution and 44 μL of potassium persulfate 140 mM solution, which was left to react for at least 7 h, at 5 $^{\circ}\text{C}$ in the dark. Then, an ethanol–water mixture was added to the solution until an absorbance value of 0.700 (0.05) at 754 nm (Jasco Inc., Easton, MD, USA). The assay was performed by adding 1 mL of diluted ABTS working solution to 100 μL of the sample. The determination of sample absorbance was accomplished after 2.5 min of reaction. All determinations were in triplicate. Blank was performed with ethanol in each assay. Inhibition was calculated according to the formula:

$$[(A_i - A_f)/A_c] \times 100, \quad (2)$$

where A_i is the absorbance of the sample at $t = 0$, A_f is the absorbance after 6 min and A_c is the absorbance of the control at time zero. Trolox was used as a standard antioxidant. The results were expressed both as μmol of TE and EC_{50} , which is the amount of antioxidant necessary to decrease the initial ABTS^{++} concentration by 50% [90].

2.2.6.3. Ferric Reducing/Antioxidant Power (FRAP) Assay

When a Fe^{3+} -TPTZ complex is reduced to the Fe^{2+} form by an antioxidant under acidic conditions, an intense blue color with an absorption maximum develops at 593 nm [90]. Therefore, the antioxidant effect (reducing ability) of the TN sample was evaluated by monitoring the formation of a Fe^{2+} -TPTZ complex with a spectrophotometer (Beckman, Los Angeles, CA, USA). The assay was performed according to Benzie and Strain (1996) and Surveswaran et al. (2007) [92,93], with some modifications. The FRAP assay reagent was prepared by adding 10 vol of 0.3 M acetate buffer, pH 3.6 (3.1 g sodium acetate and 16 mL glacial acetic acid), 1 vol of 10 mM TPTZ prepared in 40 mM HCl and 1 vol of 20 mM FeCl_3 . All solutions were used on the day of preparation. The mixture was pre-warmed at 37 °C. This reagent (2.85 mL) was mixed with 0.15 mL diluted test samples similar to those used for the ABTS and DPPH assays. The mixture was shaken and incubated at 37 °C for 4 min, and the absorbance was read at 593 nm (Jasco Inc., Easton, MD, USA). The blank is represented by the only reagent solution. Blank absorbance must be subtracted from the absorbances of the samples. All determinations were in triplicate. A standard curve was made with Trolox, and the results were expressed as μmol TE.

2.2.7. Antidiabetic Activity

2.2.7.1. α -amylase inhibitory assay

The α -Amylase inhibitory assay was performed using a modified procedure by Schisano et al. (2019) [94]. A total of 40 μ L of TN extract at different concentrations was placed in a plastic tube, adding 160 μ L of distilled water and 200 μ L of α -amylase solution (4 U/mL). This solution was pre-incubated at 37 °C for 10 min. The starch solution (1% w/v) used as the substrate was prepared by boiling potato starch in 0.02 M sodium phosphate buffer (pH 6.9). An amount of 400 μ L of the above-mentioned starch solution was added to the reaction mixture, then further incubated at 37 °C for an additional 20 min. The reaction was terminated by adding 200 μ L of DNS solution (20 mL 96 mM 3,5-dinitrosalicylic acid, 12 g sodium potassium tartrate in 8 mL of 2 M NaOH, and 12 mL deionized water). The tubes were then incubated in boiling water for 5. After cooling the tube, the reaction mixture was diluted with distilled water (2 mL). Finally, the sample's absorbance was read at 540 (Jasco Inc., Easton, MD). A control and a blank were prepared using the same procedure, replacing extract and enzyme, respectively, with distilled water. Acarbose, a well-known antidiabetic medicine, was used as a positive control. Three sets of experiments were conducted for the test: standard, blank, and control. The α -amylase inhibitory activity was calculated as follows:

$$\text{Inhibition (\%)} = \{[(A_c - A_{cb}) - (A_s - A_{sb})]/(A_c - A_b)\} \times 100, \quad (3)$$

where A_{cb} is the absorbance of the control blank, A_c is the absorbance of the control, A_{sb} is the absorbance of the sample blank, and A_s is the absorbance of the sample. The results were reported as IC_{50} , which is the amount of sample necessary to decrease the initial α -amylase activity by 50%. IC_{50} values were determined by

plotting percent inhibition (Y-axis) versus \log_{10} extract concentration (X-axis) and calculated by logarithmic regression analysis from the mean inhibitory values [95].

2.2.7.2. Advanced Glycation End-Product (AGE) inhibition

The inhibition of AGE formation by TN extract and the standard phenolic rutin was measured through the method described by Justino et al. (2019) [96], with slight modifications. An amount of 500 μ L of progressive dilutions of the samples (0.075–70 mg/mL of final concentrations for TN and 0.05–2 mg/mL for rutin) was prepared in distilled water, then added to an assay mixture containing 500 μ L of bovine serum albumin (50 mg/L), 250 μ L fructose (1.25 mol/l) and 250 μ L of glucose (25 mol/l.). All the components of the reaction mixture were solubilized in phosphate buffer (200 mmol/l; pH 7.4), containing sodium azide (0.02% w/v). The solution was incubated at 37 °C for 7 days; thereafter, fluorescence was measured at an excitation wavelength of 355 nm and an emission of 460 nm (Perkin-Elmer LS 55, Massachusetts, USA). Distilled water was used as a negative control, while the blank was carried, substituting fructose and glucose with phosphate buffer. The inhibitory activity was calculated as a percentage of glycation inhibition (GI) by using the following formula:

$$GI (\%) = [(F_s - F_{sb}) / (F_c - F_{cb})] \times 100, \quad (4)$$

where F_s is fluorescence intensity in the presence of sample; F_{sb} is fluorescence intensity in the absence of fructose and glucose; F_c is fluorescence intensity in the absence of sample; and F_{cb} is fluorescence intensity in the absence of sample, fructose, and glucose. Finally, the results were reported as EC_{50} .

2.2.8. Statistics

Unless otherwise stated, all the experimental results were expressed as the mean \pm standard deviation (SD) of three determinations. Graphics and IC₅₀ values determination were performed using GraphPad Prism 8 software.

2.3. Results

2.3.1. Validation of HPLC-DAD-FLD method

Tables 4-6 show data relating to method validation of the HPLC-DAD-FLD analysis.

Table 4. Linearity range, limit of detection (LOD), and limit of quantification (LOQ) for polyphenols analysis.

Compound	Linearity range (ppm)	Calibration curve	LOD (ppm)	LOQ (ppm)
Gallic acid	0.1 – 1000	$y = 2E+07x - 28492$	6.240	18.908
Chlorogenic acid	0.1 – 1000	$y = 3E+07x - 30148$	7.102	21.522
Catechin	0.1 – 1000	$y = 9E+06x - 11907$	5.405	16.377
Epicatechin	0.1 – 1000	$y = 1E+07x - 4563.5$	4.849	14.695
Procyanidin B1	0.5 – 1000	$y = 3E+06x - 3730.6$	5.518	16.722
Procyanidin B2	0.5 – 1000	$y = 8E+06x - 8832.4$	5.200	15.758
Rutin	0.1 – 1000	$y = 2E+07x - 1076.9$	2.372	7.189
Quercetin	0.1 – 1000	$y = 5E+07x - 41742$	2.893	8.766

Table 5. Intra- and inter-day precision for polyphenols analysis.

Analyte	Concentration (ppm)	Precision	
		Intra-day (% <i>n</i> =3)	Inter-day (% <i>n</i> =3)
Gallic acid	0.1	2.620	3.172
	0.05	1.682	1.300
	0.01	0.896	0.547
Chlorogenic acid	0.1	0.657	1.491
	0.05	2.285	2.931
	0.01	2.952	4.876
Catechin	0.1	0.611	0.122
	0.05	1.463	1.867
	0.01	8.860	7.974
Epicatechin	0.1	2.350	2.296
	0.05	7.913	1.800
	0.01	7.613	7.319
Procyanidin B1	0.1	1.539	8.147
	0.05	0.995	1.105
	0.01	2.202	2.312
Procyanidin B2	0.10	0.819	2.663
	0.05	1.328	1.949
	0.01	1.258	3.536
Rutin	0.1	1.354	1.378
	0.05	0.126	2.913
	0.01	1.922	2.920
Quercetin	0.1	0.360	4.637
	0.05	1.375	6.975
	0.01	2.276	4.260

Table 6. Intra- and inter-day accuracy for polyphenols analysis.

Analyte	Concentration (ppm)	Accuracy	
		Intra-day (% <i>n</i> =3)	Inter-day (% <i>n</i> =3)
Gallic acid	0.1	3.508	3.926
	0.05	1.272	1.506
	0.01	0.368	0.394

Chlorogenic acid	0.1	-2.960	-2.980
	0.05	-1.483	-1.574
	0.01	-0.184	-0.196
Catechin	0.1	1.312	1.284
	0.05	0.076	-0.080
	0.01	-0.564	-0.509
Epicatechin	0.1	0.894	0.882
	0.05	0.620	1.250
	0.01	-0.011	0.144
Procyanidin B1	0.1	-0,507	-1,075
	0.05	-0,488	-0,486
	0.01	-0,189	-0,192
Procyanidin B2	0.1	-0.612	0.814
	0.05	-0.390	0.007
	0.01	-0.122	0.008
Rutin	0.1	0.601	0.643
	0.05	0.100	0.001
	0.01	0.034	0.020
Quercetin	0.1	-2.765	-2.788
	0.05	-1.561	-1.709
	0.01	-0.261	-0.265

2.3.2. Qualitative polyphenols characterization by HPLC-HESI-MS/MS analysis

TN polyphenolic extract was characterized by HPLC-HESI-MS/MS. Based on a comparison with the literature data, 48 compounds were putatively identified. A total of 27 phenolic acids, 10 flavans, and 11 flavonols are displayed in Table 7. The identity of 19 compounds (3, 6-9, 13, 14, 16, 20, 24, 28, 29, 32, 34, 36, 37, 38, 43, 45) was verified by comparison with analytical standards.

Table 7. Polyphenolic composition of thinned nectarines determined by HPLC-HESI-MS/MS analysis.

Compound	<i>m/z</i>	Diagnostic Fragmentation	Reference
Hydroxycaffeic acid	195.01	177.12 [M-H-H ₂ O] ⁻ – 167.08 [M-H-CO] ⁻ – 151.00 [M-H-CO ₂] ⁻ – 133.10 [M-H-CO ₂ -H ₂ O] ⁻	[97]
Dihydroxybenzoic acid	152.97	134.93 [M-H-H ₂ O] ⁻ – 124.97 [M-H-CO] ⁻ – 108.95 [M-H-CO ₂] ⁻ – 96.99 [M-H-2CO] ⁻	[97]
Gallic acid	169.07	151.20 [M-H-H ₂ O] ⁻ – 140.93 [M-H-CO] ⁻ – 124.85 [M-H-CO ₂] ⁻	[98]
Homovanillic acid <i>O</i> -hexoside	343.01	325.13 [M-H-H ₂ O] ⁻ – 298.99 [M-H-CO ₂] ⁻ – 297.06 [M-H-CO-H ₂ O] ⁻ – 181.21 [M-H-Hex] ⁻	[99]
Quinic acid	190.97	172.95 [M-H-H ₂ O] ⁻ – 154.94 [M-H-2H ₂ O] ⁻ – 146.82 [M-H-CO ₂] ⁻ – 110.83 [M-H-CO ₂ -2H ₂ O] ⁻	[100]
Neochlorogenic acid	353.30	334.89 [M-H-H ₂ O] ⁻ – 191.02 [QA-H] ⁻ – 178.98 [CA-H] ⁻ – 134.85 [CA-H-CO ₂] ⁻	[101]
Procyanidin B1	577.14	451.23 [M-H-C ₆ H ₆ O ₃] ⁻ – 425.17 [M-H-C ₈ H ₈ O ₃] ⁻ – 288.98 [M-H-C ₁₅ H ₁₂ O ₆] ⁻ – 287.07 [M-H-C ₁₅ H ₁₄ O ₆] ⁻	[102,103]
Procyanidin B3	577.45	451.19 [M-H-C ₆ H ₆ O ₃] ⁻ – 425.25 [M-H-C ₈ H ₈ O ₃] ⁻ – 289.04 [M-H-C ₁₅ H ₁₂ O ₆] ⁻ – 287.09 [M-H-C ₁₅ H ₁₄ O ₆] ⁻	[102,103]
Catechin	289.12	271.03 [M-H-H ₂ O] ⁻ – 245.02 [M-H-C ₂ H ₄ O] ⁻ – 205.00 [M-H-C ₄ H ₄ O ₂] ⁻ – 137.00 [M-H-C ₈ H ₈ O ₃] ⁻	[102,104]
Coumaric acid <i>O</i> -hexoside	325.15	307.26 [M-H-H ₂ O] ⁻ – 289.03 [M-H-2H ₂ O] ⁻ – 162.98 [M-H-Hex] ⁻ – 118.97 [M-H-Hex-CO ₂] ⁻	[105]
3- <i>O</i> -Coumaroylquinic acid	337.25	301.77 [M-H-2H ₂ O] ⁻ – 191.02 [QA-H] ⁻ – 173.02 [QA-H-H ₂ O] ⁻ – 162.92 [M-H-QA] ⁻	[106]

Procyanidin C-type	865.25	739.34 [M-H-C ₆ H ₆ O ₃] ⁻ – 713.20 [M-H-C ₈ H ₈ O ₃] ⁻ – 695.19 [M-H-C ₈ H ₈ O ₃ -H ₂ O] ⁻ – 286.94 [M-H-C ₃₀ H ₂₆ O ₁₂] ⁻	[103]
Chlorogenic acid	353.15	335.24 [M-H-H ₂ O] ⁻ – 190.97 [QA-H] ⁻ – 179.07 [CA-H] ⁻ – 134.98 [CA-H-CO ₂] ⁻	[101]
Caffeic acid	178.92	160.96 [M-H-H ₂ O] ⁻ – 150.80 [M-H-CO] ⁻ – 134.95 [M-H-CO ₂] ⁻ – 106.86 [M-H-CO-CO ₂] ⁻	[107]
3- <i>O</i> -Feruloylquinic acid	367.18	193.04 [M-H-QA] ⁻ – 191.13 [QA-H] ⁻ – 173.02 [QA-H-H ₂ O] ⁻ – 134.02 [M-H-QA-CH ₃ -CO ₂] ⁻	[108]
Vanillic acid	167.14	151.90 [M-H-CH ₃] ⁻ – 132.92 [M-H-CH ₃ -H ₂ O] ⁻ – 122.96 [M-H-CO ₂] ⁻ – 107.90 [M-H-CH ₃ -CO ₂] ⁻	[109]
Methyl 3- <i>O</i> -Caffeoylquinic acid	367.25	335.09 [M-H-2H ₂ O] ⁻ – 191.10 [QA-H] ⁻ – 161.00 [M-H-QA-CH ₃ -H ₂ O] ⁻ – 134.97 [M-H-QA-CH ₃ -CO ₂] ⁻	[110]
4- <i>O</i> -Coumaroylquinic acid	337.12	191.13 [QA-H] ⁻ – 172.86 [QA-H-H ₂ O] ⁻ – 162.98 [M-H-QA] ⁻ – 111.03 [QA-H-2H ₂ O] ⁻	[106]
<i>Trans</i> -5- <i>O</i> -Coumaroylquinic acid	337.20	190.96 [QA-H] ⁻ – 173.02 [QA-H-H ₂ O] ⁻ – 162.94 [M-H-QA] ⁻ – 111.05 [QA-H-2H ₂ O] ⁻	[106,111]
Syringic acid	196.99	179.05 [M-H-H ₂ O] ⁻ – 168.97 [M-H-CO] ⁻ – 160.82 [M-H-2H ₂ O] ⁻ – 152.99 [M-H-CO ₂] ⁻	[112]
<i>Cis</i> -5- <i>O</i> -Coumaroylquinic acid	337.13	190.98 [QA-H] ⁻ – 172.84 [QA-H-H ₂ O] ⁻ – 163.05 [M-H-QA] ⁻ – 145.02 [M-H-QA-H ₂ O] ⁻	[106,111]
Methyl 4- <i>O</i> -Caffeoylquinic acid	367.18	296.85 [M-H-C ₃ H ₂ O ₂] ⁻ – 191.13 [QA-H] ⁻ – 160.98 [M-H-QA-CH ₃ -H ₂ O] ⁻ – 134.92 [M-H-QA-CH ₃ -CO ₂] ⁻	[110]
Caffeoylshikimic acid isomer 1	335.18	317.03 [M-H-H ₂ O] ⁻ – 179.01 [M-H-SA] ⁻ – 161.04 [M-H-SA-H ₂ O] ⁻ – 134.93 [M-H-SA-CO ₂] ⁻	[113]
Procyanidin B2	577.25	451.13 [M-H-C ₆ H ₆ O ₃] ⁻ – 425.07 [M-H-C ₈ H ₈ O ₃] ⁻ – 289.10 [M-H-C ₁₅ H ₁₂ O ₆] ⁻ – 287.14 [M-H-C ₁₅ H ₁₄ O ₆] ⁻	[102,103]

Caffeoylshikimic acid isomer 2	335.12	317.32 [M-H-H ₂ O] ⁻ – 178.99 [M-H-SA] ⁻ – 160.90 [M-H-SA-H ₂ O] ⁻ – 134.98 [M-H-SA-CO ₂] ⁻	[113]
Caffeoylshikimic acid isomer 3	335.17	317.09 [M-H-H ₂ O] ⁻ – 179.04 [M-H-SA] ⁻ – 161.01 [M-H-SA-H ₂ O] ⁻ – 134.88 [M-H-SA-CO ₂] ⁻	[113]
5- <i>O</i> -Feruloylquinic acid	367.19	349.23 [M-H-H ₂ O] ⁻ – 190.95 [QA-H] ⁻ – 172.97 [QA-H-H ₂ O] ⁻ – 134.09 [M-H-QA-CH ₃ -CO ₂] ⁻	[108]
Epicatechin	288.92	271.06 [M-H-H ₂ O] ⁻ – 245.06 [M-H-C ₂ H ₄ O] ⁻ – 205.06 [M-H-C ₄ H ₄ O ₂] ⁻ – 136.94 [M-H-C ₈ H ₈ O ₃] ⁻	[102,104]
<i>p</i> -Coumaric acid	162.88	144.92 [M-H-H ₂ O] ⁻ – 134.83 [M-H-CO] ⁻ – 118.97 [M-H-CO ₂] ⁻ – 93.08 [M-H-CO ₂ -C ₂ H ₂] ⁻	[107]
Procyanidin C-type linkage	865.45	739.33 [M-H-C ₆ H ₆ O ₃] ⁻ – 713.18 [M-H-C ₈ H ₈ O ₃] ⁻ – 695.28 [M-H-C ₈ H ₈ O ₃ -H ₂ O] ⁻ – 287.11 [M-H-C ₃₀ H ₂₆ O ₁₂] ⁻	[103]
Methyl 5- <i>O</i> -Caffeoylquinic acid	367.19	191.02 [QA-H] ⁻ – 179.00 [M-H-QA-CH ₃] ⁻ – 161.02 [M-H-QA-CH ₃ -H ₂ O] ⁻ – 135.00 [M-H-QA-CH ₃ -CO ₂] ⁻	[110]
Procyanidin C1	865.32	739.19 [M-H-C ₆ H ₆ O ₃] ⁻ – 713.19 [M-H-C ₈ H ₈ O ₃] ⁻ – 695.25 [M-H-C ₈ H ₈ O ₃ -H ₂ O] ⁻ – 287.04 [M-H-C ₃₀ H ₂₆ O ₁₂] ⁻	[103]
Procyanidin C-type linkage	865.22	739.19 [M-H-C ₆ H ₆ O ₃] ⁻ – 713.26 [M-H-C ₈ H ₈ O ₃] ⁻ – 695.32 [M-H-C ₈ H ₈ O ₃ -H ₂ O] ⁻ – 287.11 [M-H-C ₃₀ H ₂₆ O ₁₂] ⁻	[103]
Ferulic acid	193.16	177.95 [M-H-CH ₃] ⁻ – 160.02 [M-H-CH ₃ -H ₂ O] ⁻ – 148.94 [M-H-CO ₂] ⁻ – 133.94 [M-H-CH ₃ -CO ₂] ⁻	[107]
Eriodyctiol <i>O</i> -hexoside	449.20	431.11 [M-H-H ₂ O] ⁻ – 287.07 [M-H-Hex] ⁻ – 150.72 [M-H-Hex-C ₈ H ₈ O ₂] ⁻ – 135.09 [M-H-Hex-C ₇ H ₄ O ₄] ⁻	[114]
Rutin	609.34	591.40 [M-H-H ₂ O] ⁻ – 463.22 [M-H-Rha] ⁻ – 301.16 [M-H-Glu-Rha] ⁻ – 179.06 [M-H-Glu-Rha-C ₇ H ₆ O ₂] ⁻	[115,116]
Naringenin	271.04	253.07 [M-H-H ₂ O] ⁻ – 226.99 [M-H-CO ₂] ⁻ – 150.92 [M-H-C ₈ H ₈ O] ⁻ – 106.92 [M-H-C ₈ H ₈ O-CO ₂] ⁻	[117]

Quercetin-3- <i>O</i> -glucoside	463.18	445.14 [M-H-H ₂ O] ⁻ – 343.04 [M-H-C ₄ H ₈ O ₄] ⁻ – 301.03 [M-H-Glu] ⁻ – 179.09 [M-H-Hex-C ₇ H ₆ O ₂] ⁻	[116]
Quercetin- <i>O</i> -glucoside isomer	463.22	445.17 [M-H-H ₂ O] ⁻ – 343.17 [M-H-C ₄ H ₈ O ₄] ⁻ – 301.10 [M-H-Hex] ⁻ – 178.97 [M-H-Hex-C ₇ H ₆ O ₂] ⁻	[116]
Kaempferol- <i>O</i> -rutinoside isomer 1	593.32	447.21 [M-H-Pent] ⁻ – 327.18 [M-H-Pent-C ₄ H ₈ O ₄] ⁻ – 285.10 [M-H-Hex-Pent] ⁻ – 257.14 [M-H-Hex-Pent-CO] ⁻	[118]
Naringenin <i>O</i> -hexoside	433.23	415.26 [M-H-H ₂ O] ⁻ – 313.23 [M-H-C ₄ H ₈ O ₄] ⁻ – 271.11 [M-H-Hex] ⁻ – 253.07 [M-H-Hex-H ₂ O] ⁻	[119]
Dicaffeoylquinic acid isomer 1	515.07	353.17 [M-H-CA] ⁻ – 334.98 [M-H-CA-H ₂ O] ⁻ – 317.22 [M-H-CA-2H ₂ O] ⁻ – 178.91 [M-H-CA-QA] ⁻	[120]
Kaempferol-3- <i>O</i> -glucoside	447.14	428.99 [M-H-H ₂ O] ⁻ – 327.07 [M-H-C ₄ H ₈ O ₄] ⁻ – 285.07 [M-H-Glu] ⁻ – 255.01 [M-H-Glu-CH ₂ O] ⁻	[118]
Procyanidin dimer A-type linkage	575.19	557.19 [M-H-H ₂ O] ⁻ – 449.13 [M-H-C ₆ H ₆ O ₃] ⁻ – 431.13 [M-H-C ₆ H ₆ O ₃ -H ₂ O] ⁻ – 285.11 [M-H-C ₁₅ H ₁₄ O ₆] ⁻	[102,103]
Quercetin	301.18	273.17 [M-H-CO] ⁻ – 257.07 [M-H-CO ₂] ⁻ – 179.11 [M-H-C ₇ H ₆ O ₂] ⁻ – 150.88 [M-H-C ₈ H ₆ O ₃] ⁻	[121]
Dicaffeoylquinic acid isomer 2	515.18	353.04 [M-H-CA] ⁻ – 334.98 [M-H-CA-H ₂ O] ⁻ – 317.09 [M-H-CA-2H ₂ O] ⁻ – 178.84 [M-H-CA-QA] ⁻	[120]
Kaempferol- <i>O</i> -rutinoside isomer 2	593.34	447.15 [M-H-Pent] ⁻ – 327.12 [M-H-Pent-C ₄ H ₈ O ₄] ⁻ – 284.95 [M-H-Hex-Pent] ⁻ – 257.15 [M-H-Hex-Pent-CO] ⁻	[118]
Kaempferol- <i>O</i> -rutinoside isomer 3	593.38	447.13 [M-H-Pent] ⁻ – 327.09 [M-H-Pent-C ₄ H ₈ O ₄] ⁻ – 285.11 [M-H-Hex-Pent] ⁻ – 256.83 [M-H-Hex-Pent-CO] ⁻	[118]

2.3.3. Phenolic acid identification

Phenolic acids represent the most common class of polyphenols. They exhibit a generic fragmentation pattern, with a prominent fragment ion produced by the neutral loss of CO₂, due to the cleavage of the carboxylic acid group. The neutral losses of H₂O and CO, typical of the phenolic group cleavage, and the loss of sugar or organic acid for phenolic acid derivatives generate other diagnostic ions. Compound **1** showed a [M-H]⁻ ion at *m/z* 195 and a tandem mass spectrum characterized by a base peak ion at *m/z* 167 [M-H-CO]⁻ and other fragment ions at *m/z* 177 [M-H-H₂O]⁻, *m/z* 151 [M-H-CO₂]⁻ and *m/z* 133 [M-H-CO₂-H₂O]⁻. Based on this fragmentation pattern, compound **1** was putatively identified as hydroxycaffeic acid [97]. Compound **2** displayed a [M-H]⁻ ion at *m/z* 153 and a base peak ion at *m/z* 125, corresponding to the loss of CO. The minor fragment ions at *m/z* 135 [M-H-H₂O]⁻, *m/z* 109 [M-H-CO₂]⁻ and *m/z* 97 [M-H-2CO]⁻ suggested the presence of a carboxylic acid group and two phenolic groups. Therefore, compound **2** was tentatively identified as dihydroxybenzoic acid [97]. Compound **3** showed a [M-H]⁻ ion at *m/z* 169 and two fragment ions at *m/z* 141 [M-H-CO]⁻ and *m/z* 125 [M-H-CO₂]⁻. According to the literature data, this compound was identified as gallic acid [98]. Compound **4** produced a [M-H]⁻ ion at *m/z* 343 and a base peak ion at *m/z* 297, corresponding to the loss of water and CO. The minor product ions at *m/z* 299 [M-H-CO₂]⁻ and *m/z* 181 [M-H-Hex]⁻ revealed the occurrence of free carboxylic acid and a hexoside group, respectively. Consequently, compound **4** was putatively recognized as homovanillic acid *O*-hexoside [99]. Compound **5** displayed a [M-H]⁻ ion at *m/z* 191 and a base peak ion at *m/z* 147 [M-H-CO₂]⁻. The base peak ion and the fragment ions at *m/z* 173 [M-H-H₂O]⁻, *m/z* 155 [M-H-2H₂O]⁻ and *m/z* 111 [M-H-CO₂-2H₂O]⁻ highlighted the presence of free carboxylic acid and an alcoholic group. The absence of a prominent ion caused by CO loss, typical of the phenolic moiety, allowed distinguishing the alcoholic aliphatic group from the phenolic scaffold.

Based on the literature data, compound **5** was tentatively identified as quinic acid [122]. The presence of two caffeoylquinic acids (compounds **6** and **13**) was confirmed by the $[M-H]^-$ ion at m/z 353 and two fragment ions at m/z 191 and m/z 179, corresponding to quinic acid and caffeic acid ions, respectively. The identification of these compounds was supported by comparison with the authentic standards. In this way, compounds **6** and **13** were identified as neochlorogenic acid and chlorogenic acid, respectively [101]. Compound **10** showed a $[M-H]^-$ ion at m/z 325 and a base peak ion at m/z 289 $[M-H-2H_2O]^-$ due to the loss of two molecules of water. Other fragments at m/z 307 $[M-H-H_2O]^-$, m/z 163 $[M-H-Hex]^-$ and m/z 119 $[M-H-Hex-CO_2]^-$ suggested the presence of a carboxylic acid and a hexoside group. The fragment ion at m/z 163 matched to coumaric acid ion. According to this fragmentation pattern and the literature data, compound **10** was putatively identified as coumaric acid *O*-hexoside [105]. Four coumaroylquinic acid isomers (compounds **11**, **18**, **19**, and **21**) were tentatively detected. Their tandem mass spectra displayed a $[M-H]^-$ ion at m/z 337 and characteristic fragment ions at m/z 191 $[QA-H]^-$, m/z 173 $[QA-H-H_2O]^-$ and m/z 163 $[M-H-QA]^-$. Based on the literature data, the type of base peak ion allowed us to distinguish the connectivity between coumaric acid and quinic acid groups. The 3-*O*-coumaroylquinic acid can be identified by a base peak ion at m/z 163 $[M-H-QA]^-$, while 4-*O*-coumaroylquinic acid produced an intense fragment at m/z 173 $[QA-H-H_2O]^-$. Therefore, compounds **11** and **18** were putatively identified as 3-*O*-coumaroylquinic acid and 4-*O*-coumaroylquinic acid, respectively [106]. Fragmentation of 5-*O*-coumaroylquinic acid produced a base peak ion at m/z 191 $[QA-H]^-$. The determination of each geometric isomer of the 5-*O*-coumaroylquinic acid was performed considering the chromatographic elution time in reverse-phase chromatography. In particular, 5-*O*-coumaroylquinic acid *trans* isomer eluted before its *cis*-isomer. Therefore, compounds **19** and **21** were tentatively identified as *trans*-5-*O*-coumaroylquinic acid and *cis*-5-*O*-coumaroylquinic acid, respectively [106,111]. Compound **14** showed a $[M-H]^-$ ion at m/z 179 and was identified as

caffeic acid. According to the literature data, the base peak ion at m/z 135 $[\text{M-H-CO}_2]^-$ and the fragment ions at m/z 161 $[\text{M-H-H}_2\text{O}]^-$ and m/z 151 $[\text{M-H-CO}]^-$ highlighted the presence of a carboxylic acid and a phenolic group [107]. Two feruloylquinic acid isomers (compounds **15** and **27**) were putatively identified. They displayed a $[\text{M-H}]^-$ ion at m/z 367 and characteristic product ions at m/z 193 and m/z 191, which represented the fragment ions of ferulic acid and quinic acid, respectively. Compound **15** exhibited a base peak ion at m/z 193 and was tentatively annotated as 3-*O*-feruloylquinic acid. Instead, compound **27** showed a base peak ion at m/z 191 and was putatively identified as 5-*O*-feruloylquinic acid [108]. Compound **16** displayed a $[\text{M-H}]^-$ ion at m/z 167. The base peak ion at m/z 123 $[\text{M-H-CO}_2]^-$ and the product ions of its tandem mass spectrum at m/z 152 $[\text{M-H-CH}_3]^-$, m/z 133 $[\text{M-H-CH}_3\text{-H}_2\text{O}]^-$ and m/z 108 $[\text{M-H-CH}_3\text{-CO}_2]^-$ suggested the presence of a carboxylic acid and a methyl group. According to the mass fragmentation pattern, compound **16** was identified as vanillic acid [109]. Three methyl-caffeoylquinic acid isomers (compounds **17**, **22**, and **31**) were putatively detected. They showed a $[\text{M-H}]^-$ ion at m/z 367 and two characteristic fragment ions at m/z 179 $[\text{M-H-QA-CH}_3]^-$ and m/z 161 $[\text{M-H-QA-CH}_3\text{-H}_2\text{O}]^-$. Other representative fragments include the ions at m/z 191 $[\text{QA-H}]^-$ and at m/z 135 $[\text{M-H-QA-CH}_3\text{-CO}_2]^-$. This fragmentation pattern confirmed the presence of the quinic acid and the methyl ester scaffolds. Therefore, methyl-3-*O*-caffeoylquinic acid (**17**) and methyl-4-*O*-caffeoylquinic acid (**22**) can be annotated by the base peak ion at m/z 161 while methyl-5-*O*-caffeoylquinic acid (**31**) is characterized by an intense fragment ion at m/z 179 [110]. Compound **20** showed a $[\text{M-H}]^-$ ion at m/z 197. The base peak ion at m/z 153 $[\text{M-H-CO}_2]^-$ and the fragment ions of their tandem mass spectra at m/z 179 $[\text{M-H-H}_2\text{O}]^-$, m/z 169 $[\text{M-H-CO}]^-$ and m/z 161 $[\text{M-H-2H}_2\text{O}]^-$ suggested the presence of a carboxylic acid and a phenolic group. In agreement with the literature data, compound **20** was identified as syringic acid [112]. Three caffeic acid derivatives (compounds **23**, **25**, and **26**) were detected. They presented a $[\text{M-H}]^-$ ion at m/z 335 and a base peak ion at m/z 161 $[\text{M-H-SA-}$

$\text{H}_2\text{O}]^-$, due to the loss of water and shikimic acid moiety. The fragment ions at m/z 179 $[\text{M}-\text{H}-\text{SA}]^-$ and m/z 135 $[\text{M}-\text{H}-\text{SA}-\text{CO}_2]^-$ were detected in the fragmentation pattern of caffeic acid (**14**). Therefore, these compounds were tentatively identified as three caffeoylshikimic acid isomers [113]. Compound **29** showed a $[\text{M}-\text{H}]^-$ ion at m/z 163 and a base peak ion at m/z 119 $[\text{M}-\text{H}-\text{CO}_2]^-$. The fragment ions at m/z 145 $[\text{M}-\text{H}-\text{H}_2\text{O}]^-$, m/z 135 $[\text{M}-\text{H}-\text{CO}]^-$ and m/z 93 $[\text{M}-\text{H}-\text{CO}_2-\text{C}_2\text{H}_2]^-$ suggested the presence of a phenolic group and the hydroxycinnamic acid moiety. According to the mass fragmentation pattern, compound **29** was annotated as p-coumaric acid [107]. Compound **34** displayed a $[\text{M}-\text{H}]^-$ ion at m/z 193 and a base peak ion at m/z 149 $[\text{M}-\text{H}-\text{CO}_2]^-$. The base peak ion and the fragment ions at m/z 178 $[\text{M}-\text{H}-\text{CH}_3]^-$, m/z 160 $[\text{M}-\text{H}-\text{CH}_3-\text{H}_2\text{O}]^-$ and m/z 134 $[\text{M}-\text{H}-\text{CH}_3-\text{CO}_2]^-$ indicated the presence of a free carboxylic acid and a methyl group. Based on the literature data, compound **34** was identified as ferulic acid [107]. Two dicaffeoylquinic acid isomers (compounds **42** and **46**) were putatively identified and gave a $[\text{M}-\text{H}]^-$ ion at m/z 515. The base peak ion at m/z 353 $[\text{M}-\text{H}-\text{CA}]^-$, due to the loss of caffeic acid unit, and the fragment ions at m/z 335 $[\text{M}-\text{H}-\text{CA}-\text{H}_2\text{O}]^-$ and m/z 179 $[\text{M}-\text{H}-\text{CA}-\text{QA}]^-$ indicated the presence of two units of caffeic acid and one unit of quinic acid. Furthermore, the fragmentations of the two compounds followed the fragmentation pattern of chlorogenic acid and neochlorogenic acid (compounds **6** and **13**) and were in agreement with the literature data [120].

2.3.3.1. Flavans identification

Flavans are a class of 2-phenylchroman compounds largely distributed in plants. The main flavan class is represented by the flavan-3-ols, which include monomeric derivatives, such as (+)-catechin and (-)-epicatechin, and oligomeric and polymeric compounds named procyanidins. Procyanidins can be divided into A-type or B-type based on the linkage between monomers. While B-type linkage procyanidins dimers

show an interflavan single carbon–carbon bond between monomers, A-type linkage ones are characterized by two linkages between flavan units, an interflavan single carbon–carbon bond and an ether bond [123]. The ether linkage connects the monomers by a six-membered ring, resulting in a difference of 2 Da units. Procyanidins give a characteristic fragmentation pattern, which includes three types of fragmentation mechanisms: the heterocyclic ring fission (HRF), the retro Diels–Alder fission (RDA), and the quinone methide cleavage (QM). The heterocyclic ring fission (HRF) is given by the loss of a phloroglucinol unit (–126 Da), preserving the interflavanic bond between the two monomers. The quinone methide cleavage (QM) represents the fragmentation of the interflavanic bond between two monomers. Therefore, the resulting ions indicate the number of monomers in the oligomeric compounds [103]. Retro Diels–Alder fission (RDA) is given by the elimination of hydroxyvinyl benzenediol unit (–152 Da). Three procyanidins dimer B-type linkage (compounds **7**, **8**, and **24**) were detected. They showed a $[M-H]^-$ ion at m/z 577 and a base peak ion at m/z 425 $[M-H-C_8H_8O_3]^-$ due to the RDA fission. HRF fragmentation gave a fragment ion at m/z 451 $[M-H-C_6H_6O_3]^-$ while the QM cleavage produced two fragments at m/z 289 $[M-H-C_{15}H_{12}O_6]^-$ and m/z 287 $[M-H-C_{15}H_{14}O_6]^-$ [102,103]. Catechin (**9**) and epicatechin (**28**) were identified and gave a $[M-H]^-$ ion at m/z 289. The base peak ion at m/z 245 $[M-H-2H_4O]^-$ and the fragment ions at m/z 271 $[M-H-H_2O]^-$, m/z 205 $[M-H-C_4H_4O_2]^-$ and m/z 137 $[M-H-C_8H_8O_3]^-$, due to the RDA fission, agreed with the literature data [102,104]. Four procyanidins trimer B-type linkage (compounds **12**, **30**, **32**, and **33**) were putatively detected. They displayed a $[M-H]^-$ ion at m/z 865 and a base peak ion at m/z 695 $[M-H-C_8H_8O_3-H_2O]^-$, which is the product of RDA fission and the loss of a molecule of water. Other fragment ions were at m/z 739 $[M-H-C_6H_6O_3]^-$, m/z 713 $[M-H-C_8H_8O_3]^-$ and m/z 287 $[M-H-C_{30}H_{26}O_{12}]^-$, which derived from the HRF fragmentation, the RDA fission and the QM cleavage, respectively [103]. One procyanidin dimer A-type linkage (**44**) was tentatively detected and gave a $[M-H]^-$ ion at m/z 575. The base peak ion at m/z

449 [M-H-C₆H₆O₃]⁻, derived from the HRF cleavage, and the product ions at *m/z* 557 [M-H-H₂O]⁻, *m/z* 431 [M-H-C₆H₆O₃-H₂O]⁻ and *m/z* 285 [M-H-C₁₅H₁₄O₆]⁻, due to the QM cleavage, are in accordance with the fragmentation reported in the literature [102,103]. Flavanones show a different fragmentation pattern than flavan-3-ols. In fact, these compounds occur in plants as aglycone or glycosides and exhibit a characteristic fragmentation pattern, with prominent fragment ions due to the loss of sugars and retro Diels–Alder fission (RDA) [117]. Eriodyctiol *O*-hexoside (**35**) showed a [M-H]⁻ ion at *m/z* 449 and a base peak ion at *m/z* 287 [M-H-Hex]⁻ due to the loss of the hexoside unit. Secondary fragments included the *m/z* 431 [M-H-H₂O]⁻, *m/z* 151 [M-H-Hex-C₈H₈O₂]⁻, which derived from the RDA fragmentation, and *m/z* 135 [M-H-Hex-C₇H₄O₄] [114]. Compound **37** exhibited a [M-H]⁻ ion at *m/z* 271. The base peak ion at *m/z* 151 [M-H-C₈H₈O]⁻, due to the RDA pattern, and the fragment ions at *m/z* 253 [M-H-H₂O]⁻, *m/z* 227 [M-H-CO₂]⁻ and *m/z* 107 [M-H-C₈H₈O-CO₂]⁻ allowed to identify the flavanone scaffold. Based on the literature data, compound **37** was identified as naringenin [117]. Compound **41** showed a [M-H]⁻ ion at *m/z* 433, a base peak ion at *m/z* 271 [M-H-Hex]⁻ and was putatively identified as naringenin *O*-hexoside. The compound exhibited other fragment ions at *m/z* 415 [M-H-H₂O]⁻, *m/z* 313 [M-H-C₄H₈O₄]⁻, and *m/z* 253 [M-H-Hex-H₂O]⁻ [119].

2.3.3.2. Flavonols Identification

Flavanols are a class of 3-hydroxy-2-phenylchromen-4-one polyphenols and exhibit a flavanone-like fragmentation pattern. The aglycon ion represents the main fragment peak due to the cleavage of sugars, but other fragments include the neutral losses of H₂O, CO, and CO₂ and retro Diels–Alder fission (RDA). A typical fragment ion is represented by the *m/z* 179 due to the RDA fragmentation [116]. However, the glycosylated flavonols displayed two prominent fragment ions due to the loss of glucidic units and the cross-ring cleavage of the sugar moiety with a neutral loss of

$C_4H_8O_4$ (120 Da). Rutin (**36**) showed a $[M-H]^-$ ion at m/z 609 and a base peak ion at m/z 301 $[M-H-Glu-Rha]^-$ that derived from the loss of the disaccharide unit. Other fragments are the m/z 591 $[M-H-H_2O]^-$, m/z 463 $[M-H-Rha]^-$, and m/z 179 $[M-H-Glu-Rha-C_7H_6O_2]^-$, due to the RDA fragmentation. The fragments at 463 (-146 Da) and 301 (-308 Da) allowed identifying the sugars of the disaccharide moiety as glucose and rhamnose [115,116]. Two quercetin *O*-hexoside isomers (compounds **38** and **39**) were putatively detected. They displayed a $[M-H]^-$ ion at m/z 463 and a base peak ion at m/z 301 $[M-H-Hex]^-$ due to the loss of hexoside moiety. The main fragments exhibit molecular ions at m/z 445 $[M-H-H_2O]^-$, m/z 343 $[M-H-C_4H_8O_4]^-$ and m/z 179 $[M-H-Hex-C_7H_6O_2]^-$ that derived from the RDA fragmentation [116]. Three kaempferol derivative isomers (**40**, **47**, and **48**) were tentatively identified and gave a $[M-H]^-$ ion at m/z 593. The base peak ion at m/z 285 $[M-H-Hex-Pent]^-$ and the fragment ions at m/z 447 $[M-H-Pent]^-$, m/z 327 $[M-H-Pent-C_4H_8O_4]^-$ and m/z 257 $[M-H-Hex-Pent-CO]^-$ indicate the presence of the disaccharide rutinose and the aglycone kaempferol. Based on the literature data, these compounds were identified as kaempferol *O*-rutinoside isomers [118]. Kaempferol 3-*O*-glucoside (**43**) showed a $[M-H]^-$ ion at m/z 447 and a base peak ion at m/z 285 $[M-H-Glu]^-$ for the loss of the glucoside unit. The fragment ions at m/z 429 $[M-H]^-$, m/z 327 $[M-H-C_4H_8O_4]^-$ and m/z 255 $[M-H-Glu-CH_2O]^-$ confirmed the identity of the compound and are in accordance with the literature data [118]. Compound **45** displayed a $[M-H]^-$ ion at m/z 301 and a prominent fragment ion at m/z 179 $[M-H-C_7H_6O_2]^-$, due to the RDA fragmentation. Other fragment ions of the tandem mass spectrum included the m/z 273 $[M-H-CO]^-$, m/z 257 $[M-H-CO_2]^-$, and m/z 151 $[M-H-C_8H_6O_3]^-$. According to the mass fragmentation pattern, compound **45** was identified as quercetin [121].

2.3.4. Quantitative polyphenols characterization by HPLC-DAD-FLD analysis

Chromatographic analysis for the quantification of TN polyphenolic composition was conducted as reported in Section 2.3. The HPLC-DAD-FLD analysis allowed the quantification of 19 different compounds, including flavanols, procyanidin compounds, phenolic acids, and flavonol derivatives. The results are reported in Table 8.

Table 8. Quantitative analysis of thinned nectarines polyphenols determined by HPLC-DAD-FLD analysis.

Compound	Retention Time (min)	Mean Value \pm SD ($\mu\text{g/g}$)
Gallic acid	4.00	168.31 \pm 1.51
Neochlorogenic acid	7.76	1456.98 \pm 1.19
Procyanidin B1 + Procyanidin B3	12.70	8.41 \pm 0.02
Catechin	13.34	128.32 \pm 0.36
Chlorogenic acid	13.72	1496.85 \pm 0.22
Caffeic acid	13.76	15.85 \pm 0.06
Vanillic acid	14.78	19.28 \pm 0.91
Syringic acid	17.20	115.16 \pm 0.21
Procyanidin B2	18.03	6.55 \pm 0.01
Epicatechin	19.54	34.63 \pm 0.83
<i>p</i> -Coumaric acid	20.65	5.05 \pm 0.33
Procyanidin C1	22.47	12.66 \pm 0.01
Ferulic acid	24.39	10.59 \pm 0.02
Rutin	28.27	48.86 \pm 0.67
Naringenin	31.14	10.92 \pm 0.42
Quercetin-3- <i>O</i> -glucoside	32.68	166.01 \pm 3.35
Kaempferol-3- <i>O</i> -glucoside	36.84	63.65 \pm 3.01
Quercetin	46.06	17.89 \pm 0.41

Values are expressed in $\mu\text{g/g} \pm$ standard deviation (SD) of three repetitions. * Procyanidins B1 and B3 peaks were partially overlapped and were quantified as a mixture of two compounds using the procyanidin B1 calibration curve.

2.3.5. Total polyphenols and in vitro antioxidant activity of TNE

In order to obtain an overview of the total polyphenolic content, Folin–Ciocalteu’s assay was performed on hydroalcoholic TN extract (TNE). The sample exhibited a total phenol content of 17.01 ± 0.35 mg GAE/g of extract. Additionally, the antioxidant activity was evaluated by using DPPH, ABTS, and FRAP assays. As reported in Table 9, results were expressed as μmol of TE per g of dried extract.

Table 9. Antioxidant activity of Thinned Nectarine extract evaluated by DPPH, ABTS, and FRAP assays.

Antioxidant Activity ($\mu\text{mol TE/g TN} \pm \text{SD}$)		
DPPH Assay	ABTS Assay	FRAP Assay
40.09 ± 0.14	63.26 ± 0.72	58.07 ± 0.14

The results are expressed as $\mu\text{mol TE}$ per gram of TN extract. Abbreviations: TN, thinned nectarine; DPPH, 2,2-diphenyl-1-picrylhydrazyl; ABTS, 2,2’-azino-bis (3-ethylbenzothiazoline-6-sulfonic acid); FRAP, ferric reducing antioxidant power; TE, Trolox equivalent. Values are mean \pm standard deviation (SD) of three repetitions.

In order to standardize the results from various studies, DPPH and ABTS assays were also reported as EC_{50} , which is the amount of antioxidant necessary to decrease the concentration of the initial solution by 50% [90]. As displayed in Figure 7, TNE exhibited an EC_{50} of 1.57 mg/mL for the DPPH assay and 1.58 mg/mL for the ABTS assay.

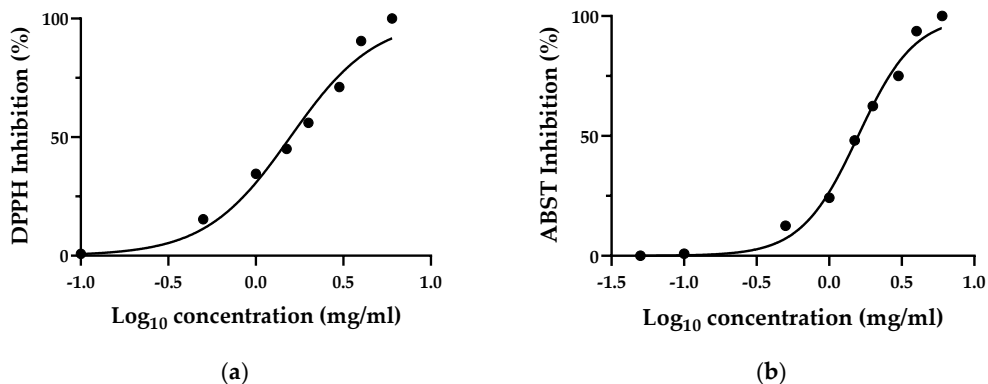


Figure 7. Antioxidant activity of the thinned nectarine extract expressed as (a) EC₅₀ of DPPH assay and (b) EC₅₀ of ABTS assay. Values represent the mean \pm standard deviation of triplicate readings.

2.3.6. *In vitro* antidiabetic activity

2.3.6.1. α -amylase inhibitory activity

The α -amylase inhibition activity of TNE was tested by an *in vitro* assay. Figure 8 shows the percentage inhibition as IC₅₀, which is the amount of compound necessary to inhibit the enzyme activity by 50% [95]. The results revealed that both acarbose and the TNE inhibited α -amylase activity in a concentration-dependent manner. The IC₅₀ values generated from the percentage inhibition revealed a result of 8.11 and 0.43 mg/mL for TNE and acarbose, respectively.

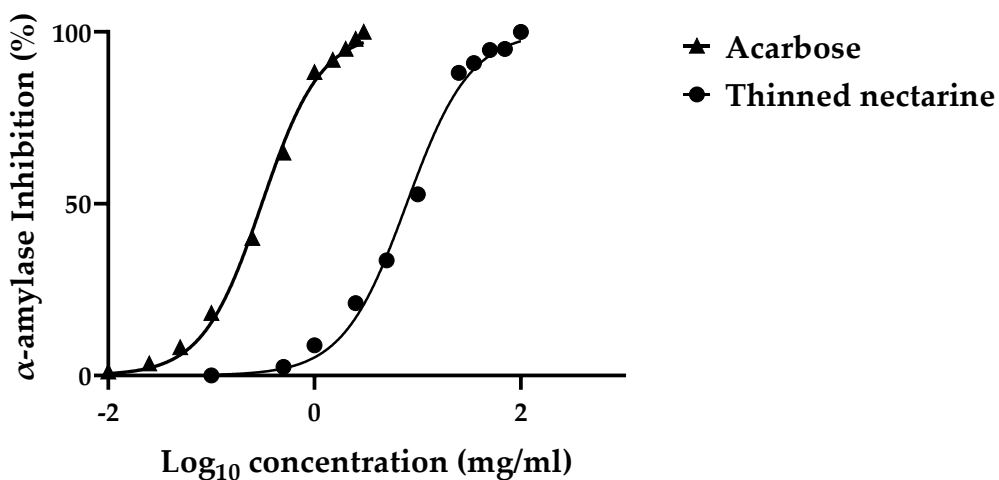


Figure 8. Inhibition of α -amylase activity (%) by thinned nectarine extract and acarbose. Values represent the mean \pm standard deviation of triplicate readings.

2.3.6.2. Advanced Glycation End-Product (AGE) inhibitory activity

The inhibitory activity of TNE on AGEs formation was also investigated. The assay is based on the inhibition of specific fluorescence generated during the course of glycation and AGEs formation. Figure 9 shows the percentage inhibition as EC_{50} , which is the concentration required to obtain a 50% effect. Under our experimental conditions, TNE and rutin produced a concentration-dependent inhibition of AGE, with an EC_{50} of 11.0 and 0.1 mg/mL for TN and rutin, respectively.

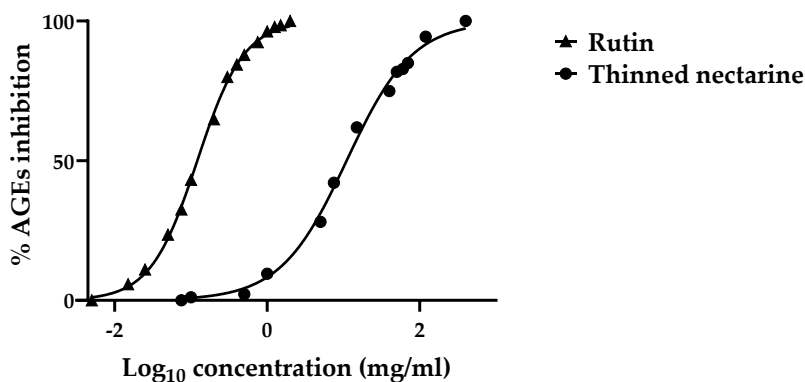


Figure 9. Inhibition of Advances Glycation End-Product formation (%) by thinned nectarine extract and rutin. Values represent the mean \pm standard deviation of triplicate readings.

2.4. Discussion

Polyphenols, a family of plant secondary metabolites naturally occurring in fruits, are considered critical not only for fruit quality but also for human health benefits [124]. Scientific data showed that polyphenolic compounds contained in nectarines and peaches could prevent cellular oxidative stress resulting from free radicals [125]. Interestingly, it was shown that thinned young fruits might exhibit significantly higher antioxidant capacity than their ripe counterparts. This was mainly due to the 5–10 times higher total polyphenol content found in thinned young fruits compared to ripe fruits [126]. In the present work, HPLC analyses allowed us to tentatively identify 48 polyphenolic compounds, 19 of which were quantified with analytical standards, confirming the high polyphenolic content of these waste-by products. In addition, the quantitative analysis of the polyphenolic profile of TNE is in line with available literature data. Specifically, Guo et al. showed that chlorogenic acid and neochlorogenic acid represent the main polyphenols of unripe nectarines, with a content of 100–500 $\mu\text{g/g}$ and 270–1250 $\mu\text{g/g}$, respectively [126].

Moreover, data presented in this part of the Ph.D. thesis demonstrated a concentration-dependent inhibitory activity of TNE on the α -amylase enzyme, with

results expressed as IC_{50} . It is well-known that the IC_{50} of an inhibitor is very dependent on the assay conditions, such as enzyme concentration and origin, substrate type and concentration, reaction duration, temperature, and pH [127]. This makes data comparison with the literature a difficult task. However, by utilizing acarbose as a benchmark, a comparison of the general inhibitory trend could be achieved. Recently, long-term excessive intake of starchy food has been reported to be one of the reasons for hyperglycemia that can even lead to type II diabetes disease [128]. In this regard, the reduction of the hydrolysis rate of starch through inhibiting digestive enzymes is one suggested way of relieving postprandial hyperglycemia [129]. Of note, the same test conducted with a standard of abscisic acid did not show any inhibitory capacity on the enzyme, highlighting that the inhibitory activity of our sample would not be ascribable to the ABA content but to the contribution of other bioactive compounds. In this regard, the role of polyphenols in modulating starch digestion and glycemic levels was widely investigated [129]. As reported by the scientific literature, compounds such as quinic acid derivatives and mono and diglycosyl flavonols (e.g., neochlorogenic acid, chlorogenic acid, and rutin) are closely correlated to the inhibition of α -amylase [130]. Therefore, the high content of these polyphenols may justify TNE inhibitory efficacy on this enzyme.

Moreover, concentration-dependent inhibition of AGEs formation was observed after testing TNE through an opportune *in vitro* assay. AGEs are proteins or fats combined with blood sugars after exposure to a glycation process through the Maillard reaction [131]. These compounds result in being highly stable and resistant to enzymatic degradation, leading to their high accumulation in different tissues, modification in cells and tissues, progressive deterioration of structural integrity and physiological function across multiple organs, and increased risk of death [132]. Regarding diabetes mellitus-related hyperglycemic conditions, it is well known that excess intracellular glucose is converted to sorbitol by the polyol pathway, mainly in tissues and organs with an insulin-independent glucose uptake (e.g., retina,

peripheral nerves, kidney, erythrocytes). This signaling pathway often results in a complex cascade of events that can culminate in tissue and vascular damage, significantly contributing to the onset of diabetes chronic complications [133]. Therefore, the inhibition of AGEs formation would represent a useful tool for the prevention of diabetes complications. In this regard, growing evidence highlighted that polyphenols are able to prevent AGEs production [134], reasonably supporting the herein observed beneficial activity exerted by TNE. Polyphenols' antiglycation properties are mainly due to the inhibition of early Maillard reaction products, especially reactive dicarbonyl as methylglyoxal (MGO) [135]. Phenolic acids and flavans (e.g., gallic acid, p-coumaric acid, and epicatechin) can directly reduce the carbonyl groups by a redox reaction, inhibiting the formation of advanced Maillard products. Differently, flavonols (e.g., quercetin, rutin) react with the MGO dicarbonyl moiety, indirectly preventing the formation of glycation products [135,136]. Therefore, it is possible to hypothesize that TNE may exert an antiglycation action with different mechanisms of action, due to the complexity of polyphenols fraction.

Considering the well-known link between diabetes and oxidative stress and considering the vegetal nature of our food matrix is highly likely to contain antioxidant polyphenols, the attention was focused on the investigation of *in vitro* antioxidant potential of TN. For these reasons, Folin–Ciocâlțeu, DPPH, ABTS, and FRAP assays were carried out on a polyphenolic extract of TN. The obtained results are in line with available studies conducted on immature nectarine, confirming the high antioxidant potential of these by-product matrices [97]. In this regard, a study conducted by Guo et al. reported that the antioxidant capacity of peaches and nectarines evaluated by DPPH, ABTS, and FRAP assays were 1.3–11.2-fold higher in thinned young fruit compared to ripe fruit [126]. Notable, increasing evidence from *in vitro* and clinical studies suggests that oxidative stress plays a pivotal role in the pathogenesis of both types of diabetes mellitus. Abnormally high levels of free

radicals and the simultaneous decline of antioxidant defense mechanisms can indeed lead to damage to biological structures. These consequences of oxidative stress can promote the development of complications of diabetes mellitus [63]. Similarly, persistent hyperglycemia is recognized as one of the main causes of oxidative stress, supporting a direct cause-and-effect relationship between hyperglycemia and oxidative stress [64]. In light of these considerations, the concomitant presence of bioactive molecules with antidiabetic and antioxidant potential in TN-based formulation would further support its supplementation for the management of diabetic pathology.

2.5. Conclusions

In conclusion, our data support TN as a source of innovative and promising nutraceutical formulations with beneficial health effects, particularly concerning the management of glucose homeostasis. According to available evidence previously described, these beneficial effects may be related to the role of ABA occurred in the TN plant matrix. Nonetheless, the results reported in this chapter have shown that the simultaneous presence of other bioactive components in TN-based nutraceutical formulation, such as polyphenols, may contribute to the management of diabetes-related oxidative stress conditions. Overall, the results obtained strongly prompted us to test the clinical potential of a TN-based nutraceutical formulation on glucose homeostasis.

Chapter 3

Validation of an LC-MS/MS method to determine the ABA serum concentration

3.1 Introduction

To date, the majority of the evidence on ABA *in vivo* hypoglycemic effects have addressed a role in the stimulation of peripheral glucose uptake by increasing the glucose transporter 4 (GLUT4) expression and translocation [34,45,48,137]. Additionally, it is noteworthy to remark that patients with type 2 diabetes mellitus (T2DM) or gestational diabetes have been found to have a decreased release of ABA following a glucose load [138]. This evidence highlights the importance of monitoring ABA serum concentrations in individuals with altered glucose metabolism and supplementing them with plant-based exogenous sources of ABA. In this regard, several studies involving both animal and human models demonstrated the significant beneficial effects on the glycemic profile of ABA-containing nutraceuticals in prediabetic and diabetic subjects, in association with an insulin-sparing mechanism of action [39,53,58,137,139,140]. In virtue of its insulin-independent mechanism of action [48], ABA supplementation may be suggested as a useful approach to improve glucose tolerance in individuals deficient in and/or resistant to insulin. On the other hand, although a wide variety of bioactive compounds of natural origin have been tested for their beneficial potential in the control of diabetic conditions [10,141], the evaluation of their bioavailability still represents a crucial aspect [142,143]. Identification of ABA as a plant hormone is usually performed with various methods, mainly in plant matrices, such as gas chromatography/mass spectrometry (GC/MS) [144] and immunological assay, i.e., enzyme-linked immunosorbent assay (ELISA) [145]. Although these methods are able to assess ABA concentration levels, they are affected by some disadvantages.

For instance, ELISA assay requires a long preparation time and has low specificity and reproducibility, while GC/MS requires derivatization of the sample [144].

Based on such considerations, the present work focused on the development and validation of a method for the determination of ABA by liquid mass spectrometry analysis (LC-MS), through liquid–liquid extraction (LLE) in a biological matrix, i.e., serum. Subsequently, the optimized and validated method was applied to test its suitability on serum samples from eight healthy volunteers that consumed a standardized test meal (STM) with the concomitant supplementation with a nutraceutical product based on TN rich in ABA, to test the method in a real-world setting. Finally, the glyceemic and insulinemic response in the above-mentioned subjects was evaluated in association with ABA serum levels at different time points of analysis.

3.2. Materials and Methods

3.2.1. Study design

3.2.1.1. Participants and standardized test meal composition

Briefly, healthy subjects of both sexes were recruited in May 2019 by Samnium Medical Cooperative (Sant’Agata De’ Goti, Italy) as a subset of volunteers participating in a randomized clinical trial. The volunteers’ letter of intent, the protocol, and the synoptic documents of the study were submitted to the Scientific Ethics Committee of AO Rummo Hospital (Benevento, Italy). The study was approved by the committee (protocol no. 28, May 15, 2017) and was conducted in accordance with the Helsinki Declaration of 1964 (as revised in 2000). The study was listed on the ISRCTN registry (www.isrctn.com) with ID ISRCTN16732651. A total of 8 healthy subjects aged 18–83 years were invited to participate. Exclusion criteria were diabetes mellitus (DM) type 1 and type 2, liver, heart, or renal disease, drug therapy or intake of dietary supplements containing ABA, underweight (body

mass index < 18.5 kg/m²), pregnancy or suspected pregnancy, birch pollen allergy. All participants received oral and written information about the study before giving written informed consent. Before inclusion in the study, volunteers were subjected to self-reporting questionnaires involving the following items: residence, occupation, smoking status, alcohol consumption, drug administration, and dietary habits. The volunteers meeting the inclusion criteria (body mass index (BMI) 27–35 kg/m²; waist circumference, men ≥102 cm and women ≥88 cm) were assigned to consume a standardized test meal (STM), immediately after the administration of TN (1 g, lyophilized) containing ABA. TN treatment was self-administered as a tablet. The STM composition consisted of white bread (100 g) with 50 g of jam and 100 g of mozzarella and 200 ml of fruit juice. These amounts were chosen based on indications of a balanced meal, as they provided 50% of calories from carbohydrates, 20% from protein, and 30% from fat [146].

3.2.1.2. Experimental procedures

At the beginning of the study, all patients underwent measurements of body height, body weight (BW), and waist circumference (WC), with the evaluation of Body Mass Index (BMI). Glucometabolic parameters were determined before the STM consumption as a baseline, except for fasting plasma glucose (FPG) and fasting plasma insulin (FPI), which were evaluated before and after consuming the STM. After a 12-hour fasting period, blood samples were collected to measure FPG, FPI, triglycerides (TG), total plasma cholesterol (TC), lipoprotein-cholesterol (HDL-C), alanine aminotransferase (ALT), aspartate aminotransferase (AST), and glycated hemoglobin (HbA1c). The concentration of the above-mentioned parameters was assayed by enzymatic colorimetric methods (Diacron International, Italy). The Friedewald formula was used to calculate LDL cholesterol levels. Plasma insulin levels were measured by ELISA (DIA-source ImmunoAssay S.A., Nivelles,

Belgium) on a Triturus analyzer (Diagnostic Grifols S.A., Barcelona, Spain). HbA1c was measured using a commercially available kit (InterMedical s.r.l, Italy).

3.2.2. Analytical method

3.2.2.1. Chemicals and reagents

The purity of ABA as primary standard was $\geq 98\%$ HPLC and purchased from Sigma-Aldrich (Milan, Italy). Chromatographic-grade solvents, methanol, formic acid, and ethyl acetate were used (minimum purity 99.9%) and purchased by Sigma Aldrich, (Milan, Italy) as well as internal standard (IS), bis 4,4'- Sulfonyldiphenol, (BPS), (minimum purity 98%). Ultra-purified water Milli Q was produced in-house (conductivity $0.055 \mu\text{S cm}^{-1}$ at 25°C , resistivity equals $18.2 \text{ M}\Omega\cdot\text{cm}$).

3.2.2.2. Real sample preparation and extraction

Vacu-test[®] tubes were employed to collect blood samples, collected from the ante-cubital vein (5 mL); the samples were immediately centrifuged at 2200 rpm for 20 min and the supernatant was frozen and stored at -80°C until processing. Both samples, synthetic and real samples, underwent liquid-liquid extraction (LLE). Briefly, the sample preparation was performed according to the following procedures: 75 μL of serum were transferred to a 2 mL vial, spiked into 40 μL of BPS 100 ppb solution, to achieve a final concentration of 40 ppb, with the addition of 340 μL of methanol and 2 μL of 12 N HCl solution. Each sample was successively vortexed and stored in ice for 2 min. Afterwards, the samples were added to 500 μL ethyl acetate, vortexed, and finally centrifuged at 10.000 rpm for 5 min at 4°C . The supernatant (a fixed volume of 700 μL) was transferred to a 4 mL vial, dried in Savant[™] SpeedVac[™] (Thermo Scientific[™], Hyannis, MA, USA) and stored until the analysis. Dried samples were dissolved in 50 μL of $\text{CH}_3\text{OH}:\text{H}_2\text{O}$ 50/50 *v/v*, vortexed, and after 45 min to facilitate the dissolution, another 50 μL of $\text{CH}_3\text{OH}:\text{H}_2\text{O}$

50/50 v/v was added. The samples were again centrifuged at 3.500 rpm for 5 min and the supernatant was transferred to a 1.5 mL glass insert and injected into liquid mass spectrometry (LC-MS). BPS was chosen for its lipophilicity feature as an internal standard (IS) to assess the recovery of each extraction.

3.2.2.3. Equipment

Analytical determination was performed on an Ultimate 3000 LC system (Dionex/Thermo Scientific) coupled to a linear ion trap LTQ XL™ Thermo Scientific™ with an electrospray ionization source. The separation was performed on Luna® Omega 3 µm Polar C18 column (100 x 2.1 mm) (Phenomenex Torrance USA). Tuning and data acquisition was carried out using Xcalibur and quantification using Qual Browser software 4.4 version.

3.2.2.4. LC-MS/MS conditions

The samples, 5 µl of each, were injected from Autosampler (Ultimate 300) and analyzed under the following chromatographic conditions: eluent A aqueous added of 0.1 % v/v formic acid and eluent B acetonitrile, added of 0.1 % v/v formic acid, flow rate set to 0.4 mL min⁻¹, at room temperature 35 ± 2 °C. Gradient elution was accomplished as follows: 0–2.0 min, 5% B; 2.0–9.0 min, 95 % B; 9.0–12.0 min, 95 % B; 12.1–16.0 min, 5 % B. All mobile phases were vacuum-filtered through 0.45 µm nylon membranes (Millipore®, Burlington, MA USA). The electrospray ionization (ESI) mass spectrometer (MS) was operated in negative ion mode using selective reaction monitoring (SRM) with nitrogen as the nebulizer, auxiliary, collision, and curtain gas. The main working source/gas parameters of the mass spectrometer were optimized and maintained as follows: curtain gas, 8; nebulizer gas, 8. The instrumental parameters employed were as follows: ESI spray voltage in the negative-ion mode, 4 kV; sheath gas flow rate, 70 arb; auxiliary gas flow-rate,

20 arb; capillary voltage, -38 V; capillary temperature, 350 °C and tube lens, 95 V. ABA was monitored as $[M-H]^-$ ion according to their m/z values.

3.2.2.5. Calibration curve and linearity

European validation guidelines were followed to validate the method [147]. Stock solutions of ABA were obtained dissolving the reference standard in 100% methanol to obtain a final concentration of 2.000 ppm. Five solutions with different concentrations (40 ppb, 20 ppb, 10 ppb, 4 ppb, 2 ppb) were prepared by diluting this stock. The linearity ranges were tested using the average peak areas against the concentration (ppm) of ABA. Linear regression analysis and calibration curve parameters (Coefficient of Determination R^2 , slope, and intercept) were back-calculated from the peak areas using the regression line by the method of least squares, and mean accuracy values were determined

3.2.2.6. Limits of Detection (LOD) and Quantification (LOQ)

LOD and LOQ were estimated to be the concentrations providing signals equal to 3 and 10 times, respectively. They were calculated based on the following equations: $LOD = SD \cdot 3/S$ and $LOQ = SD \cdot 10/S$ [148], where SD is the standard deviation of the intercept response with the y-axis of the calibration curves, and S is the slope of a calibration curve. The spike level was 2 ppb in the appropriate range using a concentration and evaluated by running the measurement ten times.

3.2.2.7. Precision and accuracy

The method's precision was evaluated by running five replicates of the sample repeated in the same day and in two different days to cover both intra-day and inter-day precision, expressed as relative standard deviation (RSD%). Repeatability was assessed using the nominal concentration of ABA (2 ppb). The accuracy of this method was determined considering samples spiked with 2–40 ppb of ABA (quality

control samples, QCs) and evaluated at each level in triplicate, and reported as a percentage of the nominal value. Serum working calibration standards were prepared by analyzing some serum from the archive and assessed showing no interfering signals eluting at the same retention time of analyte with ABA, so they were employed as blank.

3.2.2.8. Selectivity

Serum working calibration standards were prepared using sera already present in the archive of our laboratory and processed for other research, to assess the absence of ABA and that any signal interfered with the retention time of ABA. These sera, considered as blanks, were also employed to optimize the extraction process.

3.2.2.9. Carry-over

The carry-over effect of the method was evaluated by injecting methanol solvent after running the highest concentrated samples of ABA spiked in the serum (three times) and observing the occurrence of signals within the retention windows of the target chemicals.

3.2.2.10. Matrix effect

The matrix effect was investigated by calculating the ratio of the peak area in the presence of matrix (matrix spiked with ABA post extraction) to the peak area in the absence of matrix (ABA in methanol). The serum matrix blank was spiked with the analyte at each concentration of the linear range (2 ppb, 4 ppb, 10 ppb, 20 ppb, and 40 ppb). The ratio was calculated as follows:

$$\text{Matrix effect \%} = \frac{\text{peak area in presence of matrix}}{\text{area in absence of matrix}} \cdot 100$$

3.2.2.11. Recovery

The recovery was assessed by evaluating the relative abundance of the BPS peak (I.S.) spiked before the extraction procedure and calculated as follows:

$$\text{Recovery \%} = \frac{\text{found concentration}}{\text{standard concentration}} \cdot 100$$

The results of the real samples were corrected for the recovery.

3.3. Results

3.3.1. Anthropometric and glucometabolic parameters

The characteristics of the patient population at baseline are shown in Table 10. A total of 8 healthy adults (3 men and 5 women) aged 18 to 45 years, with a BMI between 18 and 25 kg/m² met the inclusion criteria and were thus eligible to participate in the study. The group was well-balanced in terms of demographic and clinical factors.

Table 10. Baseline anthropometric and glucometabolic parameters of study participants.

Characteristics	Study participants (n=8)
Demographic and anthropometric parameters	
Male sex (No (%))	3 (37.5%)
White ethnicity (No (%))	8 (100%)
Age (years)	34 ± 3.7
Height (m)	1.6 ± 0.9
Weight (kg)	71.2 ± 6.9
BMI (kg/m ²)	24.6 ± 3.3
WC (cm)	89.4 ± 5.4

Clinical parameters

HbA _{1c} (%)	6.5 ± 0.4
Triglycerides (mg/dL)	105.2 ± 14.5
Total cholesterol (mg/dL)	171.3 ± 11.9
HDL-C (mg/dL)	46.7 ± 5.4
LDL-C (mg/Dl)	89.5 ± 7.6
AST (U/L)	25.6 ± 3.9
ALT (U/L)	18.7 ± 2.8
Creatinine (mg/dL)	0.9 ± 0.1

Data are expressed as mean ± standard deviation. Abbreviations: AST: aspartate aminotransferase; ALT: alanine aminotransferase; BMI, Body Mass Index; Cre: creatinine; F, females; FPG: fasting plasma glucose; FPI: fasting plasma insulin; HbA_{1c}: glycated hemoglobin; HDL-C: high-density lipoprotein-cholesterol; LDL-C: low-density lipoprotein-cholesterol; M: males; TG: triglycerides; WC: waist circumference.

3.3.2. Two-hour glycemic and insulinemic responses to standardized test meal

Following the STM, which was preceded by the administration of the nutraceutical supplement containing ABA, mean plasma glucose levels reached a peak at 30 min and gradually decreased to pre-prandial levels by 120 min. According to the plasma glucose response curve, the post-prandial insulinemic response curve peaked at 30 min and gradually declined to the pre-prandial level by 120 min (Figure 10). A similar trend can be observed for serum ABA concentrations after the consumption of STM and the TN-based nutraceutical product in volunteers under our investigation as shown in Figure 11.

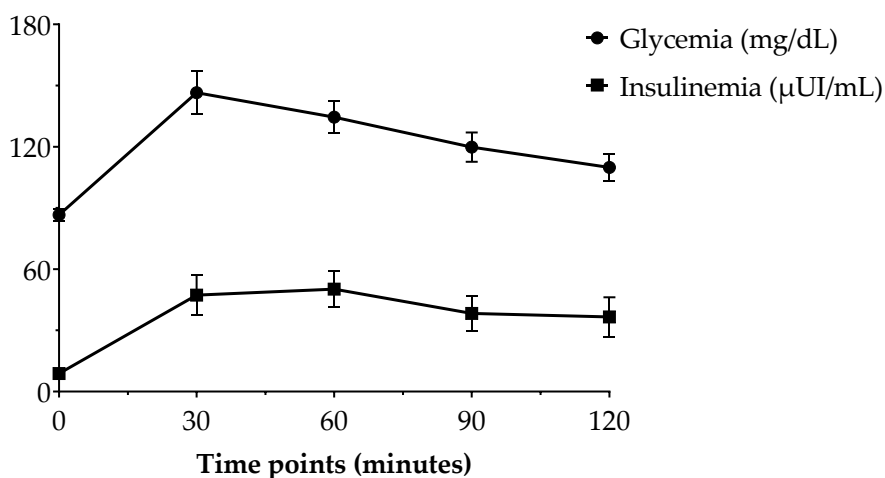


Figure 10. Change in postprandial plasma glucose and insulin concentration in healthy adults (n=8). Data are expressed as mean \pm SEM.

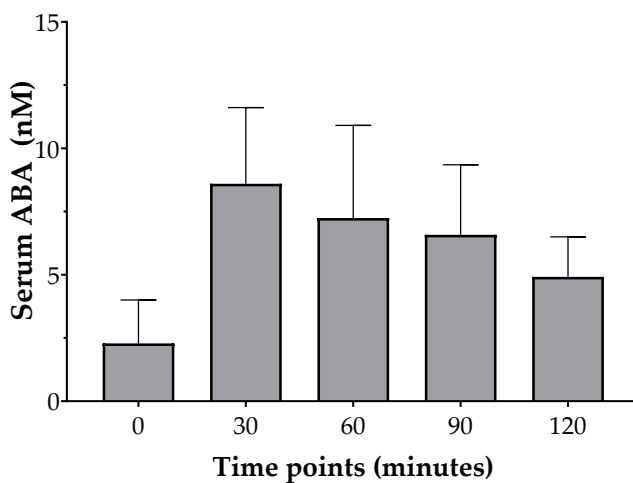


Figure 11 ABA concentration change after the consumption of STM and TN-based product in healthy adults (n=8). Data are expressed as mean \pm SEM.

3.3.3. Optimization of chromatographic method

Different “synthetic” samples with known ABA concentrations, i.e., methanolic solutions and serums spiked with ABA, were used for the method development.

These samples were subjected to the above-mentioned method in order to evaluate the efficiency in isolating and detecting abscisic acid in the context of complex biological matrices. The proposed method of extraction and quantification of ABA was easy to handle and sensitive to the analysis in serum matrix, optimizing the method after several changes in operating. For the extraction procedures, there were distinct organic solvents in various percentages with water. Ethyl acetate as an extraction solvent was the most efficient solvent to extract ABA from the serum matrix (data not shown). The spike levels (40.0 ppb and 2.0 ppb) were in the recommended range, i.e., calculated LOD < spike level < 10 × calculated LOD. For LC-MS analysis, we optimized the method using different stationary reversed-phases (Luna® Omega 3 µm Polar C18 column (100 × 2.1 mm) (Phenomenex Torrance USA) and an Inertsil ODS-3 column (2.1 mm × 100 mm, 5 µm) (Torrance, CA, USA), and by a varying gradient elution program, to achieve an adequate resolution for the two analytes from the interferences. Optimal transitions were obtained for ABA (C₁₅H₂₀O₄, MW: 264.32 g/mol) at *m/z* 152.000, and for BPS (C₁₂H₁₀O₄S, MW: 250.27 g/mol) at *m/z* 107.000. The linear R-squared values ($r^2 = 0.9981$) show a good linearity in the range of the calibration curves performed in the serum matrix from 40 ppb to 2 ppb. The sensitivity of the developed method is appreciable from the listed LOD and LOQ parameters, with values of 1.59 ppb and 5.31 ppb, respectively. The RSD% of within-run precision was 2.30%, while the RSD% between-run precision was 12.01%. Repeatability was performed using the repeatedly frozen and thawed ABA samples, and we did not observe any differences in the raw data and degradation products. Recovery from the serum matrix, evaluated at high and low spiking concentrations (40 ppb and 2.0 ppb), resulted in 70.3%. Matrix effect was 39.97% and variations in the experimental parameters did not result in any appreciable change in the method performance. Table 11 summarizes all method validation parameters.

Table 11. Summary of LC-MS/MS method validation parameters.

Linear Range (ppb)	Slope	Intercept	R ²	Repeatability (n = 5) RSD %	Intermediate Precision (n = 10) RSD%	LOQ (ppb)	LOD (ppb)	Matrix Effect
40.0–2.0	92.84	-32.45	0.9981	2.30	12.01%	5.31	1.59	39.97%
Spiking level (ppb)	2	4	10	20	40			
Recovery (%)	71.8	73.3	77.7	65.5	63.5			

These results demonstrate that the developed analytical method provides a reliable response relevant to the analysis of ABA in such a complex biological matrix. Selectivity is the ability of an analytical method to differentiate and quantify the analyte in the presence of other components in the sample. The selectivity of the method was evaluated by analyzing a blank sample, compared to a blank sample spiked with the lower limit of quantitation LOQ, (ABA equal to 2.00 ppb). As can be seen in Figure 12 the selectivity of this method was good.

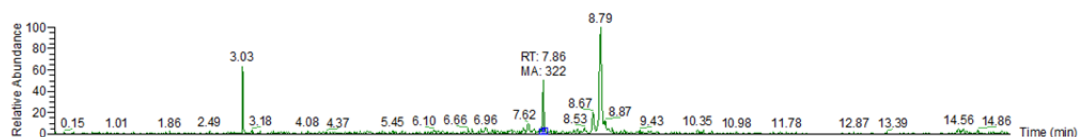


Figure 12. Chromatogram of ABA in serum matrix.

3.4. Discussion

In the present work a method for the determination of ABA in biological samples by liquid-liquid extraction (LLE), followed by liquid mass spectrometry (LC-MS) of the extract, was developed and validated. The above-reported method has significant advantages, as it does not require expensive operations, in terms of procedures and amounts of solvents used, and leads to results with a good level of accuracy, reproducibility, LOD, and LOQ values. These resulted in the same order of magnitude as those achieved by other authors, even if scientific literature reports

methods for determination of ABA, but a) in different matrices, such as in *Arabidopsis thaliana* [149], b) in serum matrix, but without reporting all the validation parameters [150,151]. Moreover, the application of the optimized method on serum samples of healthy volunteers who consumed a STM together with a nutraceutical product rich in ABA, allowed us to evaluate its applicability in a suitable biological model. Accordingly, the STM composition of the present work provided 50% of calories from carbohydrates, 20% from protein, and 30% from fat, in agreement with the guidelines for balanced nutrition [146]. In this manner, the glyceic and insulinemic response, together with the increase in plasmatic ABA, was evaluated in the closest to a real-life setting.

The LC-MS analysis performed on the serums obtained from the eight volunteers showed different ABA levels at each time point. As observed in Figure 11, the found data confirmed the involvement of this endogenous hormone in the human response to glucose-containing foods. For all subjects, indeed, the serum ABA levels reached the highest concentration 30 min after the consumption of the STM and the nutraceutical product based on TN. In this regard, various studies carried out on human serums attempted to identify and quantify ABA levels, by performing different isolation and detection methods [34,138]. Specifically, plasma ABA has been shown to increase in normal glucose tolerant (NGT) subjects after an oral glucose load [14], but not in patients with T2D or in pregnant women with gestational diabetes mellitus (GDM). On the other hand, the resolution of GDM one month after childbirth is associated with a restoration of ABA response to glucose load [138]. Interestingly, a significant increase in ABA was observed in obese patients after biliopancreatic diversion (BPD), a bariatric surgery performed to reduce body weight and ameliorate glucose tolerance, compared to pre-surgery levels [138]. Another observed difference between T2D and NGT individuals was related to fasting ABA values, which were significantly higher in T2D compared to NGT subjects (1.15 vs 0.66 as median values, respectively). Nevertheless, the

distribution of ABA levels was found to be normal in NGT but not in T2D patients [138]. These alterations could be due to the heterogeneity of ABA-related dysfunction occurring in T2D, such as the inability of ABA to increase in response to hyperglycemia or the resistance to the activity of ABA. Collectively, these observations suggest a role for ABA as pivotal hormone involved in the management of glucose homeostasis and highlight the importance of monitoring ABA levels in these categories of individuals. Notably, based on reports about the daily consumption of fruits and vegetables containing ABA, epidemiological evidence have shown that the majority of the population assumes a very low intake of ABA from dietary sources [152]. Due to the multiple beneficial effects on health status ascribed to the role of ABA [153], interest in supplementing this bioactive molecule by administering nutraceutical products rich in ABA is increasing over time, also with regard to the nanomolar blood concentrations of this hormone requested for its efficacy.

3.5. Conclusions

In conclusion, we herein developed and validated a method for the extraction and LC-MS/MS analysis of ABA in biological samples. Even if limited by the small sample size, requiring therefore confirmation through larger clinical evaluation, an added value is represented by the successful application of this method to real samples, which allowed the evaluation of ABA serum changes after the consumption of STM and an ABA-rich nutraceutical product. Overall, the results shown could provide a starting point for determining the response to a glucose-containing meal in clinical practice, in terms of ABA concentration. Indeed, serum detection of this endogenous hormone may be considered a marker to assess the presence of an impaired ABA response in dysglycemic subjects. Undoubtedly, the use of this analysis would be of great interest for clinical trials involving the chronic administration of ABA-rich nutraceutical supplements with hypoglycemic potential.

Chapter 4

Clinical efficacy of a TN-based nutraceutical formulation (TNnf) on glucose homeostasis

4.1. Introduction

Diabetes is a metabolic disease that has reached epidemic proportions: the latest edition of the IDF Diabetes Atlas shows that in 2021 10.5% of adults were affected by diabetes and this percentage will further increase, along with 12% of global health expenditure destined to treat this condition [1]. The use of therapeutic strategies aimed to contrast hyperglycemia is essential, especially to avoid diabetes-related microvascular and macrovascular complications [154]. As previously reported in this Ph.D. thesis, ABA has recently aroused considerable interest in scientific literature as an endogenous hormone with hypoglycemic potential in the management of glucose homeostasis [44,153]. ABA is produced and released by pancreatic β -cells in response to high glucose concentrations in humans [34]. As a result, this molecule would promote stimulation of both glucose-dependent and glucose-independent insulin release [32], and stimulation of glucose uptake by upregulation of GLUT4 expression and translocation [34,45,48]. Despite this, recent findings demonstrated how the *in vivo* administration of ABA at low doses may lead to the improvement of glucose tolerance in association with an ameliorated insulin profile [53]. Overall, this evidence clarifies the role played by this hormone as a key actor in the control of diabetic pathology. In support of this consideration, an impaired release of ABA has been also reported after a glucose load in patients with T2DM or gestational diabetes [138], further highlighting the potential of thinning by-products as precious supplements of this hypoglycemic hormone. As shown in the previous chapters, the high concentration of polyphenolic compounds, together with the antioxidant and

antidiabetic results obtained from in vitro assays attributed to the TN product [155], reasonably prompted us to test its clinical potential on glucose homeostasis in patients with T2DM. In light of these considerations, we aimed to evaluate the effects on glucose homeostasis after supplementation with two different doses of a TN-based nutraceutical formulation (TNnf), through a randomized controlled trial (RCT) conducted on patients with T2DM. Moreover, the correlation between glycemia and ABA plasmatic levels was also evaluated in a subgroup of patients undergoing the clinical trial.

4.2. Material and methods

4.2.1. Study population and design

Study participants were recruited by the Samnium Medical Cooperative (Sant'Agata De' Goti, Italy). Patients were enrolled in May 2019. Protocol, letter of intent of volunteers, and synoptic documents about the study were submitted to the Scientific Ethics Committee of AO Rummo Hospital (Benevento, Italy). The study was approved by the committee (protocol n°28 of 15/05/2017) and carried out in accordance with the Helsinki Declaration of 1964 (as revised in 2000). The sample size was calculated using G*Power 3.1.9.4 statistical analysis software to achieve 80% power. Patients aged 18–83 years with T2DM, as defined by the American Diabetes Association [156], for more than one year were eligible for enrolment. Figure 13 shows the flow of participants through the trial according to the criteria recommended in the CONSORT guidelines [157]. A total of 80 T2DM were initially invited to participate. Exclusion criteria were: type 1 diabetes mellitus (T1DM), smoking, hepatic disease, renal disease, heart disease, drug therapy or supplement intake containing ABA or polyphenols, heavy physical exercise (> 10 h/week), underweight (Body Mass Index < 18.5 kg/m²), pregnant women, women suspected

of being pregnant, women who hoped to become pregnant, breastfeeding, use of vitamin/mineral supplements 2 weeks before starting the study, birch pollen allergy, and donation of blood less than 3 months before the study. The occurrence of any of the above exclusion criteria during the trial resulted in the immediate cessation of participation in the study seven patients did not qualify for the study due to improper inclusion/exclusion criteria. Finally, a total of sixty-seven patients received the allocated intervention, and sixty-one of them completed the study. All the participants received oral and written information concerning the study before they gave their written consent.

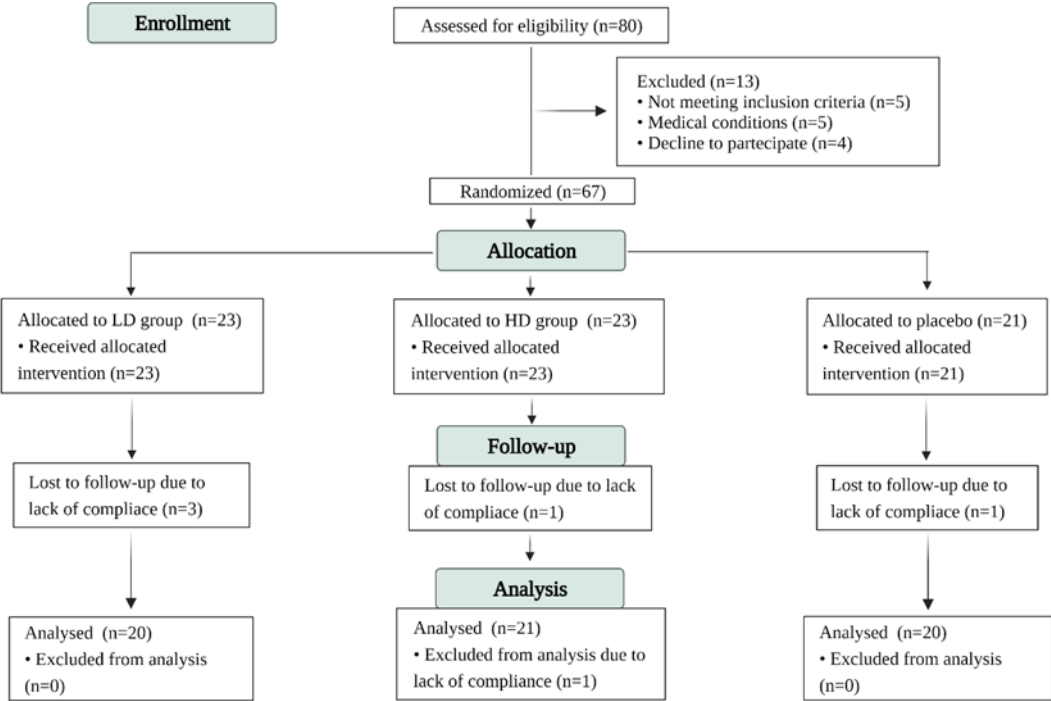


Figure 13. Study Consolidated Standards of Reporting Trials (CONSORT) flow diagram. HD, high dose of thinned nectarine group; LD, low dose of thinned nectarine group.

This study was designed as a 12-week, monocentric, double-blind, randomized, placebo-controlled, 3-arm parallel-group trial. Patients were randomly allocated to

three intervention groups: placebo group (500 mg of maltodextrins three times/day), low dose of TNnf (LD) group (500 mg three times/day, lyophilized), or high dose of TNnf (HD) group (750 mg three times/day, lyophilized). Both placebo and TNnf treatments were self-administered as tablets. Treatment compliance was assessed by counting the number of tablets returned at the time of specified clinic visits. Throughout the study, we instructed patients to take their first dose of new medication on the day after they were given the appropriate treatments. All treatments were provided free of charge. Randomization was done using a drawing of envelopes containing randomization numbers. The random number list was generated by an investigator with no clinical involvement in the trial. Patients, core laboratories, clinicians, and trial staff were blind to treatment allocation. Periodic and standardized telephone interviews were performed by qualified personnel to verify and increase protocol compliance. Moreover, a secondary outcome of the study was represented by the measurement of plasmatic ABA (ABAp) levels through an LC-MS/MS analysis. This evaluation was only performed on a small subgroup of patients undergoing the clinical trial, due to depletion of available samples (LD group at baseline, n=9; LD group after 3 months, n=6; HD group at baseline, n=10; HD group after 3 months, n=7).

4.2.2. Assessments

At the study start, all patients underwent a standardized physical examination, assessment of medical history (for up to five years before enrolment) and of vital signs (blood pressure and heart rate, laboratory examination, measurements of body height, body weight (BW), and waist circumference (WC), with the evaluation of Body mass index (BMI). BMI was calculated from the body height and body weight. Blood samples were collected after 12 h of fasting at weeks 0, 4, 8, and 12 in 10-mL EDTA-coated tubes (Becton Dickinson, Plymouth, United Kingdom), and plasma

was immediately isolated by centrifugation (20 min, 2.200 g, 4°C). All samples were stored at -80°C until analysis. Subjects were asked to abstain from alcohol consumption and practice hard physical activity 48 h prior to blood sampling. Plasma total cholesterol (TC), high-density lipoprotein-cholesterol (HDL-C), low-density lipoprotein-cholesterol (LDL-C), fasting plasma glucose (FPG), triglyceride (TG), aspartate aminotransferase (AST), alanine aminotransferase (ALT), and creatine levels were determined using commercially available kits from Diacron International (Grosseto, Italy). Analyses were performed on a Diacron International Free Carpe Diem. Glycated hemoglobin (HbA_{1c}) was determined with a commercially available kit (InterMedical s.r.l, Italy). Fasting plasma insulin (FPI) was measured using an enzyme-linked immunosorbent (ELISA) assay commercial kit (InterMedical s.r.l, Italy). Homeostatic model assessment of insulin resistance (HOMA index) was calculated with the formula: FPG (mg/dl) times FPI (μUI/ml) divided by 22.5 [158].

4.2.3. *Quantification of serum ABA levels by LC-MS/MS analysis*

The determination of serum ABA concentration was carried out at T0 and T90 following the optimized and validated protocol previously described (see Chapter 3).

4.2.4. *Statistics*

Unless otherwise stated, all the experimental results were expressed as the mean ± standard deviation (SD). Statistical analysis of data was performed by the Student's t-test or Pearson's correlation test. *P*-values less than 0.05 were regarded as statistically significant. The degree of the linear relationship between the two variables was measured using the Pearson product-moment correlation coefficient (*R*). Correlation coefficients (*R*) were calculated using GraphPad Prism 8.4.3.

4.3. Results

4.3.1. Study sample

A total of eighty patients were initially enrolled in the trial; nineteen patients were then lost due to different reasons. Finally, sixty-one participants (Placebo group, $n = 20$; LD group, $n = 20$, HD group, $n = 21$) completed the 3 months of intervention. The baseline and 3-month general data and anthropometric parameters of patients are reported in Table 12. The groups were well-balanced for demographics and anthropometric factors. No changes were observed in BMI and circumferences in the three treatment groups at the end of the clinical trial.

Table 12. Baseline, and 3-month general data and anthropometric parameters of randomized subjects in placebo, high dose of TNnf group, and a low dose of TNnf group.

Parameters	Low dose group		High dose group		Placebo	
	Baseline	T90	Baseline	T90	Baseline	T90
Patients (n)	20	20	21	21	20	20
M/F	11/9	-	12/9	-	13/7	-
Age (years)	63 ± 6.5	-	64 ± 7.8	-	64 ± 5.9	-
Height (m)	1.69 ± 0.1	-	1.66 ± 0.1	-	1.68 ± 0.1	-
Weight (kg)	83.4 ± 7.9	83.2 ± 6.8	86.1 ± 6.2	85.9 ± 4.2	85.4 ± 4.5	85.3 ± 4.4
BMI (kg/m^2)	29.2 ± 4.1	29.1 ± 4.1	31.6 ± 4.5	31.6 ± 4.5	30.5 ± 4.3	30.5 ± 4.2
WC (cm)	99.0 ± 8.5	98.9 ± 8.6	103 ± 6.8	103 ± 6.9	99.5 ± 7.8	99.5 ± 7.9

Data are expressed as mean \pm standard deviation. TNnf: thinned nectarine-based nutraceutical formulation; M: males; F: females; BMI: body mass index; WC: waist circumference.

4.3.2. Glucometabolic parameters

As shown in Table 13, a significant increase was observed for HDL-C values in both the treatment groups compared to baseline values ($p < 0.05$ vs. baseline), while no significant differences were observed in the placebo group. Additionally, a non-significant decrease and a significant decrease ($p < 0.05$ vs. baseline) of TG levels were observed in the HD group and LD group, respectively. As regards glyceamic parameters, a significant decrease in FPG, FPI, HOMA-IR, and HbA1c was observed in the HD and LD of TNnf treatment groups, compared to the baseline values ($p < 0.05$ vs. baseline), while no significant differences were observed in the placebo group.

Table 13. Baseline and 3-month biochemical parameters of patients of placebo, high dose, and low dose of TNnf groups.

Parameters	Low dose group (<i>n</i> = 20)		High dose group (<i>n</i> = 21)		Placebo (<i>n</i> = 20)	
	Baseline	T90	Baseline	T90	Baseline	T90
FPG (mg/dL)	151.4 ± 28.6	129.9 ± 12.7**	147.2 ± 36.8	137.1 ± 26.9*	155.1 ± 31.5	154.6 ± 30.6
FPI (μU/mL)	12.0 ± 9.1	8.5 ± 4.0*	15.22 ± 7.6	12.77 ± 6.6*	15.9 ± 6.7	15.4 ± 6.9
HbA _{1c} (%)	8.0 ± 0.9	6.9 ± 0.7***	7.8 ± 0.6	6.9 ± 0.4***	7.7 ± 0.5	7.7 ± 0.3
HOMA-IR	4.7 ± 4.0	2.7 ± 1.2*	5.6 ± 3.3	4.4 ± 2.6*	5.8 ± 3.2	5.8 ± 3.2
TC (mg/dL)	146.4 ± 36.1	152.8 ± 30.9	164.2 ± 27.0	167.5 ± 26.5	150.5 ± 28.9	151.6 ± 29.8
LDL-C (mg/dL)	83.4 ± 28.8	83.7 ± 26.5	109.5 ± 19.8	108.8 ± 31	84.5 ± 35.9	84.6 ± 34.8
HDL-C (mg/dL)	36.2 ± 8.1	39.0 ± 8.3*	34.2 ± 8.7	39.0 ± 7.9*	36.7 ± 7.5	36.6 ± 7.2
TG (mg/dL)	134.3 ± 42.1	100.6 ± 22.1**	102.7 ± 27.5	98.5 ± 28.5	130.5 ± 32.1	133.6 ± 33.2
AST (U/L)	25.7 ± 8.2	21.7 ± 6.2	21.5 ± 6.3	21.1 ± 5.6	24.5 ± 4.6	24.3 ± 4.8
ALT (U/L)	18.9 ± 6.3	20.0 ± 6.3	19.3 ± 4.7	18.4 ± 3.6	19.8 ± 5.6	19.9 ± 5.5
Cre (mg/dL)	0.9 ± 0.2	0.9 ± 0.1	1.2 ± 0.1	1.1 ± 0.2	0.9 ± 0.3	0.9 ± 0.1

Data are expressed as mean ± standard deviation. Statistical significance is calculated by Student's t-test analysis; * $p < 0.05$; ** $p < 0.01$; *** $p < 0.001$ vs. baseline. Abbreviations: ALT, alanine aminotransferase; AST, aspartate aminotransferase; FPG: fasting plasma glucose; Cre, creatinine; FPI, fasting plasma insulin; HbA_{1c}, glycated hemoglobin; HD, high doses; HDL-C, high density lipoprotein-cholesterol; HOMA-IR, homeostatic model assessment of insulin resistance; LD, low doses; LDL-C, low density lipoprotein-cholesterol; TC, total cholesterol; TG, triglycerides; TNnf, thinned nectarine-based nutraceutical formulation.

Noteworthy, although a significant decrease of glycemic parameters was observed in both TNnf treatment groups, treatment with LD showed a greater decrease of FPG values (-14.8%, $p < 0.01$ vs baseline), compared to TNnf HD group (-6.9%, $p < 0.05$ vs baseline) and a greater insulin sparing effect (FPI: -29.2%, $p < 0.05$ vs baseline), compared to HD group (FPI: -16.5%, $p < 0.05$ vs baseline). Overall, as reported in Table 14, these results determined a greater decrease of HOMA-IR values in the LD group (-41.6%, $p < 0.05$ vs baseline), compared to the HD group (-22.2%, $p < 0.05$ vs baseline).

Table 14. Effects of low and high doses of thinned nectarine-based nutraceutical formulation on glycemic parameters at baseline and after 3 months.

	Fasting plasma glucose		Fasting plasma insulin		HOMA-IR	
	Baseline	T90	Baseline	T90	Baseline	T90
HD group						
Mean ±	147.2 ± 36.8	137.1 ± 26.9	15.2 ± 7.6	12.7 ± 6.6	5.6 ± 3.3	4.4 ± 2.6
SD						
CV %		- 6.9 %		- 16.5 %		- 22.2 %
<i>p</i> -value		0.0472		0.0345		0.0482
LD group						
Mean ±	151.4 ± 28.6	129.9 ± 12.7	12.0 ± 9.1	8.5 ± 4.0	4.7 ± 4.0	2.5 ± 1.2
SD						
CV %		- 14.8 %		- 29.2 %		- 41.6 %
<i>p</i> -value		0.0035		0.0404		0.0230

Abbreviation: CV, coefficient of variation; HD, high dose of thinned nectarine-based nutraceutical formulation group; LD, low doses of thinned nectarine-based nutraceutical formulation group; SD, Standard deviation; HOMA-IR: homeostatic model assessment of insulin resistance.

4.3.3. Correlation analysis of serum ABA levels and glycemia

A secondary outcome of the present work included the investigation of the relationship between plasma ABA concentration (ABAp) and changes in plasma glucose levels in patients supplemented with LD or HD of TNnf at baseline and after 3 months. To achieve this purpose, an LC-MS/MS analysis was performed to

determine the ABAp levels, and the obtained data were correlated to the corresponding glyceimic values in a small subgroup of patients (LD group at baseline, n=9; LD group after 3 months, n=6; HD group at baseline, n=10; HD group after 3 months, n=7). As shown in Figure 14, a negative correlation was observed for both the groups treated with the TNnf at baseline, and at the end of the 3 months. Specifically, these correlations were statistically significant in the LD group at T0 ($r = - 0.9012$, $p < 0.001$), in the HD group at T0 ($r = - 0.6388$, $p = 0.0468$), and in the HD group at T90 ($r = - 0.8068$, $p = 0.0283$), although a not significant negative correlation was also observed in the LD group at T90 ($r = - 0.7686$, $p = 0.0742$).

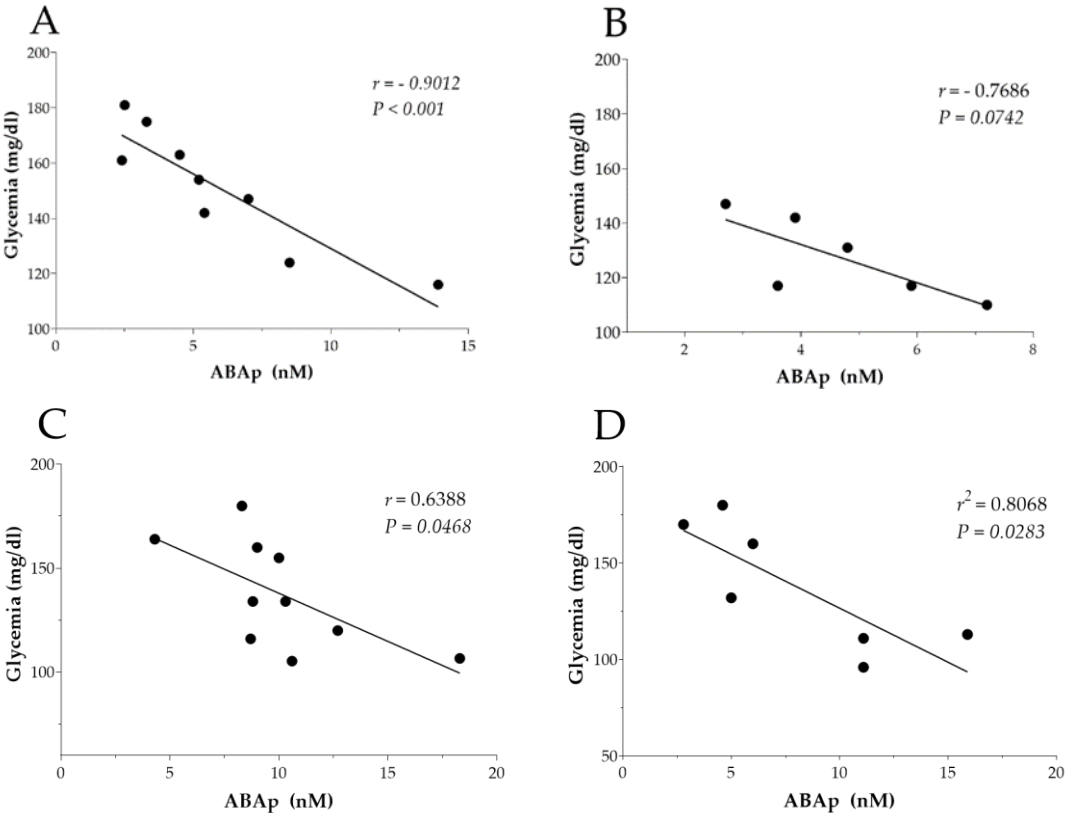


Figure 14. Correlation analysis of serum ABA levels and glycemia. The Pearson correlation analysis was calculated to evaluate the link between plasmatic ABA levels and glycemia in the following groups: (A) low doses of TNnf group (500 mg of TN three times/day) at baseline (T0), (B) low doses of TNnf group (500 mg of TN three times/day) after 90 days (T90), (C) high doses of TNnf group (750 mg of TN three times/day) at baseline (T0), (D) high doses of TNnf group (750 mg of TN three times/day) after 90 days (T90). Abbreviations: ABA, abscisic acid; TNnf, thinned nectarines- based nutraceutical formulation.

4.4. Discussion

Abscisic acid is widely described as a terpenoid phytohormone naturally present in fruits and vegetables [66], with a crucial role in managing glucose homeostasis in humans [44]. This bioactive compound is currently and extensively being investigated for different therapeutic purposes, such as diabetes, cancer, ischemic retinopathy, and neurodegenerative diseases, due to the broad biological activity spectrum attributed to it [159–162]. The first aim of this study was to evaluate the potential beneficial effects on glucose homeostasis after supplementation with two different doses of the TNnf rich in ABA. Specifically, the two doses tested (500 mg and 750 mg TNnf three times/day) were selected based on evidence that the hypoglycemic effect of ABA *in vivo* at low doses (0.5-1 $\mu\text{g}/\text{kg}$ BW) result to be associated with an insulin-sparing mechanism of action [53]. Based on the previously quantified TN content of ABA (see Chapter 1), daily administration with the two TNnf would therefore promote an exogenous ABA intake of ~ 0.45 and $0.7 \mu\text{g}/\text{kg}$ BW (considering an average adult weight of 70 kg) for the LD and HD groups, respectively. In addition, doses outside this range were excluded due to the results of a previously conducted pilot study (data not shown). Interestingly, supplementation with TNnf showed to significantly reduce fasting glycemia in both the intervention groups, with a greater decrease of FPG values in the LD group (-14.8% , $p < 0.01$, vs baseline), compared to the HD group (-6.9% , $p < 0.05$ vs baseline). Moreover, a greater insulin-sparing effect was reported in

patients treated with LD of TNnf (FPI: -29.2%, $p < 0.05$ vs baseline), compared to the HD group (FPI: -16.5%, $p < 0.05$ vs baseline). Overall, these results seem to be consistent with available scientific data involving the supplementation with low doses of ABA [53]. Although the reasons for this unexpected effect have not yet been fully elucidated, various hypotheses have been proposed. Based on these assumptions, the stimulation of glucose uptake in GLUT4-expressing cells by ABA could precede in time and/or exceed in extent the stimulation of insulin release or, in a not necessarily exclusive manner, these cells may result to be more sensitive to the effect of ABA than pancreatic β -cells in vivo [153]. Therefore, the administration of ABA at low doses may be suggested as a useful tool for the improvement of glucose tolerance in subjects with a deficiency of/or insulin resistance. In this regard, there is a rising consensus within the scientific community that the protracted stimulation of insulin release from pancreatic β -cells under conditions of chronic hyperglycemia may finally contribute to their eventual exhaustion [54]. Taking into account this evidence, antidiabetic molecules capable of lowering glycemia without increasing insulinemia are highly desirable, since they could improve the survival and function of these cells. In this context, by-product nectarines derived from fruit thinning may be considered valuable matrices for nutraceutical applications. In particular, the results herein presented may direct physicians toward novel treatment/intervention which may represent a useful alternative/support in the clinical practice.

One of the objectives of the present work included the investigation of the relationship between plasma ABAP levels and changes in plasma glucose levels in patients undergoing the clinical trial at baseline, and after 3 months. Interestingly, although not always significant, a negative correlation was observed for both the groups treated with the TNnf at baseline and at the end of the trial. Noteworthy, and in agreement with the observed data, an impaired release of ABA has been reported after a glucose load in patients with T2DM or gestational diabetes [138]. Another convincing evidence that ABA could be involved in glycemia control derives from

the observation that nanomolar ABA stimulated glucose uptake, similarly to insulin, in rat L6 myoblasts and in murine 3T3-L1 cells differentiated to adipocytes, by upregulating GLUT-4 translocation to the plasma membrane [34]. Additionally, the insulin-independent hypoglycemic activity of ABA has been proposed by recent *ex vivo* experiments, in which ABA demonstrated to stimulate the uptake of a fluorescent glucose analog by mouse skeletal muscle in the absence of insulin, and the LANC2 silencing reduced all the observed effects [48]. These results were also confirmed *in vivo* on rats undergoing an oral glucose load, as the ABA-induced glucose and storage in skeletal muscle were detected by micro-PET [48]. From a mechanistic point of view, the activation of AMPK would result to be responsible for these effects. More specifically, the incubation with ABA showed to increase the phosphorylation of AMPK, thus leading to the phosphorylation and activation of PGC-1 α in skeletal muscle. Eventually, the main consequence of this process would be represented by the increase in GLUT4 expression and glycogen accumulation [48,49]. AMPK also represents an upstream positive regulator of p38 MAPK [50], which has been attributed to the ability to promote PPAR- γ phosphorylation on Ser122, thus preventing PPAR- γ -induced inhibition of GLUT4 expression [48,51,52]. Altogether, these observations about the non-overlapping signaling pathways and the metabolic effects of ABA and insulin suggest a role for ABA as an upstream regulator in the glycemic response.

As regards the lipid profile, a significant increase in HDL-C values was observed in both the groups treated with TNnf, compared to baseline, while no significant differences were observed in the placebo group. This unexpected result could be explained by the high content of polyphenolic compounds in our food matrix. As indeed reported by scientific studies, polyphenols can positively influence cholesterol metabolism, especially regarding the class of dimeric procyanidins B2 [163]. Moreover, the decrease of TG levels observed in the TNnf treatment groups may be justified both by the reported beneficial effects exerted by polyphenols on

the management of hypertriglyceridemia [164] and by the positive response of plasma TG levels after the improved glycemic control, as described by scientific evidence [165]. In agreement with this hypothesis, the previous characterization of TN polyphenolic profile, performed by a validated HPLC-DAD method [166], highlighted the high potential of this matrix in terms of polyphenol content [155]. In this sense, increasing evidence suggests a pivotal role played by oxidative stress in the pathogenesis of both types of DM [167,168] and the related beneficial role exerted by polyphenolic compounds [63,169]. Specifically, high levels of free radicals and the simultaneous decline of antioxidant defense mechanisms can lead to damage of biological structures, with a resulting increased risk of diabetes-related complications [63]. Similarly, persistent hyperglycemia is recognized as one of the main causes of oxidative stress, supporting a direct cause-and-effect relationship between hyperglycemia and oxidative stress [64]. In light of these considerations, the concurrent presence of bioactive molecules with antidiabetic and antioxidant potential in TN plant matrix further suggests its synergistic efficacy for the management of diabetic pathology.

4.4.1. Strengths and limitations

One of the strengths of the clinical trial herein presented resides in the originality of the study that involves the administration of an agricultural by-product as a source of bioactive compounds with hypoglycemic potential. This is in line with the current worldwide trend to reevaluate such agro-food wastes for purposes of environmental sustainability and circular economy. Secondly, the study population represented by patients with T2DM that maintained their usual daily diets allowed us to evaluate treatment effects in a real-world setting. Moreover, the two different doses of TNnf tested in the intervention groups contributed to evaluating a dose-response relationship, helping to identify the adequate dose of the food supplement. In this

context, the results herein reported can inform physicians about a novel intervention, which can represent a valuable alternative in the clinical practice. Finally, although the measurement of the ABAP concentration was only performed on a limited number of samples, the analysis allowed us to highlight an existing correlation between the circulating amount of ABA and the observed effects on glycemic levels. Doubtless, these preliminary results strongly encourage us in future considering the measurement of ABAP levels as a primary outcome in study including a greater number of patients. The main limitations of our study include the choice of exclusively white race, the short-term assessment for the treatment of a chronic condition, and the wide age range due to the availability of such individuals at the stage of the recruitment. Therefore, randomized, placebo-controlled studies with larger numbers of participants are warranted to further confirm our observations.

4.5. Conclusions

In conclusion, the present study indicated that TN-based nutraceutical product may significantly and clinically reduce glucose levels, in association with an insulin-saving effect. Overall, these results reasonably support TN as an innovative and promising nutraceutical formulation able to contribute to the management of glucose homeostasis. According to scientific available data, these beneficial actions may be related to the role of ABA occurred in TN, particularly relating to the insulin-sparing mechanism of action. Moreover, the negative correlations observed between glycemia and ABA plasmatic levels in patients treated with TN further support the observed beneficial results. Undoubtedly, the present work needs to be supported by further investigations to confirm the proposed results.

Chapter 5

In vitro antioxidant and antidiabetic properties of a TNE-based nanoformulation in a pancreatic β -cell line

5.1. Introduction

Pancreatic β -cells play a pivotal role in maintaining whole-body glucose homeostasis by synthesizing and secreting insulin at appropriate rates. At low levels, oxidative stress is essential for normal β -cell function and has a role in different activities, such as the stimulation of basal insulin secretion [170]. However, these cells are profoundly susceptible to oxidative damage upon sustained insult [171], due to relatively low expression of antioxidant enzymes (e.g. catalase and glutathione peroxidase) [172]. Notably, reactive oxygen species (ROS) represent key mediators for nucleic acids, lipids, and proteins damage, resulting in undesirable biochemical and functional modifications [173]. Sustained excessive iron and glucose exposure have been shown to be key mediators of oxidative stress occurring in pancreatic β -cells, ultimately resulting in mitochondrial and cellular membrane damage and disruption [174]. ROS generation induced by the high amount of free ferrous iron generated through the Fenton and Haber-Weiss reaction leads to terminal hydroxyl radical ($\cdot\text{OH}$) production. Lipid peroxidation is a representative biological process related to metal-induced generation of ROS, leading to production of reactive aldehydes such as malondialdehyde (MDA) and 4-hydroxy-2-nonenal (4-HNE) production [175]. These free radicals can rapidly react with biological molecules causing significant damage to cellular components and disruptions in function, including insulin resistance and eventual β -cell failure [176]. In this context, recent evidence has demonstrated that high iron exposure (100 μM) can result in a marked decrease in MIN6 insulin secretory capacity (64% reduction) as well as cellular

insulin content (10% reduction). Moreover, this insulin secretory dysfunction was suggested to be partially due to the impairment of the exocytotic machinery, as shown by the significant reduction in SNAP-25 (synaptosomal-associated protein of 25 kDa) expression, a key element of the β -cell exocytotic machinery, following exposure to high iron and elevated glucose concentrations [167]. From a mechanistic point of view, the perturbations in mitochondria functionality related to iron-induced oxidative stress would correlate with diminishing of MIN6 β -cell insulin secretion, suggesting a fundamental role for iron overload in the development and progression of T2DM [167].

The potential role of polyphenolic compounds in the treatment of diabetes has been well described in scientific literature, being able to act on the control of blood sugar at different levels and through diverse mechanisms of actions [63]. From this perspective, natural products containing bioactive molecules with antioxidant potential may be particularly relevant for more efficient management of diabetic pathologies. Based on this rationale, the concomitant presence of different bioactive compounds in TN, such as ABA and polyphenols, would reasonably support this vegetable matrix as a source of innovative nutraceutical formulations useful for the management of glucose homeostasis [155]. Although several botanical compounds have shown therapeutic promise, their application has often been limited by issues related to their stability, bioavailability and efficacy at site of action [177]. Notably, nanotechnology based formulations, such as micelles, nanoliposomes and solid lipid nanoparticles, have been shown to be beneficial in overcoming these limitations and enhancing the potential of bioactive molecules [178].

Polymeric micelles (PM) are used as drug carriers due to the relatively simple preparation methods, narrow size distribution with a diameter up to 100 nm, and the ability to solubilize hydrophobic drugs. PM's are formed by self-assembly of amphiphilic block copolymers, making up a core-shell structure. Polymeric nanoparticles (PNPs) refer to polymeric particles in the form of either capsules or

solid spheres. A drug or bioactive is typically incorporated in the polymer matrix, and its release is driven by polymer degradation and/or drug diffusion. Polymers used for this application include natural polymers such as albumin, dextran, and chitosan and synthetic polymers such as Polyethylene glycol (PEG) [179,180]. PEG has been in use for several decades as a surfactant and for steric stabilisation and conjugation of ligands to drug nanocarriers.

The polyethylene glycol grafted 1,2-distearoyl-sn-glycero-3-phosphatidylethanolamine (DSPE-PEG) is a PEGylated phospholipid frequently used to develop drug nanocarrier systems due to its ability to form micellar rather than bilayered structures by self-assembly in a suitable aqueous environment. Ascorbyl palmitate is a palmitic acid ester of ascorbic acid that is lipophilic in nature and has been used as an excipient in the cosmetic industry as a stable form of ascorbic acid. Due to its hydrophobic nature, ascorbyl palmitate requires the amphiphilic derivative DSPE-PEG to spontaneously form vesicle structures in an aqueous medium. The nanocarriers thus formed provide a suitable platform for the incorporation of active ingredients, and previous studies have successfully demonstrated the use of such vesicles as carriers for a hydrophobic drug [178,181]. Nanocarriers can enhance the potency, stability, bioavailability, and passage across biological membranes of incorporated compounds. As regards stability, evidence has shown that nanocarriers remain stable in the bloodstream, thus resisting aggregation or premature drug leakage and avoiding removal by renal filtration and by the organs of the reticuloendothelial system (RES) [182]. They can also improve the delivery across biological barriers (e.g. lipid-based nanocarriers can more easily bind the cell membrane) and their uptake can be mediated by endocytosis [181,183]. These effects are related to several characteristics, such as small particle size (<200 nm), surface charge, physical and/or chemical interactions among the components, etc., overall leading to an improved targeting delivery to the site of action. Moreover, following cellular internalization, the nanoformulations may allow temporal control of

encapsulated molecule release [179]. Various mechanisms drive drug release from the carriers. For example, drug release kinetics can be controlled by the diffusion of a drug molecule through a carrier matrix or a barrier surrounding the matrix. Alternatively, degradation or swelling of the carrier matrix and the cleavage of drug-polymer linkage can control the drug release rate from the carrier [179,184]. Based on these considerations, the following aims were pursued during my Ph.D. research period abroad:

1) To develop nanoformulations based on TNE and ABA (pure standard) with the use of specific nanocarriers (i.e. DSPE-PEG and ascorbyl palmitate/DSPE-PEG)

2) To evaluate the physiochemical characteristics of the above-mentioned nanoformulations, in collaboration with the UCL, School of Pharmacy of London.

3) To investigate and compare properties of TNE and ABA-based nanoformulations in a pancreatic β -cell line. Specifically:

3.1.) To assess the cytotoxicity of the unencapsulated and nanoformulated samples through MTT assay and their antioxidant potential using an in vitro cellular antioxidant activity assay.

3.2) To evaluate the potential insulinotropic effect of the above-mentioned nanoformulations in MIN6 cells incubated with varying glucose concentrations (5.5 mM and 20 mM).

3.3) To investigate the antioxidant and protective effects against β -cell dysfunction induced by a challenge with high iron concentrations (100 μ M).

5.2. Materials and methods

5.2.1. Reagents and materials

All chemicals and reagents used for the HPLC-DAD analysis were either analytical-reagent or HPLC grade. The water was treated in a Milli-Q water purification system (Millipore, Bedford, MA) before use. (\pm)-2-*Cis*-4-*trans*-abscisic acid (ABA), 2',7'-Dichlorofluorescein diacetate (DCFH-DA), ethanol, methanol, acetonitrile, and formic acid were all purchased from Sigma–Aldrich (Milano, Italy). All chemicals for cell culture experiments were of cell culture grade and purchased from Sigma-Aldrich (Dorset, UK) unless otherwise stated. Protease Inhibitor Cocktail (PIC, catalog no. P8340), dimethyl sulfoxide (DMSO), Thiazolyl, and Blue Tetrazolium Blue (MTT) were obtained from Sigma-Aldrich (Dorset, UK). Fisher Scientific (Loughborough, UK) supplied Minimum Essential Medium (MEM), Dulbecco's modified Eagle's medium (DMEM) Glutamax[®], fetal bovine serum (FBS), and 100× antibiotic-antimycotic solution. The 12-well cell culture dishes, 96-well microtiter plates, and flasks were purchased from Nunc (Roskilde, Denmark). A mouse insulin ELISA kit was supplied by Mercodia (Cat No. 10-1247-01—Mercodia, D.B.A., Milan, Italy). Ascorbyl palmitate was purchased from Sigma–Aldrich (Dorset, UK), and DSPE-PEG was from Lipoid (Steinhausen, Switzerland). Experimental reagents were prepared using ultrapure water (resistivity of 18.2 M Ω cm).

5.2.2. Preparation of thinned nectarine extract

TN were collected in June 2019 at the orchards of “Giaccio Frutta” society (Vitulazio, Caserta, Italy, 41°10' N–14°13' E), about one month after full bloom, coinciding with the fruit thinning stage. The whole fruits (pulp, peel, and seed) were

frozen at $-20\text{ }^{\circ}\text{C}$, lyophilized, and ground to obtain a homogenous powder. As regards the extraction procedure, a previous method reported by Schiano et al. was used with slight modifications [155]. Briefly, 2.5 g of homogenized sample was suspended in 25 mL of a 100% ethanolic solution and thoroughly vortexed for 1 min. The suspension was then sonicated for 10 minutes using a VWR Ultrasonic cleaner bath USC300T (VWR International Limited, Lutterworth, UK) and stirred lightly for 40 min at 25° , 600 speed. After centrifugation (10 min, $9000 \times g$, 25°), the supernatant was decanted, filtered with a $0.22\text{ }\mu\text{m}$ nylon filter (CellTreat, Shirley, MA, USA), and evaporated using a rotary evaporator (Hei-VAP Advantage Rotary Evaporator, Heidolph, Germany). The ABA content of the dried extract was evaluated as reported in section 1.2.3. of the present thesis. Moreover, for all experiments described below, the dried extract was dissolved with a defined volume of media (MEM) in order to obtain the equivalent ABA concentrations contained in Free-ABA and NF-ABA samples.

5.2.3. *Preparation of ABA and TNE-based nanoformulations*

DSPE-PEG or DSPE-PEG Ascorbyl palmitate nanocarriers were prepared by the thin-film hydration method as previously described [178,185]. Briefly, DSPE PEG alone or ascorbyl palmitate (AP) and DSPE-PEG were dissolved in methanol in a round bottom flask. A dry lipid film was formed by removing the solvent under reduced pressure for 10 min at $60\text{ }^{\circ}\text{C}$ using a rotary evaporator (Hei-VAP Advantage Rotary Evaporator, Heidolph, Schwabach, Germany), with residual solvent removed by purging the lipid film with nitrogen gas. The film was hydrated with an ABA or TNE solution (4 mg/10 ml or 52 mg/5 ml) or distilled water in case of corresponding blank nanocarrier formulations. In order to remove any unloaded compound, the obtained solution was filtered through a sterile $0.22\text{ }\mu\text{m}$ filter. The nanocarriers were then stored in 10 ml vials at $4\text{ }^{\circ}\text{C}$ until use. Preparations were coded: 1. DSPE-PEG-

TNE, 2. DSPE-PEG-ABA, 3. DSPE-PEG-blank, 4. DSPE-PEG-AP-TNE, 5, DSPE-PEG-AP-ABA, 6. and DSPE-PEG-AP-blank. To enable storage of samples for further analysis, some samples were lyophilized using a Virtis AdVantage 2.0 BenchTop freeze dryer (SP Industries, UK).

5.2.4. Size and surface charge of the nanoformulations

The particle size and surface charge of nanoformulations were measured using the Zetasizer Nano ZS (Malvern Instruments, Malvern UK). The nanodispersions were added individually to the ZetaMaster electrophoresis cell and size distribution was measured via photon correlation spectroscopy as mean volume diameters (MVD) and polydispersity index (PDI) carrying out three measurements on each sample. Nanoformulation zeta potential was determined similarly using the electrophoretic light-scattering technique (Zeta-sizer Nano ZS, Malvern Instruments, UK) measuring electrophoretic mobility in triplicate for all samples (Table 15).

Table 15. Particle size and zeta potential of ABA and TNE-based nanoformulations.

Sample	Particle size (nm)	Zeta potential (mV)
DSPE-PEG-AP-ABA	52 ± 3.2	-0.01 ± 0.04
DSPE-PEG-AP-TNE	24 ± 2.1	0.03 ± 0.04
DSPE-PEG-AP-BLK	173 ± 59	-5.3 ± 4.4
DSPE-PEG – ABA	5.2 ± 1.3	-0.001 ± 0.03
DSPE-PEG – TNE	6.2 ± 0.7	0.0051 ± 0.002
DSPE-PEG – BLK	3.6 ± 1.5	0.0861 ± 1.5

Data represent the mean ± standard deviation (SD) of six replicates. Abbreviations: ABA, abscisic acid; AP, ascorbyl palmitate; BLK, blank; DSPE-PEG: Polyethylene glycol grafted 1,2-distearoyl-sn-glycerol-3-phosphatidylethanolamine; TNE, thinned nectarine extract.

5.2.5. *Nanoformulation morphology*

Transmission electron microscopy (TEM) analysis was performed to analyze the morphology (size and surface characteristics) of the nanoformulation complexes using an FEI CM 120 BioTwin transmission electron microscope (Philips Electron Optics BV, Netherlands) at acceleration voltage 120.0 kV. Approximately 40 μl of the nanoparticle dispersion was placed on a Formvar/carbon coated copper grid and negatively stained with 1% uranyl acetate. Digital images were taken at 13,500, 17,500, 46,000, and 65,000 times magnification (Figure 15).

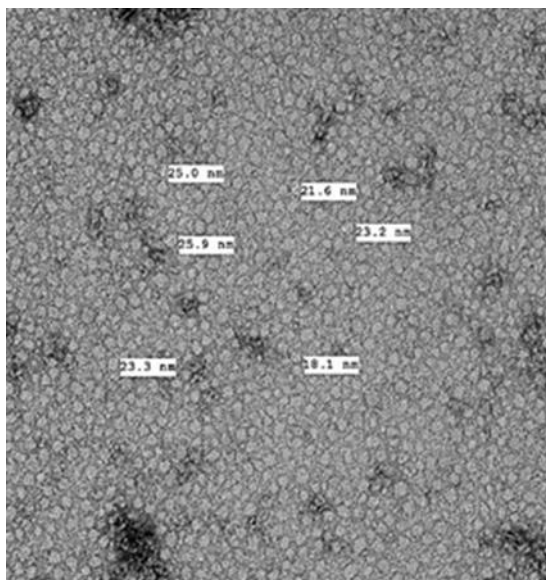


Figure 15. Representative image of DSPE-AP nanocarriers imaged at 13,500 magnification.

5.2.6. *Determination of nanoformulation loading and encapsulation efficiency*

HPLC-DAD analysis was employed to study drug loading and encapsulation efficiency of the nanoformulations, following the method previously described in section 1.2.3. The percentage of drug loading (DG) and encapsulation efficiency

(EE) was calculated using the following equations:

$$DG (\%) = \frac{\text{Determined mass of drug within nanocarriers}}{\text{Mass of drug – loaded nanocarriers}} \times 100$$

$$EE (\%) = \frac{\text{Determined mass of drug within nanocarriers}}{\text{Theoretical mass of drug within nanocarriers}} \times 100$$

5.2.7. MIN6 cell culture

MIN6 beta cells from mice (originally from Prof. Jun-ichi Miyazaki, Osaka University, Osaka, Japan) were kindly provided by Dr. Bo Liu (Department of Diabetes, King's College London, London, United Kingdom) at passage 35. Cells stored at cryogenic temperatures (-196°C) in a liquid-nitrogen freezer were reconstituted by placing them in incubator with an atmosphere of 95% air and 5% CO₂ for 10 min. Subsequently, cells were transferred to a 15 ml centrifuge tube followed by the addition of 5 ml of fresh growth medium. The cell suspension finally underwent centrifugation at 5000 RPM for 5 min and the pellet was resuspended in a 75 cm² T-flasks containing 10 ml of fresh growth. Complete Dulbecco's Modified Eagle Medium (DMEM)—GlutaMax[®], pH 7.4 supplemented with 1% antibiotic/antimycotic solution, 15% Fetal Bovine Serum (FBS) was used for MIN6 culture. Cells were incubated in an atmosphere of 95% air and 5% CO₂ at constant humidity. Stock cultures were grown at 37 °C in 75 cm² T-flasks, with the medium replaced every two days. Cells were seeded in 12-well plates or 6-well plates for all experimental procedures. MIN6 cells reached confluence within day 5 after seeding. At this time, small clusters of cells were formed (Figure 16), indicating that the cells were assembled as physiologically relevant mature pseudoislets and were viable and functional [186].

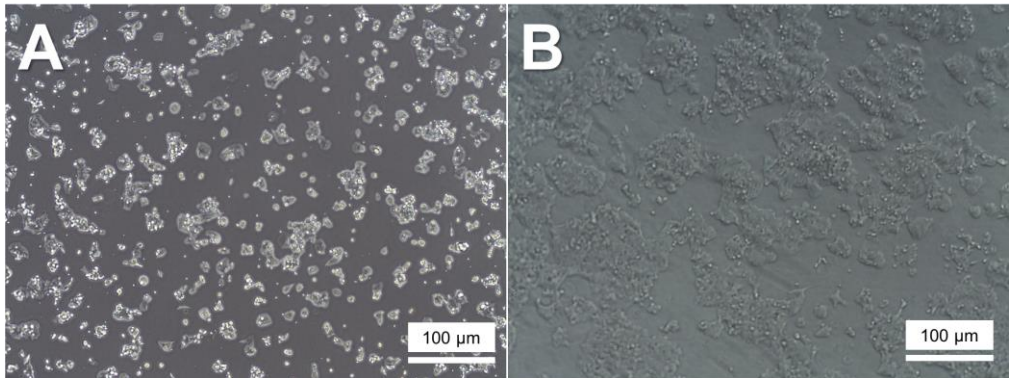


Figure 16. Growth pattern of MIN6 cells into mature pseudoislets. Stock MIN6 cell cultures were grown at 37°C in 75 cm² T-flasks, replacing the medium every two days. Cells were seeded in 12-well plates with density of 75×10^4 cells/cm² for all experimental cultures (panel A). MIN6 cells reached confluence on day 5 post-seeding by which point the phenotype of small clusters of cells (pseudoislets) was formed, indicating the cells were functional and capable of secreting insulin (panel B). Cells were imaged through a microscope at 10x magnification.

5.2.8. *Determination of cell viability by MTT assay*

To assess any potential cytotoxicity of the testing samples (free-ABA, free-TNE, NF-ABA, and NF-TNE) on MIN6 beta cells, cells were incubated with each sample at three different ABA concentrations (0.001, 0.01, and 0.1 µM) or media (MEM) for 24, 48, and 72 hours. After each incubation time, a volume of 20 µL of 3-(4,5-Dimethylthiazol-2-yl)-2,5-diphenyltetrazolium bromide (MTT) solubilized in sterile DPBS was added to the wells at the concentration of 5 mg/mL [187]. Cells were further incubated at 37 °C for 4 hours, and the resulting formazan crystals were then dissolved in 100 µL of DMSO, following aspiration. Plates were ultimately incubated on The MaxQ 4000 benchtop orbital shaker (Thermo Fisher Scientific, Loughborough, UK) at 75 rpm for 15 min to ensure the DMSO was mixed well. Absorbance was measured at 570 nm and compared to control cells (MEM).

5.2.9. Cellular antioxidant activity (CAA) assay

The cellular antioxidant activity (CAA) assay was conducted to assess and compare the antioxidant power and cellular accessibility of the formulated and unformulated samples at varying concentrations. To this end, a pre-incubation with a cell-permeable 2',7'-Dichlorofluorescein diacetate (DCFH-DA) fluorescence probe dye is performed. DCFH-DA is indeed deacetylated by cellular esterase and turns into its fluorescent form DCFH upon oxidation triggered by the addition of iron (100 μM) as a prooxidant agent. The cellular antioxidant activity was measured based on a slightly modified protocol of the original assay developed by Wolfe and colleagues [188], as reported by previous works [189]. MIN6 cells were first cultured in a 96-well black fluorescence cell culture plate until reaching confluence. Cells were then washed with DPBS and treated with 200 μL of one of the testing samples (free-ABA, free-TNE, NF-ABA, and NF-TNE) at the same ABA concentration (0.05 μM) for 1 h at 37 $^{\circ}\text{C}$. Subsequently, cells were washed with MEM and mixed with 200 μL of DCFH-DA (100 μM) and further incubated for 30 min at 37 $^{\circ}\text{C}$. Following aspiration, each well was treated with 100 μL of iron 00 μM . Cell fluorescence was read every 5 min for 1 h at 528 and 485 nm emission and excitation wavelength, respectively, using a Fluostar Optima Fluorescence Plate Reader. The bioflavonoid Quercetin, ranging from 0 to 2000 μM , was used as a positive control. Based on the hypothesis of the assay, quercetin and test antioxidant samples inhibit the formation of free radicals, and thus DCF formation, in a concentration dependent manner. The CAA units were calculated using the following equations:

$$\mathbf{CAA\ unit} = 100 - \frac{\text{AUC of the treatment}}{\text{AUC of the control}} \times 100$$

$$\mathbf{AUC} = \left(1 + \left(\frac{\text{RFU1}}{\text{RFU0}}\right) + \left(\frac{\text{RFU2}}{\text{RFU0}}\right)\right),$$

where RFU0 is the relative fluorescence value of time zero and RFU_x is the relative fluorescence at each time point (e.g., RFU10 is the relative fluorescence value at minute 10). The results of the positive control Quercetin were also reported as IC₅₀, while the samples antioxidant values were expressed as both CAA units and Quercetin equivalents (QE).

5.2.10. MIN6 cells exposure to glucose and iron at different concentrations

Cells were seeded at 75×10^4 cells/cm² for the glucose-stimulated insulin secretion (GSIS) and the iron challenge assay. The day before the experiment MIN6 cells were iron depleted with a serum-free MEM media (glucose 5.5 mM, supplemented with 2 mM L-glutamine and 1% antibiotic/antimycotic) and incubated overnight at 37°C with 5% CO₂. For the GSIS experiment, MIN6 cells were washed with DPBS and preincubated in a Krebs–Ringer Bicarbonate (KRB) buffer (119 mM NaCl, 4.74 mM KCl, 2.54 mM CaCl₂·6H₂O, 1.19 mM KH₂PO₄, 1.19 mM MgSO₄·7H₂O, 25 mM NaHCO₃, 10 mM HEPES, pH 7.4, and 1% BSA) containing 1.1 mM glucose (basal level) for 2.5 h. As regards the iron challenge assay, cells were incubated in a KRB buffer containing a high iron concentration (100 μM) for 2.5 h. Afterward, as reported in Table 16, an aliquot of the supernatant was collected for T0 analysis and cells were then preincubated for 30 minutes with the different sample treatments (free-ABA, free-TNE, NF-ABA, NF-TNE). A negative control (represented by MEM) was also tested. Finally, media was aspirated from all the wells, followed by 2 h exposure to KRB solution at two glucose concentrations, which were 5.5 mM (physiological glucose concentration) and 20 mM (supraphysiologic glucose concentration). Immediately after the exposure to glucose, the supernatants were collected at different time points of analysis (i.e. T5, T10, T30, T60 minutes), while cells were lysed at the end of the incubation time (60

min). All supernatants and cell lysates were aliquoted and stored at -20°C, to use them for multiple experiments, avoiding freeze-thaw cycles.

Table 16. List of samples at different glucose and iron concentrations.

Treatment	Abbreviation	Glucose Concentration (mM)	Iron Concentration (µM)
DSPE-PEG/AP nanoformulation of TNE	NF-TNE 1	5.5	0
	NF-TNE 2	20	0
	NF-TNE 3	5.5	100
	NF-TNE 4	20	100
DSPE-PEG/AP nanoformulation of ABA	NF-ABA 1	5.5	0
	NF-ABA 2	20	0
	NF-ABA 3	5.5	100
	NF-ABA 4	20	100
Free nanocarriers	BLK-NF 1	5.5	100
	BLK-NF 2	20	100
Free TNE	Free-TNE 1	5.5	0
	Free-TNE 2	20	0
	Free-TNE 3	5.5	100
	Free-TNE 4	20	100
Free ABA	Free-ABA 1	5.5	0
	Free-ABA 2	20	0
	Free-ABA 3	5.5	100
	Free-ABA 4	20	100
Media (MEM)	Ctrl-Glu 1	5.5	0
	Ctrl-Glu 2	20	0
	Ctrl-Iron 1	5.5	100
	Ctrl-Iron 2	20	100

Figure 17 shows the workflow of the metabolic experiment at different glucose and iron concentrations.

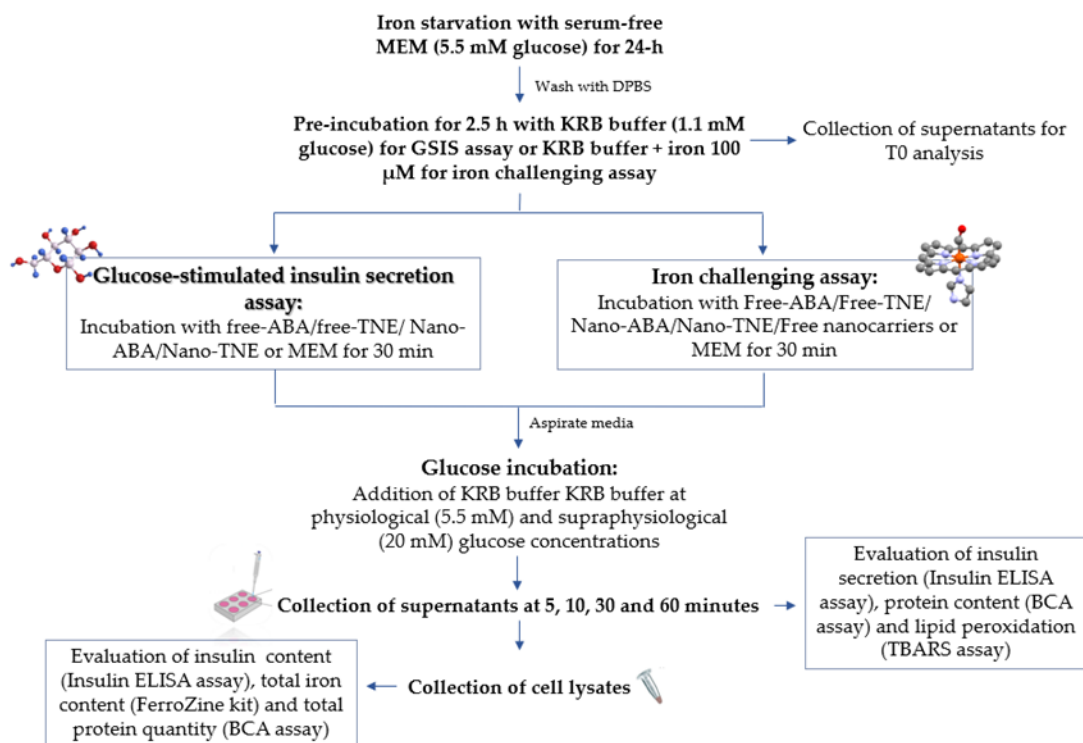


Figure 17. Workflow of metabolic experiments at different glucose and iron concentrations.

5.2.11. Cell harvesting

All steps for cell harvesting were carried out at 4 °C by keeping the experiment plates on an ice tray. A NaOH 40 mM solution was prepared from the 1 M NaOH stock using Milli-Q water as a diluent. The cell lysis buffer was prepared by adding 140 μl PIC and 14 ml of 50 mM NaOH stock solution. Firstly, media was aspirated from the wells. Then, a volume of 350 μl or 175 μl of lysis buffer was added to each well of 6-well plates and 12-well plates, respectively. Plates were then incubated on a plate rocker (8 rpm) for 40 minutes. The resulting cell lysates were collected using a sterile cell scraper and collected into microcentrifuge tubes. Using a 1 ml syringe

with 25-gauge needles, each lysate sample was passed six times to resuspend the lysates and reduce viscosity. Samples were immediately stored at -20° until analysis.

5.2.12. Intracellular total iron quantification

Intracellular total iron content was quantified using an optimized FerroZine™-based iron protocol developed by Reimer et al., with slight modifications [190]. Briefly, 200 µL of 0.1M HCl solution was added to tubes containing 200 µL of the sample, while 200 µL of 50 mM NaOH solution was used for tubes containing 200 µL of each standard of iron (from 0 to 120 µM). A blank solution was represented by 400 µl of 50 mM NaOH. Subsequently, a volume of 200 µl of the freshly prepared iron-releasing agent, consisting of an equal volume of 1.4 M HCl and 4.5% (w/v) KMnO₄ solution, was added to each tube to promote the iron release from proteins, including ferritin [191]. Samples were incubated for 2 hours in a 60 °C dry bath within a fume hood and then cooled to room temperature for 10 mins. Afterwards, a volume of 60 µL of the iron detection reagent (6.5 mM FerroZine™, 2.5 M ammonium acetate, and 1 M ascorbic acid dissolved in water) was mixed to each tube and samples were incubated at 25° for 60 min. Lastly, a volume of 200 µL from standard and sample tubes was placed in duplicate into a 96-well and the colour development was spectrometrically monitored by measuring the absorbance at 550 nm using a microplate reader. Intracellular iron concentration was determined by normalizing the obtained results against the total protein content of each well evaluated by the BCA (bicinchoninic acid) assay.

5.2.13. Evaluation of insulin secretion

Measurement of insulin secretion is considered pivotal for the investigation of β-cell function. To this aim, supernatants were obtained from MIN6 cells exposed to

different concentrations of glucose and iron at various time points (T0, T5, T10, T30, T60 minutes) to determine the temporal profile of insulin secretion under these conditions and were then analyzed by insulin ELISA assay. Briefly, a volume of 10 μ L of standards and samples was transferred into a 96-well plate in duplicate followed by the incubation steps, as described by the manufacturer's protocol. Finally, the absorbance was measured at 450 nm using a microplate reader.

5.2.14. Statistical analysis

For all the experiments, the mean of at least four replicates was calculated for each condition, with the data expressed as mean \pm standard error mean (SEM), otherwise stated. The MTT results were statistically analyzed using one-way analysis of variance (ANOVA) followed by Dunnett's post hoc test and two-way ANOVA followed by Sidak's posthoc test. The results about the total iron quantification were analyzed by two-way ANOVA followed by Sidak's posthoc test. A two-tailed Student's t-test was used for CAA results, while two-way ANOVA followed by Tukey's multiple comparisons post hoc test was used to analyze the insulin ELISA results (PRISM software package, Version 8, Graphpad Software Inc., San Diego, USA).

5.3. Results

5.3.1. Size, charge, and loading efficiency

In all cases, the NF was found to be in the nanometer size range. This data is in line with the project objectives, as the aim was to create nanocarriers loaded with bioactive compounds, as particles in this size range may exhibit enhanced cellular uptake and longer drug retention time in the bloodstream by potentially avoiding

phagocytic clearance. The incorporation of AP resulted in an increase in the particle size of the NF, although in all cases the bioactive-loaded NFs were smaller compared to the corresponding blanks. The zeta potential results do not differ significantly between the formulations but show a shift towards a positive charge in the case of ABA and TNE NF compared to the blank. Overall, these data are also in general agreement with the results of previous studies using a similar carrier system for iron delivery [178]. Furthermore, the results of the loading efficiency of the nanocarriers reveal a very high encapsulation of 95% and 99 % in the case of the ABA and TNE formulations, respectively. These results demonstrate the successful incorporation of both ABA and TNE into the carrier systems. High encapsulation efficiency allows the delivery of a higher payload with a lower dose and is a desirable property in formulation design. The observed high encapsulation efficiency demonstrates the suitability of the carrier system and the formulation method used for the entrapment of both the bioactive ABA and TNE.

5.3.2. *Assessment of cellular viability*

The results shown in Figure 18 demonstrate the effects of the tested samples (free-ABA, free-TNE, NF-ABA, and NF-TNE) at three different ABA concentrations (0.001, 0.01, and 0.1 μM) on MIN6 cell viability at 24, 48, and 72 h. As evident, all cells exposed at the ABA concentration of 0.001 and 0.01 μM did not show reduced cell viability, whereas 0.1 μM ABA concentration caused a significant reduction of cell survival in the Free-ABA ($p < 0.05$ vs Ctrl at 72-h), NF-ABA ($p < 0.001$ vs Ctrl at 24-h) and NF-TNE ($p < 0.0001$ vs Ctrl at 24-h) groups. Interestingly, the 24-h incubation with Free-TNE was demonstrated to significantly increase cell viability for all ABA concentrations tested ($p < 0.001$ vs Ctrl). Moreover, a clear trend of increase in MIN6 cell survival was observed over the 72-hour incubation

period in both NF-ABA and NF-TNE groups at most of the concentrations tested, compared to the control.

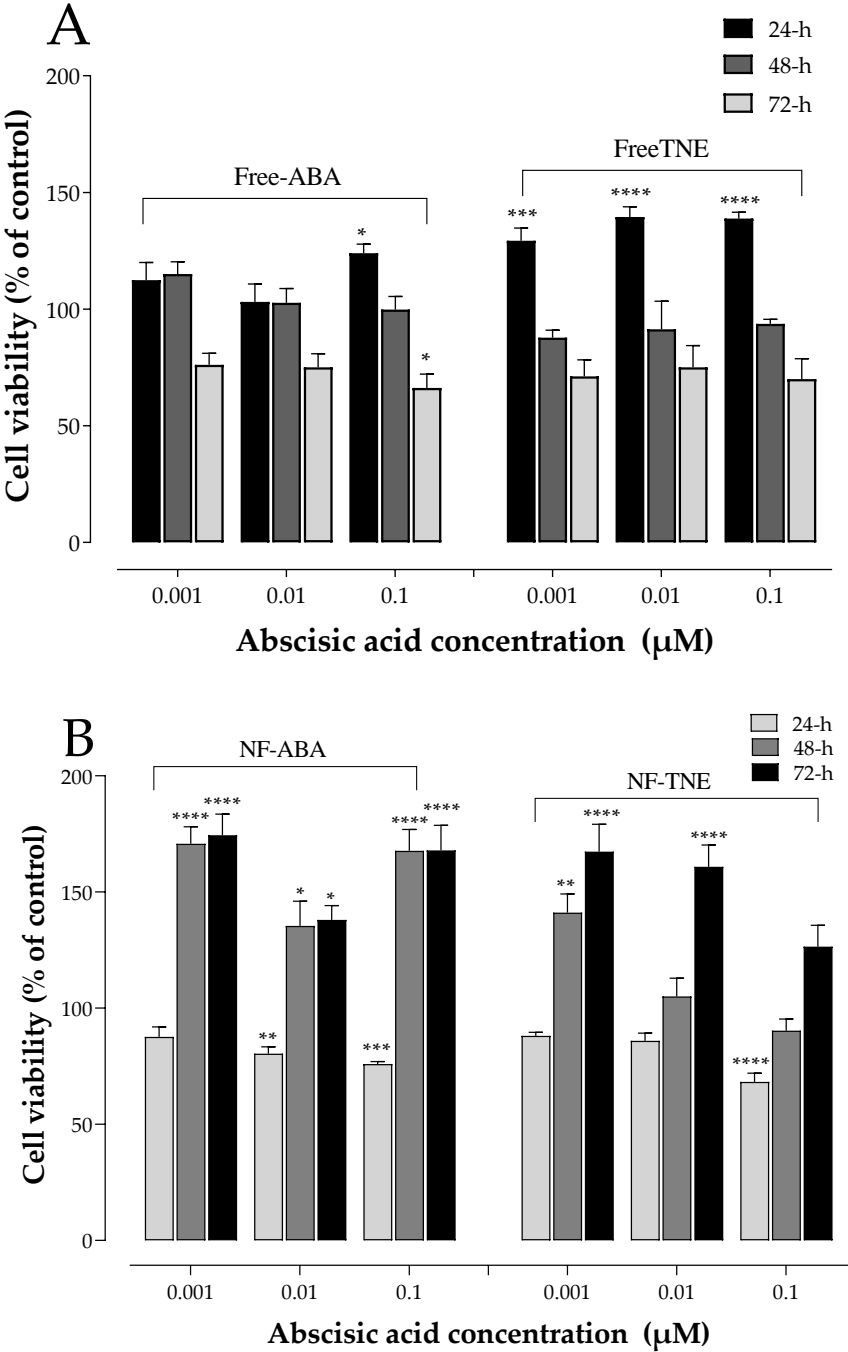
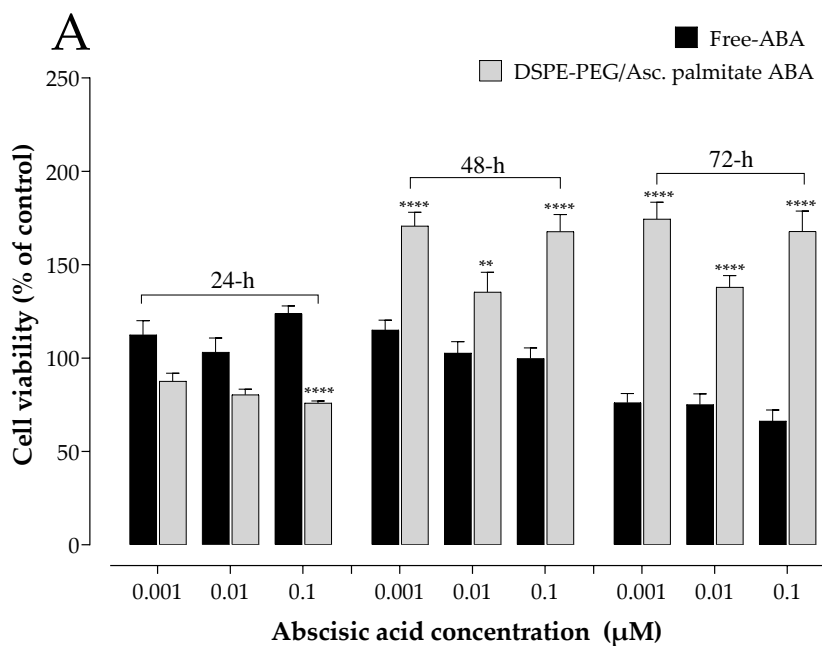


Figure 18. MTT analysis on MIN6 cell viability at 24, 48, and 72 hours. (A) Cells treated with free-ABA and free-TNE; (B) Cells treated with NF-ABA (ascorbyl palmitate/DSPE-PEG nanoformulated abscisic acid) and NF-TNE (ascorbyl palmitate/DSPE-PEG nanoformulated thinned nectarine extract); values are presented as means \pm S.D. of 4 replicates. ABA (0 μ M) was regarded as a control in this analysis; data were analyzed with one-way ANOVA followed by Dunnett's post hoc test; * $p \leq 0.05$, ** $p \leq 0.01$, *** $p \leq 0.001$, **** $p < 0.0001$, significantly different from the control group. ABA, abscisic acid; TNE, thinned nectarine extract.

Similarly, the increased cell viability observed in the nanoformulated samples was significantly higher compared to free samples at the same ABA concentrations (Figure 19). Besides the novel results in terms of ameliorated cell survival for the nanoformulated samples, these data indicated that concentrations lower than 0.1 μ M ABA did not compromise β -cell viability in all cases. Based on the outcomes of these experiments, an intermediate ABA concentration of 0.05 μ M was therefore selected for further experiments involving the investigation of the role of the various samples in regulating MIN6 cell function, as this concentration can be regarded as the compromise that may evoke functional effects without compromising cell viability.



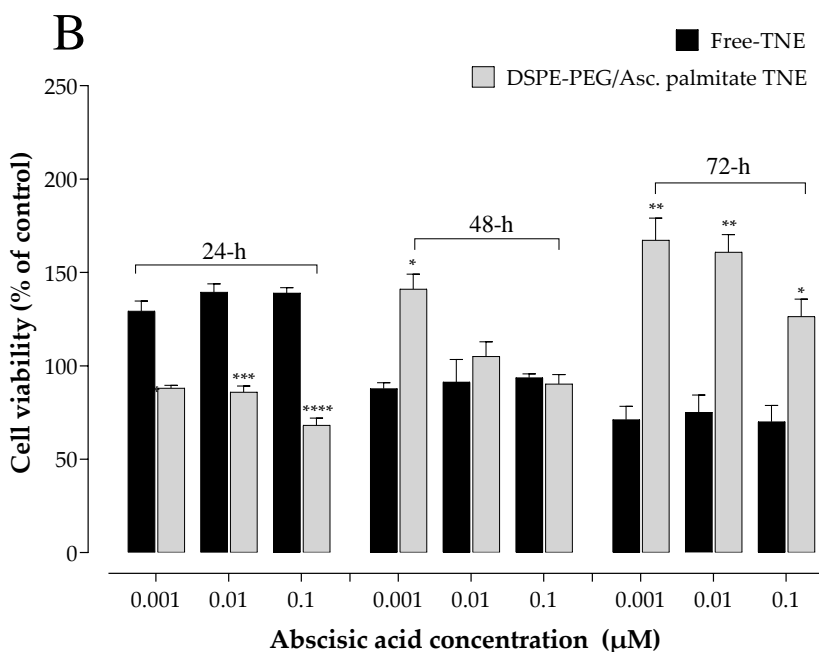


Figure 19. MTT results of 24-, 48- and 72-hours pre-treatment with (A) DSPE-PEG/Ascorbyl palmitate nanoformulated ABA and Free ABA, (B) DSPE-PEG/Ascorbyl palmitate nanoformulated TNE and Free TNE on MIN6 cells; values are presented as means \pm SEM of 4 replicates. ABA (0 μ M) was regarded as a control in this analysis; data were analyzed with two-way ANOVA followed by Sidak's posthoc test; * $p < 0.05$, ** $p < 0.01$, *** $p < 0.001$, **** $p < 0.0001$ vs not nanoformulated sample at the same treatment concentrations; ABA, abscisic acid; TNE, thinned nectarine extract; DSPE-PEG,1,2-distearoyl-sn-glycero-3-phosphatidylethanolamine-N-(polyethylene glycol-2000).

5.3.3. Determination of cellular antioxidant activity

As reported in the Materials and methods section, the bioflavonoid Quercetin, ranging from 0 to 2000 μ M, was used as a positive control. This latter showed to exert cellular antioxidant activity in a concentration-dependent manner, with an IC_{50} value of 482.7 μ M (Figure 20).

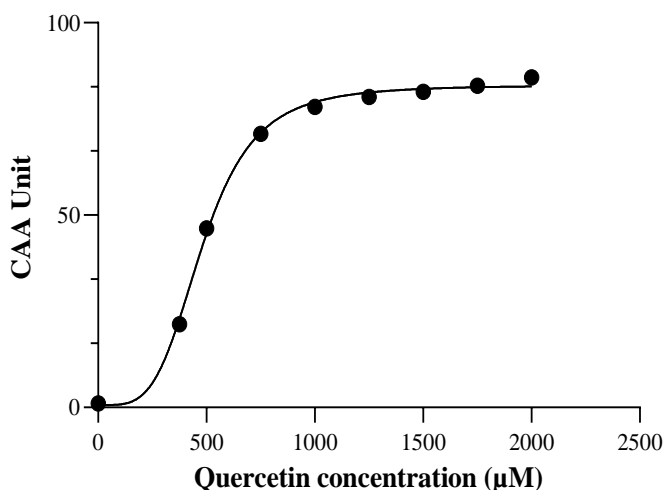


Figure 20. Cellular antioxidant activity of the positive control Quercetin at different concentrations (0-2000 μM); values are presented as means \pm S.D. of 6 replicates.

Furthermore, as shown in Figure 21, Free-ABA did not demonstrate to counteract oxidative stress in our experiment, while the results obtained with TNE treatment showed the ability of this vegetal extract to exert cellular antioxidant properties when cells endure oxidative stress (CAA units: 42.17 ± 4.92 ; Quercetin Equivalents: $482.64 \mu\text{M}$). However, the nanoformulated form of TNE (NF-TNE) showed significantly higher antioxidant activity compared with the Free-TNE sample (CAA units: 83.81 ± 0.74 ; Quercetin Equivalents: $1589.39 \mu\text{M}$; $p < 0.001$ vs Free-TNE).

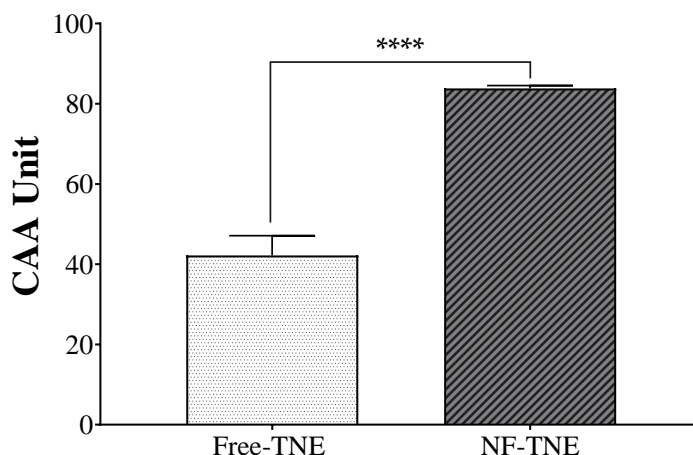


Figure 21. Cellular antioxidant activity (CAA) assay results of nanoformulated and unencapsulated TNE. Values are presented as means \pm S.D. of 6 replicates; data were analyzed with two-tailed Student's t-test; **** $p < 0.0001$, significantly different from not nanoformulated samples at the same treatment concentration (ABA 0.05 μ M); NF-TNE, ascorbyl palmitate/DSPE-PEG nanoformulated TNE; TNE, thinned nectarine extract.

5.3.4. Evaluation of total cellular iron content

For the iron challenge assay, MIN6 cells were pre-incubated in the presence of 100 μ M iron before the addition of glucose at both physiological (5.5 mM) and supraphysiological (20 mM) levels. Evaluation of total iron content in the cell lysates allows us to assess if the exposure to high iron levels results in a proportional higher accumulation of iron into MIN6 cells. In this regard, as shown in Figures 22 and 23, greater iron content was exhibited in all cells pre-incubated with iron, compared to cells incubated with the same glucose concentration without iron. Additionally, the ANOVA analysis showed that this increase was found to be significant for almost all the samples tested. The highest iron content was exhibited upon treatment with 100 μ M iron and at 5.5 mM glucose in cells treated with NF-ABA, demonstrating a 5-fold increase compared to the same condition without iron incubation. Thus, cellular iron levels were shown to be increased in all cases, demonstrating that iron

uptake increases in response to iron exposure, and the presence of the nanoformulation system does not adversely interfere with cellular iron uptake.

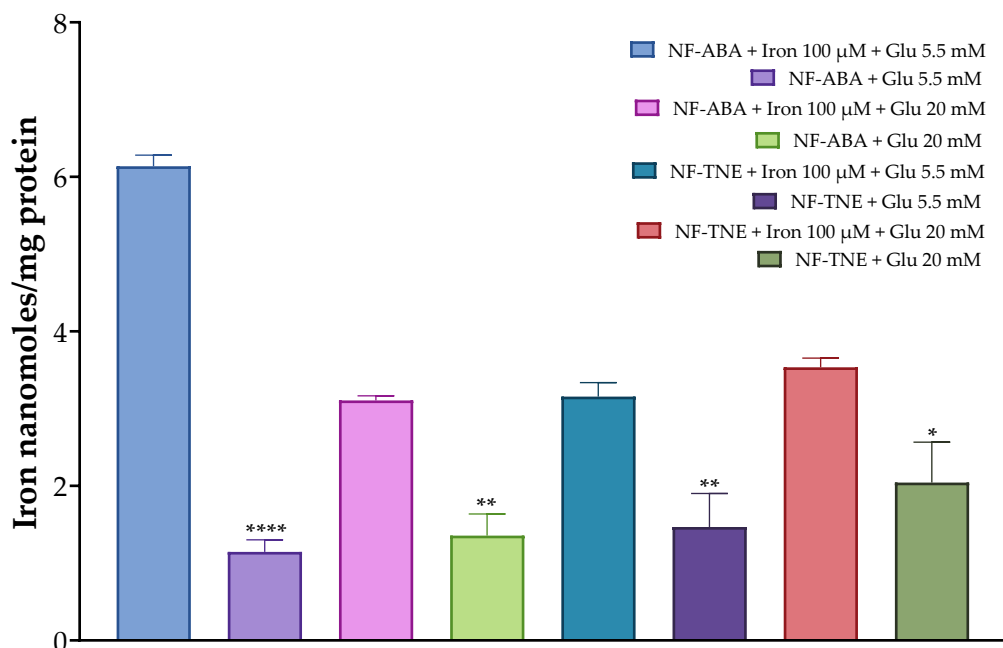


Figure 22. Effects of iron (100 μM) preincubation on MIN6 cells. The data represent mean ± SEM, n = 4. Data were analyzed with one-way ANOVA followed by Sidak's posthoc test; * $p \leq 0.05$, ** $p \leq 0.01$, *** $p \leq 0.001$, **** $p \leq 0.0001$ significantly different from samples incubated without iron at the same glucose concentration. Abbreviations: Glu, glucose; NF-ABA, ascorbyl palmitate/DSPE-PEG nanoformulated abscisic acid; NF-TNE, ascorbyl palmitate/DSPE-PEG nanoformulated thinned nectarine extract.

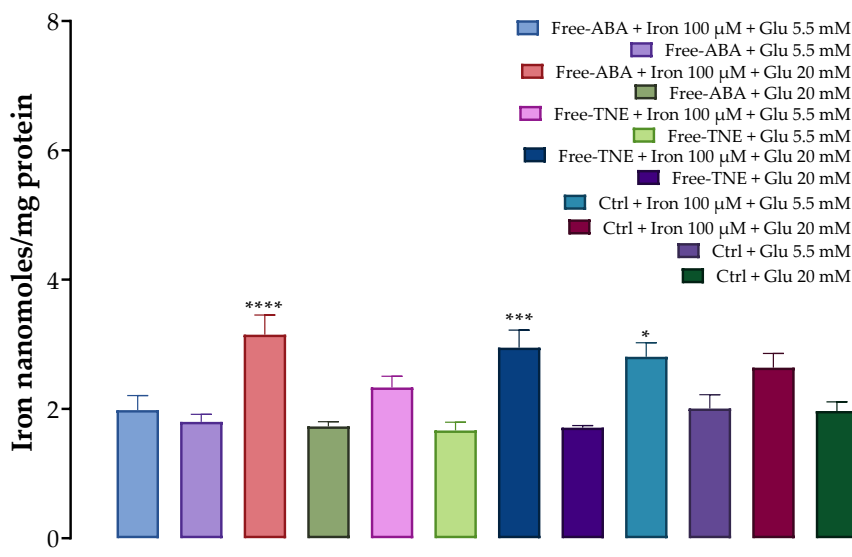


Figure 23. Effects of iron (100 μM) preincubation on MIN6 cells. The data represent mean \pm SEM, $n = 4$. Data were analyzed with one-way ANOVA followed by Sidak's posthoc test; $*p \leq 0.05$, $**p \leq 0.01$, $***p \leq 0.001$, $****p \leq 0.0001$ significantly different from samples incubated without iron at the same glucose concentration. Abbreviations: ABA, abscisic acid; Ctrl, control (MEM); TNE, thinned nectarine extract.

5.3.5. Effects of glucose and iron on MIN6 cell's insulin secretion

The first result that can be highlighted relates to the different insulin responses observed after incubation with two different glucose concentrations (5.5 mM and 20 mM) and the combination of glucose and iron exposure in our cellular model. As indeed shown in Figure 24, a significant increase in insulin AUC was observed in the Ctrl group incubated with 20 mM glucose compared to the group incubated with glucose 5.5 mM ($p < 0.05$). Of note, pre-incubation with high levels of iron (100 μM) dramatically decreased insulin secretion in the Ctrl groups at both glucose concentrations, suggesting that treatment with this prooxidant agent was responsible for the functional disruption in the MIN6 cells subjected to the iron-

challenging experiments. As reported in the following sections, this reduction in insulin AUC observed after iron incubation was reproducible for all conditions.

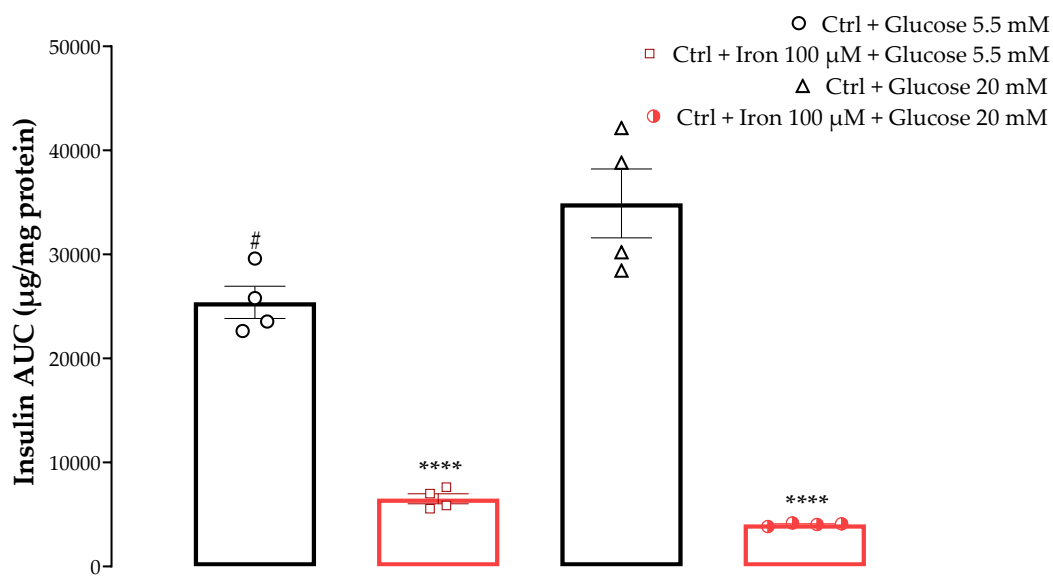


Figure 24. The effect of treatment with two different concentrations of glucose (5 mM and 20 mM) w/wo iron (100 µM) on MIN6 cells insulin secretion. The data represent mean \pm SEM, n = 4. Data were analyzed with one-way ANOVA followed by Tukey's multiple comparison test; * $p \leq 0.05$, ** $p \leq 0.01$, *** $p \leq 0.001$, **** $p \leq 0.0001$ significantly different from Ctrl samples incubated with the same glucose concentrations without iron; # $p \leq 0.05$ significantly different from Ctrl + Glucose 20 mM. Abbreviations: AUC, area under the curve; Ctrl, control (MEM).

5.3.6. Assessment of insulin secretion in GSIS experiment

As shown in Figure 25, in cells incubated with physiological glucose levels (5.5 mM) a statistical increase in insulin AUC was observed in the NF-TNE group ($p < 0.05$ vs Ctrl group), resulting in a 40% increase in AUC compared with the Ctrl group. In contrast, the other treatment groups showed no significant effects on insulin secretion in MIN6 cells. A similar trend can be observed in cells incubated with supraphysiological glucose levels (20 mM), as treatment with each of the samples

tested showed no significant changes in insulin AUC, although a slight increase was observed in the NF-TNE group (+ 8.2% vs Ctrl group).

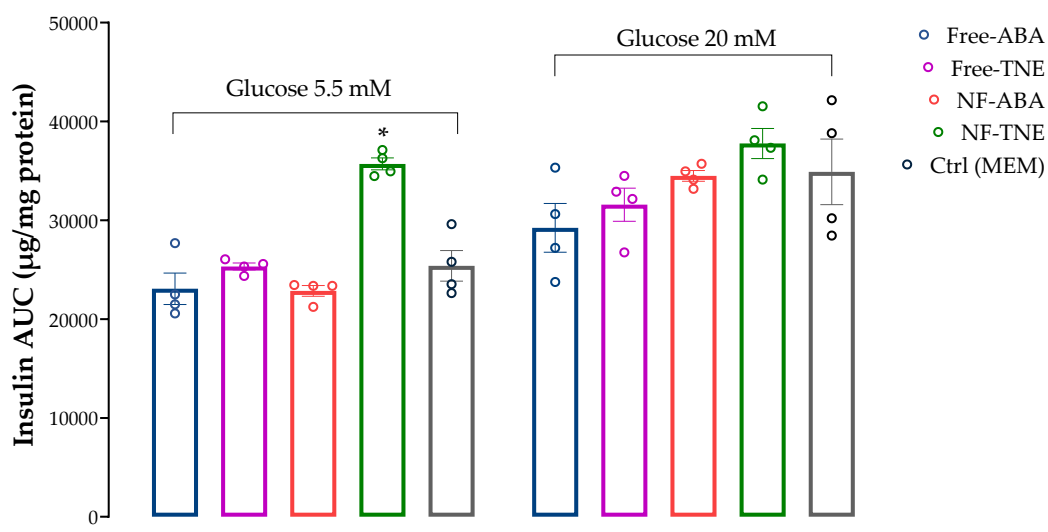
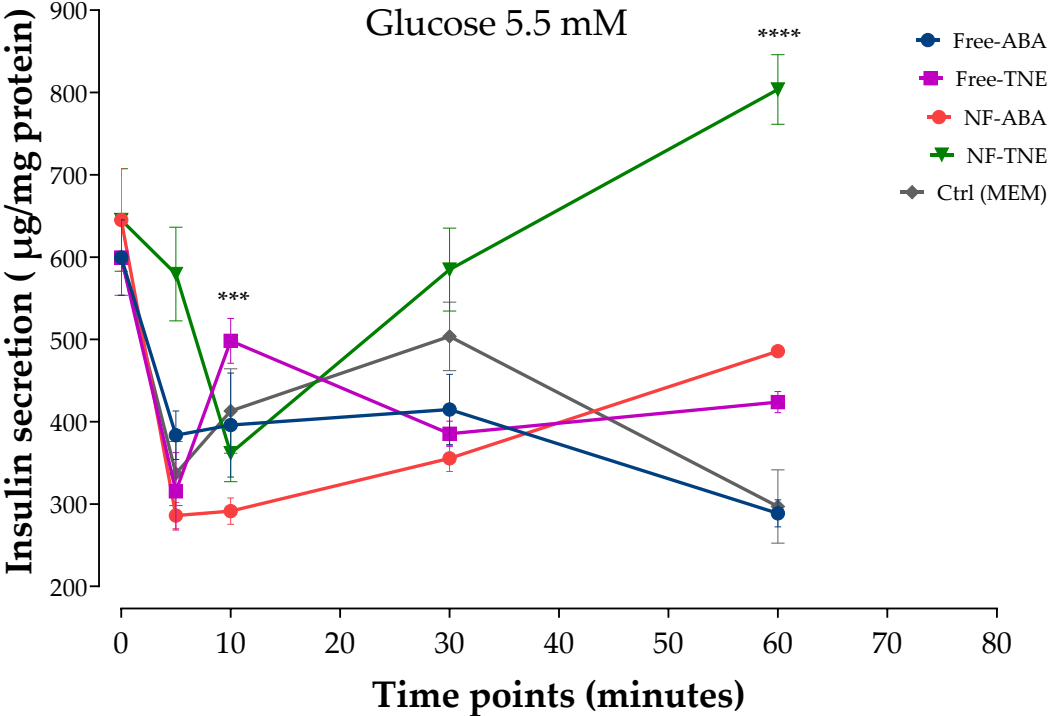


Figure 25. The effect on MIN6 cells insulin secretion after incubation with two different glucose concentrations (5.5 mM and 20 mM). Unencapsulated abscisic acid (Free-ABA), unencapsulated thinned nectarine extract (Free-TNE), ascorbyl palmitate/DSPE-PEG nanoformulated abscisic acid (NF-ABA), ascorbyl palmitate/DSPE-PEG nanoformulated thinned nectarine extract (NF-TNE) and MEM (Ctrl) were used as treatments. The data represent mean \pm SEM, $n = 4$. Data were analyzed with one-way ANOVA followed by Tukey's multiple comparison test; $*p \leq 0.05$, $**p \leq 0.01$, $***p \leq 0.001$, $****p \leq 0.0001$ significantly different from the Ctrl sample at the same glucose concentrations. Abbreviations: AUC, area under the curve AUC; Ctrl, control.

Furthermore, if we consider insulin secretion at the various sample collection time points (Figure 26), incubation with both 5.5 mM and 20 mM glucose concentrations resulted in a biphasic insulin secretion profile in our model. The two peaks of secretion are observed at T5 and T60 min. These two peaks may be explained in a physiological context by the rapid release of preformed insulin from cellular granules docked at the periphery of the cells, and the subsequent release of insulin granules that were newly synthesized and more gradually transported from within the cellular organelles to be exocytosed [192]. In addition, the NF-TNE group

showed a statistical increase in insulin secretion at both T5 and T60 min in cells incubated with 5.5 mM glucose, ($p < 0.001$ vs Ctrl), or only at T5 when cells were incubated with 20 mM glucose ($p < 0.01$ vs Ctrl, Figure 26). In contrast, a significant reduction ($p < 0.001$) in insulin release at T60 was observed in the Free-ABA group compared with the Ctrl group in response to 20 mM glucose exposure. Since there is no clear explanation for this result based on the available scientific available data, it remains to be further investigated and elucidated as this is possible within the scope of the current work.



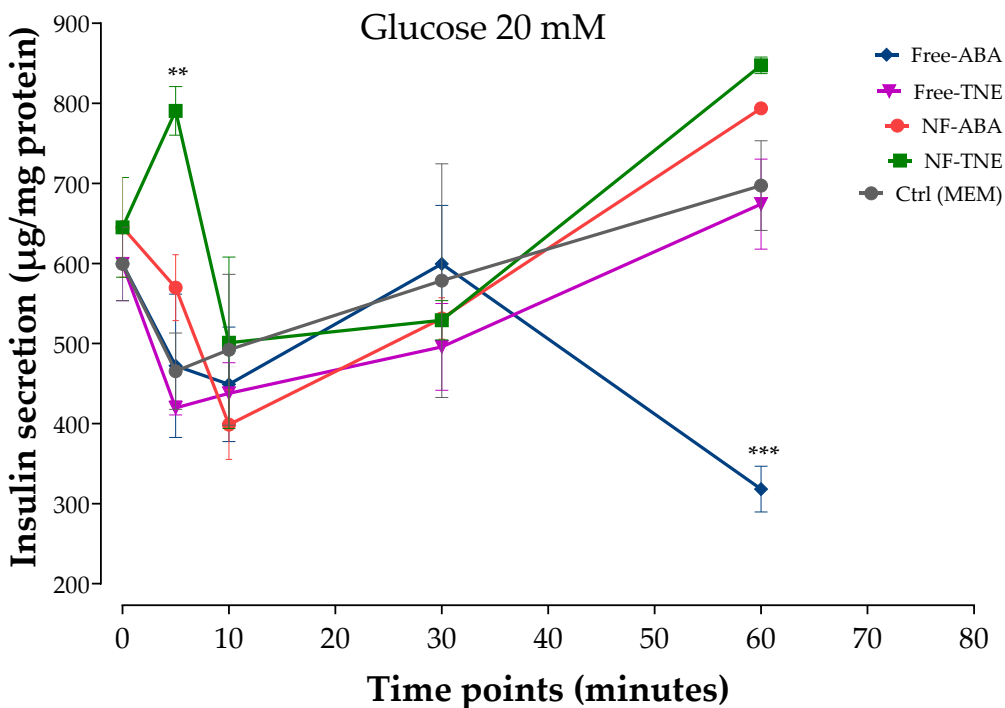


Figure 26. The effect on MIN6 cells insulin secretion after incubation with glucose 5.5 mM (upper graph) and glucose 20 mM (lower graph). Insulin secretion was evaluated at different time points of analysis (T0, T5, T10, T30, and T60 minutes). Unencapsulated abscisic acid (Free-ABA), unencapsulated thinned nectarine extract (Free-TNE), ascorbyl palmitate/DSPE-PEG nanoformulated abscisic acid (NF-ABA), ascorbyl palmitate/DSPE-PEG nanoformulated thinned nectarine extract (NF-TNE) and MEM (Ctrl) were used as treatments. The data represent mean \pm SEM, $n = 4$. Data were analyzed with two-way ANOVA followed by Tukey's multiple comparison test; * $p \leq 0.05$, ** $p \leq 0.01$, *** $p \leq 0.001$, **** $p \leq 0.0001$ significantly different from Ctrl sample (MEM) at the same time point of analysis.

5.3.7. Assessment of insulin secretion in the iron-challenge assay

Interestingly, as shown in Figure 27, significantly higher insulin AUC values were observed for all test samples compared with the Ctrl group in both experiments that included preincubation with high iron levels (100 μ M). Notably, the highest insulin response was obtained in the NF-TNE group, exhibiting 54% higher insulin levels compared with the Ctrl group, ($p < 0.0001$). Similar to results from the GSIS

experiment, the nanoformulated samples showed a greater effect on insulin release compared to unencapsulated treatments. Another interesting result is related to the cells incubated with high glucose and iron concentrations (Figure 27). In this regard, significantly higher insulin secretion was observed at the same significance level for all test groups compared with the Ctrl group ($p < 0.0001$ vs Ctrl group). These results are consistent with observations in the previous section, as the highest insulin concentration was achieved in the NF-TNE group (+235% vs Ctrl group).

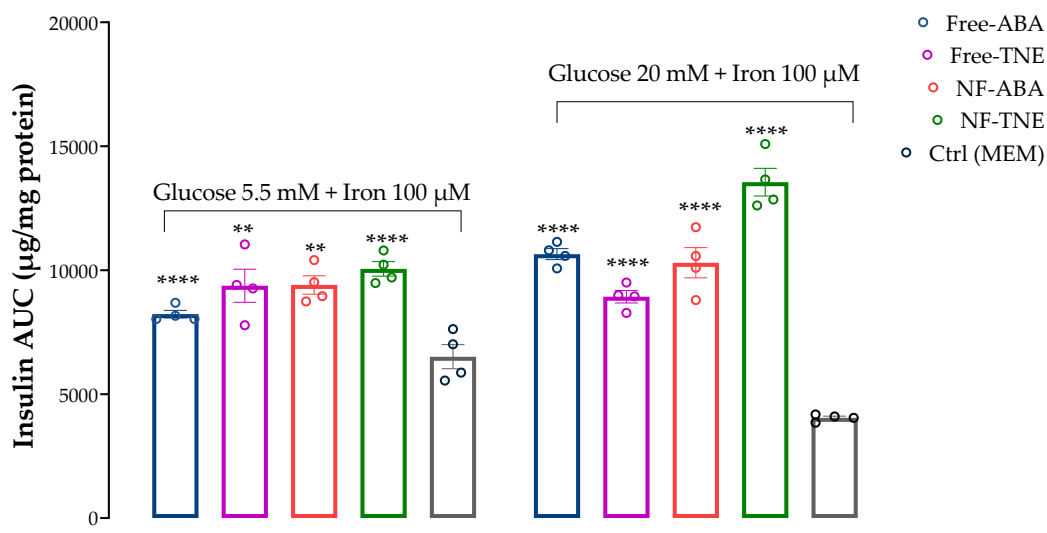
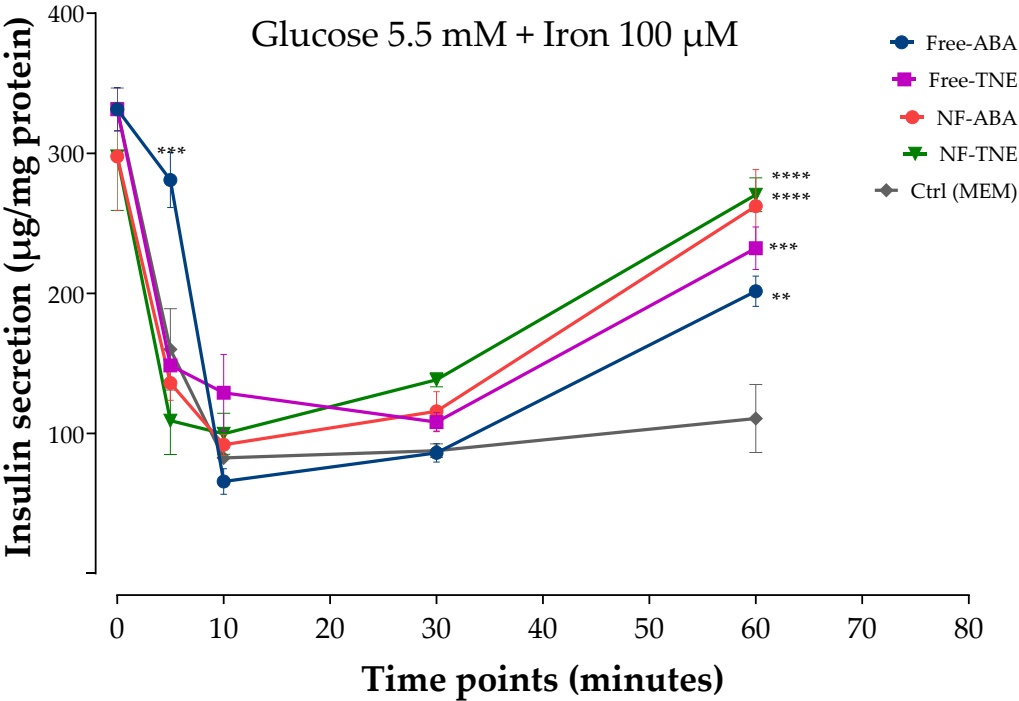


Figure 27. The effect on MIN6 cells insulin secretion after incubation with two different glucose concentrations (5.5 mM and 20 mM) and high iron levels (100 µM). Unencapsulated abscisic acid (Free-ABA), unencapsulated thinned nectarine extract (Free-TNE), ascorbyl palmitate/DSPE-PEG nanoformulated abscisic acid (NF-ABA), ascorbyl palmitate/DSPE-PEG nanoformulated thinned nectarine extract (NF-TNE) and MEM (Ctrl) were used as treatments. The data represent mean \pm SEM, $n = 4$. Data were analyzed with one-way ANOVA followed by Tukey's multiple comparison test; $*p \leq 0.05$, $**p \leq 0.01$, $***p \leq 0.001$, $****p \leq 0.0001$ significantly different from the Ctrl sample at the same glucose concentrations. Abbreviations: AUC, area under the curve AUC; Ctrl, control.

In terms of insulin response at different analysis time points (Figure 28), the detrimental effect caused by iron incubation can be clearly observed in our cellular model, as only a slight increase in insulin response or a flat-shaped insulin profile

was observed in Ctrl cells incubated with the combination of iron and 5.5 mM glucose or 20 mM glucose, respectively. Nevertheless, as shown in the upper graph of the mentioned Figure, insulin secretion at T5 ($p < 0.001$) significantly increased in the Free-ABA group compared to the Ctrl group, while a clear trend of increase over the incubation period was observed for all the treatment groups, with a significant increase at T60 ($p < 0.01$, $p < 0.001$, $p < 0.0001$ and $p < 0.0001$ for the Free-ABA, Free-TNE, NF-ABA, and NF-TNE groups, respectively, compared with Ctrl group). Finally, following incubation with high glucose and iron levels, a significant increase in insulin levels was detected for all the analysis timepoint in the NF-TNE group, or only at T30 and T60 for the other treatment groups, compared to the Ctrl group (Figure 28, lower graph).



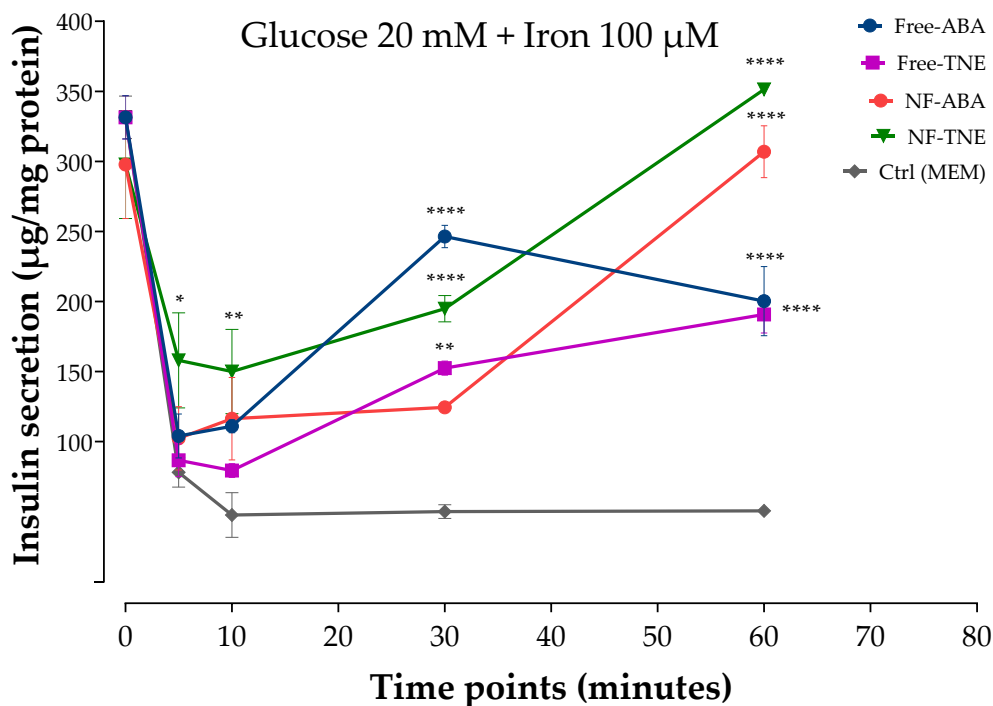


Figure 28. The effect on MIN6 cells insulin secretion after incubation with a combination of glucose 5.5 mM (upper graph) and glucose 20 mM (lower graph) with high iron levels (100 μM). Insulin secretion was evaluated at different time points of analysis (T0, T5, T10, T30, and T60 minutes). Unencapsulated abscisic acid (Free-ABA), unencapsulated thinned nectarine extract (Free-TNE), ascorbyl palmitate/DSPE-PEG nanoformulated abscisic acid (NF-ABA), ascorbyl palmitate/DSPE-PEG nanoformulated thinned nectarine extract (NF-TNE) and MEM (Ctrl) were used as treatments. The data represent mean \pm SEM, $n = 4$. Data were analyzed with two-way ANOVA followed by Tukey's multiple comparison test; * $p \leq 0.05$, ** $p \leq 0.01$, *** $p \leq 0.001$, **** $p \leq 0.0001$ significantly different from Ctrl sample (MEM) at the same time point of analysis.

5.4. Discussion

The first set of experiments of the present work involved the assessment of cell viability on MIN6 cells after treatment with the tested samples (free-ABA, free-TNE, NF-ABA, and NF-TNE) at three different ABA concentrations (0.001, 0.01, and 0.1 μM) at 24, 48, and 72 h. The time points represent short-term to extended chronic

exposure, while the concentrations were selected based upon prior work [32]. In addition to assessing any potential cytotoxic effects of the formulations, another objective of these experiments was to determine the optimum concentration range to be used for further cell exposure experiments involving NF and free ABA/TNE.

An interesting observation was that free-TNE increased MIN6 cell viability at all concentrations at the initial 24 h time point (Figure 18). One probable explanation may be that the TNE extract contains a complex blend of bioactive compounds in addition to ABA, and it is possible that at the initial time point these act in concert at the tested concentration range to evoke an acute proliferative effect on cell viability, which is then gradually blunted over time [155]. Furthermore, as reported in the same figure, a clear trend of increase in MIN6 cell survival was observed over the 72-hour incubation period in both NF-ABA and NF-TNE groups at almost all the concentrations tested, compared to the control group. Similarly, the increased cell viability observed in the nanoformulated samples resulted to be significant compared to free samples at the same ABA concentrations (Figures 19A and 19B). One possible explanation could be that the free compounds in their native unformulated form evoke rapid effects on intracellular organelles, thereby compromising cell viability to some extent. In the case of formulated delivery systems of standards and extracts, the carrier system may facilitate a more gradual and temporal release of its payload into the intracellular environment upon cellular entry [177]. In this way, the observed effects may be sustained and gradually mitigate any potential adverse effects that may occur within the cells following sudden exposure to high levels of bioactive molecules. In addition, the specific composition of nanoformulated samples may influence cell viability. In this regard, the nanoformulations contain ascorbyl palmitate, a stable form of ascorbic acid containing palmitic acid. The presence of the fatty acid palmitic acid may present a nutrient for cells over the 72-h incubation, therefore promoting their eventual proliferation [6]. In summary, the cytotoxicity results demonstrate the suitability of the nanoformulations for further

cellular experiments and provide information about the concentrations of ABA that may be utilized in subsequent experiments. Doubtless, the obtained results have also revealed intriguing trends that call for future more comprehensive studies to further investigate this phenomenon.

Moreover, the antioxidant potential on a MIN6 pancreatic line of pure ABA and TNE containing ABA at the same ABA concentration was evaluated and compared by performing the CAA assay. Since the cellular antioxidant activity of a bioactive compound depends on its cellular uptake, this assay also indicates the relative cellular uptake potential of the ABA from the free extracts compared to the formulations, as well as the differences between the formulations. Free-ABA did not show the ability to counteract oxidative stress in our assay, while the obtained results from the TNE treatment demonstrated the ability of this vegetal extract to exert antioxidant properties when cells endure oxidative stress. However, the nanoformulated form of TNE (NF-TNE) showed significantly higher antioxidant activity compared to the Free-TNE sample ($p < 0.001$). This result could be explained in part based on the rationale that the unencapsulated compounds had compromised antioxidant activity before and upon entry into the cellular environment. As explained earlier, many potent natural compounds, most notably curcumin, suffer from issues of stability and degradation that affect their potency [177]. A formulation strategy, such as the one used in this study, not only preserves the stability and integrity of the bioactive, but can also improve cellular delivery. Indeed, the DSPE-PEG-AP delivery system used in this study has been shown to significantly increase cellular delivery of iron as the payload in human Caco-2 intestinal cells [178]. Thus, the higher antioxidant activity may be attributed in part to better preservation of antioxidant activity as well as enhanced cellular delivery, highlighting the beneficial potential of this approach. Furthermore, the components of the nanoformulation system retain their antioxidant activity which may also have influenced cellular antioxidant behavior. As indeed reported in the literature, the

ascorbyl moiety of ascorbyl palmitate nanocarrier has been demonstrated to exert even much higher antioxidant activity than ascorbic acid itself [193]. This observation further strengthens the beneficial potential of the nanoformulated form of TNE, as it contains different bioactive compounds that could act synergistically to exert significant cellular antioxidant activity.

In the GSIS and Iron-challenging assays we aimed to evaluate the insulin response in MIN6 cells incubated with two different glucose concentrations, which were chosen to replicate physiological and supraphysiological glucose levels (5.5 and 20 mM respectively), w/wo preincubation with high iron levels (100 μ M). The prooxidant role of excess free iron and its detrimental consequences have been demonstrated in various organ systems and disease states. Elevated iron levels have been shown to correlate with the pathogenesis of type-2 diabetes [194] and previous studies in MIN6 cells studying β -cell function have demonstrated 100 μ M iron to cause cellular and mitochondrial dysfunction [167].

Pre-treatment with one of the test samples (free-ABA, free-TNE, NF-ABA, and NF-TNE) or MEM (Ctrl) was then evaluated under the above-described conditions. The initial observation relates to the observed significant increase in insulin AUC of the Ctrl group incubated with 5.5 mM glucose compared with the same group incubated with higher glucose levels ($p < 0.05$, Figure 24). This is consistent with evidence from the literature on the profile of GSIS in MIN6 cells upon exposure to these glucose levels [195]. In this regard, a progressive response starting at 5 mM glucose has been reported for this cell line, reaching its maximum level at 25 mM and remaining at this level up to 50 mM [195]. Moreover, a statistical decrease in insulin secretion was observed for both Ctrl groups incubated with 5.5 and 20 mM glucose together with 100 μ M iron, compared to the same groups without iron treatment. This is in agreement with data obtained in a previous work on the same pancreatic β -cell line [167]. Accordingly, exposure of β -cells to high iron concentrations can lead to oxidative stress, which eventually results in cellular

dysfunction and toxicity [168]. In particular, by increasing mitochondrial iron transport, overaccumulation of this element in β -cells may eventually cause mitochondrial dysfunction and impairment of the insulin secretory machinery [167,196]. In this regard, it has been reported that the expression of SNAP-25, a key protein in the core SNARE (soluble N-ethylmaleimide-sensitive factor attachment protein receptor) complex responsible for insulin exocytosis, is vulnerable towards oxidative stress [167]. Furthermore, if we consider Ctrl cells exposed to glucose 20 mM and iron 100 μ M, an even lower level of insulin AUC can be observed compared to cells incubated with glucose 5.5 mM and iron 100 μ M, probably due to the detrimental combination of glucose and iron-induced toxicity to which these cells were exposed. Therefore, these results further support the validity of using these conditions as a model to study β -cell disruption and insulin secretory dysfunction.

In the present work we chose to evaluate and compare the effects of different samples on insulin secretion, using the same ABA concentration (0.05 μ M) for all test treatments [32]. This concentration was selected based on what has been previously reported in the literature about the role of this bioactive molecule in pancreatic β -cell lines. Specifically, Bruzzone et al. reported the ability of ABA to significantly increase insulin secretion from RIN-m and INS-1 cells and murine and human pancreatic islets incubated at both low and high glucose levels (i.e., 5.5 and 16.7 mM glucose) [32]. This effect was observed after treatment with ABA at a concentration of 0.01 μ M, while no statistical differences were observed when the concentration of the pure standard was increased (from 0.01 to 10 μ M ABA, $p = 0.6$). From a mechanistic point of view, the reported increase in intracellular levels of the Ca^{2+} mobilizer cADPR (cyclic ADP-ribose) [197] led to its identification as the main contributor to ABA-triggered insulin secretion. Compared to these outcomes, treatment with ABA-containing samples did not show any significant increase in insulin response in our cellular model after incubation with physiological and supraphysiological glucose concentrations (Figure 25). The only exception was

represented by the treatment with Free- and NF-TNE samples, which resulted in a slight increase in insulin secretion compared with the Ctrl group. A completely different observation arises from the results obtained in MIN6 cells incubated with both glucose and iron. In this regard, significantly higher insulin AUC levels were observed for all test samples compared with the Ctrl group, with the greatest effect obtained after treatment with the NF-TNE sample (+54% vs Ctrl group incubated with glucose 5.5 mM + iron 100 μ M; +235% vs Ctrl group incubated with glucose 20 mM + iron 100 μ M). As previously reported, the role of excessive iron accumulation in damaging essential biological components (e.g., DNA, proteins, and lipids) through the generation of ROS is well established [171,174,198]. Therefore, ROS clearly has the ability to behave like a destructive agent that eventually leads to insulin resistance and β -cell failure [174]. Notably, impairment of insulin secretion due to iron-induced oxidative stress can lead to hyperglycemia and insulin resistance conditions, which are well-known features of T2DM. In this context, a considerable amount of evidence indicates that excess iron increases the risk of insulin resistance in diabetes mellitus, while a recent study conducted on healthy subjects concluded that iron excess negatively affected insulin activity [174,194,199,200]. In virtue of these considerations, the presence of bioactive compounds with antioxidant potential [155], especially polyphenols, in the TNE-based sample has been shown to contribute to the protection of these cells by counteracting cellular dysfunction induced by ROS in our model. Moreover, in both experiments involving exposure to high iron levels, the NF samples were found to be more efficient in terms of insulin release compared to unencapsulated samples. These data are also supported by the results of our cell viability and antioxidant activity assays where the NF-samples generally demonstrated prominent positive effects. This can be explained by the higher stability, bioavailability and delivery at the site of action of the bioactive compounds contained in the nanoformulated treatments, further supporting the

advantages of using a formulation-based approach for the delivery of bioactive molecules [177,178,187].

The originality of the present project lies in the first-time evaluation and comparison of the TNE efficacy on pancreatic β -function at the same ABA concentrations contained in the pure standard and the first-time incorporation of these molecules into formulations using novel delivery systems. In this way, the effects of the TNE-based samples and the pure standard were compared in terms of antioxidant and insulinotropic potential, and the effects of the NF samples were compared with their free counterparts. Specifically, the evaluation at the same concentration of the active ABA allowed us to distinguish the additional activity of TNE in relation to its content of bioactive compounds, especially polyphenols, which can contribute positively and synergistically to cellular antioxidant protection.

5.5. Conclusions

In the last part of this Ph.D. project, two nanoformulations containing a pure standard of ABA or TNE at the same ABA concentration were developed and optimized, using ascorbyl palmitate/DSPE-PEG as the nanocarrier delivery system. Interestingly, a significantly greater effect on MIN6 cell viability was observed in cells incubated with NF-ABA and NF-TNE compared to free samples. Also, cellular antioxidant activity improved after treatment with NF-TNE compared to Free-TNE, while no antioxidant activity was observed in both ABA-based groups. Finally, MIN6 cells exposed to two different glucose concentrations (5.5 and 20 mM) and iron (100 μ M) as a prooxidant agent showed significantly higher insulin AUC levels after treatment with all test samples compared to the Ctrl group, with the superior effect observed after pre-treatment with the NF-TNE sample. Overall, we herein showed the higher efficacy of the tested nanoformulated samples in terms of cell viability, antioxidant activity, and insulin secretion in our pancreatic β -cell model. Furthermore, the improved results obtained in cells treated with the NF-TNE sample

support its additional potential to enhance cellular antioxidant defence due to the synergistic combination of bioactive compounds contained in the TNE phytocomplex. Taken together, the novel results from this aspect of the project demonstrate not only the unique efficacy of TNE as a bioactive agent with therapeutic potential but also a significant advantage of using a nanoformulation approach to further increase the benefits of this and similar phyto-bioactive molecules. This novel work lays the foundation for future studies in cellular models to further clarify the mechanisms underlying these observed effects and progress to subsequent human clinical trials.

Conclusions

In conclusion, our data reasonably support TN as a source of innovative and promising nutraceutical formulations with beneficial effects on the management of glucose homeostasis. According to the observed results, these beneficial activities may be attributed to the concomitant presence of different bioactive compounds, such as ABA and polyphenols, in the TN vegetable matrix. An aspect of major interest of the present Ph.D. thesis is represented by the nutraceutical application of an agricultural by-product, in line with the current worldwide trend to recover agro-food wastes for environmental, economic, and health purposes. Moreover, clinical results obtained in subjects with T2DM demonstrated the beneficial potential of a TN-based nutraceutical formulation (TNnf) as a source of ABA able to positively regulate blood glucose levels, in association with a valuable insulin-sparing effect. More remarkably, its supplementation would be particularly advantageous in patients with endogenous ABA deficiency, as the pleiotropic functions ascribed to this hormone can only be replicated by the exogenous administration of the molecule itself. Undoubtedly, the clinical results obtained highlight the need for further *in vitro* and *in vivo* studies aimed at clarifying the mechanism of actions underlying the beneficial effects of TNnf in humans.

References

1. Sun, H.; Saeedi, P.; Karuranga, S.; Pinkepank, M.; Ogurtsova, K.; Duncan, B.B.; Stein, C.; Basit, A.; Chan, J.C.N.; Mbanya, J.C.; et al. IDF Diabetes Atlas: Global, regional and country-level diabetes prevalence estimates for 2021 and projections for 2045. *Diabetes Res. Clin. Pract.* **2022**, *183*, 109119, doi:10.1016/j.diabres.2021.109119.
2. Zheng, Y.; Ley, S.H.; Hu, F.B. Global aetiology and epidemiology of type 2 diabetes mellitus and its complications. *Nat. Rev. Endocrinol.* **2018**, *14*, 88–98, doi:10.1038/nrendo.2017.151.
3. Weires, M.B.; Tausch, B.; Haug, P.J.; Edwards, C.Q.; Wetter, T.; Cannon-Albright, L.A. Familiality of diabetes mellitus. *Exp. Clin. Endocrinol. Diabetes* **2007**, *115*, 634–640, doi:10.1055/s-2007-984443.
4. Aschner, P. New IDF clinical practice recommendations for managing type 2 diabetes in primary care. *Diabetes Res. Clin. Pract.* **2017**, *132*, 169–170, doi:10.1016/j.diabres.2017.09.002.
5. Krass, I.; Schieback, P.; Dhipayom, T. Adherence to diabetes medication: A systematic review. *Diabet. Med.* **2015**, *32*, 725–737, doi:10.1111/dme.12651.
6. Quality, A. for H.R. and Diabetes Medications for Adults with Type 2 Diabetes: An Update Focused on Monotherapy and Add-on Therapy to Metformin. *Ahrq* **2015**, *4*, 1–19.
7. Tan, S.Y.; Mei Wong, J.L.; Sim, Y.J.; Wong, S.S.; Mohamed Elhassan, S.A.; Tan, S.H.; Ling Lim, G.P.; Rong Tay, N.W.; Annan, N.C.; Bhattamisra, S.K.; et al. Type 1 and 2 diabetes mellitus: A review on current treatment approach and gene therapy as potential intervention. *Diabetes Metab. Syndr. Clin. Res. Rev.* **2019**, *13*, 364–372, doi:10.1016/j.dsx.2018.10.008.
8. Chaturvedi, R.; Desai, C.; Patel, P.; Shah, A.; Dikshit, R.K. An evaluation of the impact of antidiabetic medication on treatment satisfaction and quality of life in patients of diabetes mellitus. *Perspect. Clin. Res.* **2018**, *9*, 15–22,

doi:10.4103/picr.PICR_140_16.

9. Osadebe, P.; Odoh, E.; Uzor, P. Natural Products as Potential Sources of Antidiabetic Drugs. *Br. J. Pharm. Res.* **2014**, *4*, 2075–2095, doi:10.9734/bjpr/2014/8382.
10. Ota, A.; Ulrich, N.P. An overview of herbal products and secondary metabolites used for management of type two diabetes. *Front. Pharmacol.* **2017**, *8*, 1–14, doi:10.3389/fphar.2017.00436.
11. Mukherjee, A.; Gaurav, A.K.; Singh, S.; Yadav, S.; Bhowmick, S.; Abeysinghe, S.; Verma, J.P. The bioactive potential of phytohormones: A review. *Biotechnol. Reports* **2022**, *35*, e00748, doi:10.1016/j.btre.2022.e00748.
12. Newman, D.J.; Cragg, G.M. Natural products as sources of new drugs over the 30 years from 1981 to 2010. *J. Nat. Prod.* **2012**, *75*, 311–335, doi:10.1021/np200906s.
13. Xu, L.; Li, Y.; Dai, Y.; Peng, J. Natural products for the treatment of type 2 diabetes mellitus: Pharmacology and mechanisms. *Pharmacol. Res.* **2018**, *130*, 451–465, doi:10.1016/j.phrs.2018.01.015.
14. Finkelstein, R. Abscisic Acid Synthesis and Response. *Arab. B.* **2013**, *11*, e0166, doi:10.1199/tab.0166.
15. Liao, P.; Wu, Q.Y.; Li, S.; Hu, K. Bin; Liu, H.L.; Wang, H.Y.; Long, Z.Y.; Lu, X.M.; Wang, Y.T. The ameliorative effects and mechanisms of abscisic acid on learning and memory. *Neuropharmacology* **2023**, *224*, 109365, doi:10.1016/j.neuropharm.2022.109365.
16. Nambara, E.; Marion-Poll, A. Abscisic acid biosynthesis and catabolism. *Annu. Rev. Plant Biol.* **2005**, *56*, 165–185, doi:10.1146/annurev.arplant.56.032604.144046.
17. Spinelli, S.; Magnone, M.; Guida, L.; Sturla, L.; Zocchi, E. The ABA / LANCL Hormone / Receptor System in the Control of Glycemia , of

Cardiomyocyte Energy Metabolism , and in Neuroprotection : A New Ally in the Treatment of Diabetes Mellitus ? **2023**.

18. Leng, P.; Yuan, B.; Guo, Y.; Chen, P. The role of abscisic acid in fruit ripening and responses to abiotic stress. *J. Exp. Bot.* **2014**, *65*, 4577–4588, doi:10.1093/jxb/eru204.
19. Zhang, D.P.; Chen, S.W.; Peng, Y.B.; Shen, Y.Y. Abscisic acid-specific binding sites in the flesh of developing apple fruit. *J. Exp. Bot.* **2001**, *52*, 2097–2103, doi:10.1093/jexbot/52.364.2097.
20. Ghosh, S.; Sengupta, S.; Pal, A. Abscisic Acid, One of the Key Determinants of in Vitro Shoot Differentiation from Cotyledons of <i>Vigna radiata</i>. *Am. J. Plant Sci.* **2014**, *05*, 704–713, doi:10.4236/ajps.2014.55085.
21. Brookbank, B.P.; Patel, J.; Gazzarrini, S.; Nambara, E. Role of Basal ABA in Plant Growth and Development. **2021**, doi:10.3390/genes12121936.
22. Sun, L.; Sun, Y.; Zhang, M.; Wang, L.; Ren, J.; Cui, M.; Wang, Y.; Ji, K.; Li, P.; Li, Q.; et al. Suppression of 9-cis-epoxycarotenoid dioxygenase, which encodes a key enzyme in abscisic acid biosynthesis, alters fruit texture in transgenic tomato. *Plant Physiol.* **2012**, *158*, 283–298, doi:10.1104/pp.111.186866.
23. Zhao, S.L.; Qi, J.X.; Duan, C.R.; Sun, L.; Sun, Y.F.; Wang, Y.P.; Ji, K.; Chen, P.; Dai, S.J.; Leng, P. Expression analysis of the DKNCED1, DKNCED2 and DKCYP707A1 genes that regulate homeostasis of abscisic acid during the maturation of persimmon fruit. *J. Hortic. Sci. Biotechnol.* **2012**, *87*, 165–171, doi:10.1080/14620316.2012.11512848.
24. Stewart, G.R.; Smith, H. Effects of abscisic acid on nucleic acid synthesis and the induction of nitrate reductase in *Lemna polyrhiza*. *J. Exp. Bot.* **1972**, *23*, 875–885, doi:10.1093/jxb/23.4.875.
25. Mullins, M.G.; Osborne, D. Effect of abscisic acid on growth correlation in

- vitis vinifera L. *Aust. J. Biol. Sci.* **1970**, *23*, 479–484, doi:10.1071/BI9700479.
26. Wang, H.; Qi, Q.; Schorr, P.; Cutler, A.J.; Crosby, W.L.; Fowke, L.C. ICK1, a cyclin-dependent protein kinase inhibitor from *Arabidopsis thaliana* interacts with both Cdc2a and CycD3, and its expression is induced by abscisic acid. *Plant J.* **1998**, *15*, 501–510, doi:10.1046/j.1365-313X.1998.00231.x.
 27. Świątek, A.; Lenjou, M.; Van Bockstaele, D.; Inzé, D.; Van Onckelen, H. Differential effect of jasmonic acid and abscisic acid on cell cycle progression in tobacco BY-2 cells. *Plant Physiol.* **2002**, *128*, 201–211, doi:10.1104/pp.010592.
 28. Le Page-Degivry -Th., M.; Bidard, J.N.; Rouvier, E. Presence of abscisic acid, a phytohormone, in the mammalian brain. *Proc. Natl. Acad. Sci. U. S. A.* **1986**, *83*, 1155–1158, doi:10.1073/pnas.83.4.1155.
 29. Bruzzone, S.; Moreschi, I.; Usai, C.; Guida, L.; Damonte, G.; Salis, A.; Scarfi, S.; Millo, E.; De Flora, A.; Zocchi, E. Abscisic acid is an endogenous cytokine in human granulocytes with cyclic ADP-ribose as second messenger. *Proc. Natl. Acad. Sci. U. S. A.* **2007**, *104*, 5759–5764, doi:10.1073/pnas.0609379104.
 30. Magnone, M.; Bruzzone, S.; Guida, L.; Damonte, G.; Millo, E.; Scarfi, S.; Usai, C.; Sturla, L.; Palombo, D.; De Flora, A.; et al. Abscisic acid released by human monocytes activates monocytes and vascular smooth muscle cell responses involved in atherogenesis. *J. Biol. Chem.* **2009**, *284*, 17808–17818, doi:10.1074/jbc.M809546200.
 31. Magnone, M.; Sturla, L.; Jacchetti, E.; Scarfi, S.; Bruzzone, S.; Usai, C.; Guida, L.; Salis, A.; Damonte, G.; De Flora, A.; et al. Autocrine abscisic acid plays a key role in quartz-induced macrophage activation. *FASEB J.* **2012**, *26*, 1261–1271, doi:10.1096/fj.11-187351.
 32. Bruzzone, S.; Bodrato, N.; Usai, C.; Guida, L.; Moreschi, I.; Nano, R.;

- Antonioli, B.; Fruscione, F.; Magnone, M.; Scarfi, S.; et al. Abscisic acid is an endogenous stimulator of insulin release from human pancreatic islets with cyclic ADP ribose as second messenger. *J. Biol. Chem.* **2008**, *283*, 32188–32197, doi:10.1074/jbc.M802603200.
33. Scarfi, S.; Ferraris, C.; Fruscione, F.; Fresia, C.; Guida, L.; Bruzzone, S.; Usai, C.; Parodi, A.; Millo, E.; Salis, A.; et al. Cyclic ADP-Ribose-Mediated Expansion and Stimulation of Human Mesenchymal Stem Cells by the Plant Hormone Abscisic Acid. *Stem Cells* **2008**, *26*, 2855–2864, doi:10.1634/stemcells.2008-0488.
34. Bruzzone, S.; Ameri, P.; Briatore, L.; Mannino, E.; Basile, G.; Andraghetti, G.; Grozio, A.; Magnone, M.; Guida, L.; Scarfi, S.; et al. The plant hormone abscisic acid increases in human plasma after hyperglycemia and stimulates glucose consumption by adipocytes and myoblasts; The plant hormone abscisic acid increases in human plasma after hyperglycemia and stimulates glucose consumption by adipocytes and myoblasts. *FASEB J. • Res. Commun.*, doi:10.1096/fj.11-190140.
35. Coates, D.R.; Chin, J.M.; Chung, S.T.L. 基因的改变 NIH Public Access. *Bone* **2011**, *23*, 1–7, doi:10.1016/j.jnutbio.2009.10.003.Abscisic.
36. Baliño, P.; Gómez-Cadenas, A.; López-Malo, D.; Romero, F.J.; Muriach, M. Is there a role for abscisic acid, a proven anti-inflammatory agent, in the treatment of ischemic retinopathies? *Antioxidants* **2019**, *8*, doi:10.3390/antiox8040104.
37. Guri, A.J.; Hontecillas, R.; Bassaganya-Riera, J. Abscisic acid ameliorates experimental IBD by downregulating cellular adhesion molecule expression and suppressing immune cell infiltration. *Clin. Nutr.* **2010**, *29*, 824–831, doi:10.1016/j.clnu.2010.02.009.
38. Zocchi, E.; Carpaneto, A.; Cerrano, C.; Bavestrello, G.; Giovine, M.; Bruzzone, S.; Guida, L.; Franco, L.; Usai, C. The temperature-signaling

- cascade in sponges involves a heat-gated cation channel, abscisic acid, and cyclic ADP-ribose. *Proc. Natl. Acad. Sci. U. S. A.* **2001**, *98*, 14859–14864, doi:10.1073/pnas.261448698.
39. Derosa, G.; Maffioli, P.; D'angelo, A.; Preti, P.S.; Tenore, G.; Novellino, E. Abscisic acid treatment in patients with prediabetes. *Nutrients* **2020**, *12*, 1–11, doi:10.3390/nu12102931.
40. Landlinger, C.; Salzer, U.; Prohaska, R. Myristoylation of human LanC-like Protein 2 (LANCL2) is essential for the interaction with the plasma membrane and the increase in cellular sensitivity to adriamycin. *Biochim. Biophys. Acta - Biomembr.* **2006**, *1758*, 1759–1767, doi:10.1016/j.bbamem.2006.07.018.
41. Cichero, E.; Fresia, C.; Guida, L.; Booz, V.; Millo, E.; Scotti, C.; Iamele, L.; de Jonge, H.; Galante, D.; De Flora, A.; et al. Identification of a high affinity binding site for abscisic acid on human lanthionine synthetase component C-like protein 2. *Int. J. Biochem. Cell Biol.* **2018**, *97*, 52–61, doi:10.1016/j.biocel.2018.02.003.
42. Fresia, C.; Vigliarolo, T.; Guida, L.; Booz, V.; Bruzzone, S.; Sturla, L.; Di Bona, M.; Pesce, M.; Usai, C.; De Flora, A.; et al. G-protein coupling and nuclear translocation of the human abscisic acid receptor LANCL2. *Sci. Rep.* **2016**, *6*, 1–11, doi:10.1038/srep26658.
43. Vigliarolo, T.; Zocchi, E.; Fresia, C.; Booz, V.; Guida, L. Abscisic acid influx into human nucleated cells occurs through the anion exchanger AE2. *Int. J. Biochem. Cell Biol.* **2016**, *75*, 99–103, doi:10.1016/j.biocel.2016.03.006.
44. Magnone, M.; Sturla, L.; Guida, L.; Spinelli, S.; Begani, G.; Bruzzone, S.; Fresia, C.; Zocchi, E. Abscisic acid: A conserved hormone in plants and humans and a promising aid to combat prediabetes and the metabolic syndrome. *Nutrients* **2020**, *12*, 1–13, doi:10.3390/nu12061724.
45. Sturla, L.; Mannino, E.; Scarfi, S.; Bruzzone, S.; Magnone, M.; Sociali, G.; Booz, V.; Guida, L.; Vigliarolo, T.; Fresia, C.; et al. Abscisic acid enhances

- glucose disposal and induces brown fat activity in adipocytes in vitro and in vivo. *Biochim. Biophys. Acta - Mol. Cell Biol. Lipids* **2017**, *1862*, 131–144, doi:10.1016/j.bbali.2016.11.005.
46. Holst, J.J.; Gasbjerg, L.S.; Rosenkilde, M.M. The Role of Incretins on Insulin Function and Glucose Homeostasis. *Endocrinol. (United States)* **2021**, *162*, 1–10, doi:10.1210/endo/bqab065.
 47. Bruzzone, S.; Magnone, M.; Mannino, E.; Sociali, G.; Sturla, L.; Fresia, C.; Booz, V.; Emionite, L.; De Flora, A.; Zocchi, E. Abscisic acid stimulates glucagon-like peptide-1 secretion from L-cells and its oral administration increases plasma glucagon-like peptide-1 levels in rats. *PLoS One* **2015**, *10*, 1–12, doi:10.1371/journal.pone.0140588.
 48. Magnone, M.; Emionite, L.; Guida, L.; Vigliarolo, T.; Sturla, L.; Spinelli, S.; Buschiazzo, A.; Marini, C.; Sambuceti, G.; De Flora, A.; et al. Insulin-independent stimulation of skeletal muscle glucose uptake by low-dose abscisic acid via AMPK activation. *Sci. Rep.* **2020**, *10*, 1–14, doi:10.1038/s41598-020-58206-0.
 49. Leick, L.; Fentz, J.; Biensø, R.S.; Knudsen, J.G.; Jeppesen, J.; Kiens, B.; Wojtaszewski, J.F.P.; Pilegaard, H. PGC-1 α is required for AICAR-induced expression of GLUT4 and mitochondrial proteins in mouse skeletal muscle. *Am. J. Physiol. - Endocrinol. Metab.* **2010**, *299*, 456–465, doi:10.1152/ajpendo.00648.2009.
 50. Xi, X.; Han, J.; Zhang, J.Z. Stimulation of Glucose Transport by AMP-activated Protein Kinase via Activation of p38 Mitogen-activated Protein Kinase. *J. Biol. Chem.* **2001**, *276*, 41029–41034, doi:10.1074/jbc.M102824200.
 51. Armoni, M.; Kritz, N.; Harel, C.; Bar-Yoseph, F.; Chen, H.; Quon, M.J.; Karnieli, E. Peroxisome proliferator-activated receptor- γ represses GLUT4 promoter activity in primary adipocytes, and rosiglitazone alleviates this

- effect. *J. Biol. Chem.* **2003**, 278, 30614–30623, doi:10.1074/jbc.M304654200.
52. Magnone, M.; Spinelli, S.; Begani, G.; Guida, L.; Sturla, L.; Emionite, L.; Zocchi, E. Abscisic Acid Improves Insulin Action on Glycemia in Insulin-Deficient Mouse Models of Type 1 Diabetes. **2022**.
53. Magnone, M.; Ameri, P.; Salis, A.; Andraghetti, G.; Emionite, L.; Murialdo, G.; De Flora, A.; Zocchi, E. Microgram amounts of abscisic acid in fruit extracts improve glucose tolerance and reduce insulinemia in rats and in humans. *FASEB J.* **2015**, 29, 4783–4793, doi:10.1096/fj.15-277731.
54. Muoio, D.M.; Newgard, C.B. Mechanisms of disease: Molecular and metabolic mechanisms of insulin resistance and β -cell failure in type 2 diabetes. *Nat. Rev. Mol. Cell Biol.* **2008**, 9, 193–205, doi:10.1038/nrm2327.
55. Despoudi, S.; Bucatariu, C.; Otles, S.; Kartal, C. *Food waste management, valorization, and sustainability in the food industry*; Elsevier Inc., 2020; ISBN 9780128205631.
56. Pour, F.H.; Makkawi, Y.T. A review of post-consumption food waste management and its potentials for biofuel production. *Energy Reports* **2021**, 7, 7759–7784, doi:10.1016/j.egy.2021.10.119.
57. Rao, P.; Rathod, V. Valorization of Food and Agricultural Waste: A Step towards Greener Future. *Chem. Rec.* **2019**, 19, 1858–1871, doi:10.1002/tcr.201800094.
58. Tenore, G.C.; Caruso, D.; D'avino, M.; Buonomo, G.; Caruso, G.; Ciampaglia, R.; Schiano, E.; Maisto, M.; Annunziata, G.; Novellino, E. A pilot screening of agro-food waste products as sources of nutraceutical formulations to improve simulated postprandial glycaemia and insulinaemia in healthy subjects. *Nutrients* **2020**, 12, 1–14, doi:10.3390/nu12051292.
59. Raak, N.; Symmank, C.; Zahn, S.; Aschemann-Witzel, J.; Rohm, H. Processing- and product-related causes for food waste and implications for the

- food supply chain. *Waste Manag.* **2017**, *61*, 461–472, doi:10.1016/j.wasman.2016.12.027.
60. Mengyuan, W.; Haoli, W.; Tingting, M.; Qian, G.; Yulin, F.; Xiangyu, S. Comprehensive Utilization of Thinned Unripe Fruits from Horticultural Crops. *Foods* **2021**, *10*.
61. Guo, C.; Bi, J.; Li, X.; Lyu, J.; Wu, X.; Xu, Y. Polyphenol metabolic diversity of Chinese peach and nectarine at thinned and ripe stages by UPLC-ESI-Q-TOF-MS combined with multivariate statistical analysis. *J. Food Compos. Anal.* **2020**, *90*, doi:10.1016/j.jfca.2020.103502.
62. Sun, J.; Chu, Y.-F.; Wu, X.; Rui, A.; Liu, H. Antioxidant and Antiproliferative Activities of Common Fruits. **2002**, doi:10.1021/jf0207530.
63. Maritim, A.C.; Sanders, R.A.; Watkins, J.B. Diabetes, oxidative stress, and antioxidants: A review. *J. Biochem. Mol. Toxicol.* **2003**, *17*, 24–38, doi:10.1002/jbt.10058.
64. Tangvarasittichai, S. Oxidative stress, insulin resistance, dyslipidemia and type 2 diabetes mellitus. *World J. Diabetes* **2015**, *6*, 456, doi:10.4239/wjd.v6.i3.456.
65. Cantín, C.M.; Gogorcena, Y.; Moreno, M.Á. Phenotypic diversity and relationships of fruit quality traits in peach and nectarine [*Prunus persica* (L.) Batsch] breeding progenies. *Euphytica* **2010**, *171*, 211–226, doi:10.1007/s10681-009-0023-4.
66. Brookbank, B.P.; Patel, J.; Gazzarrini, S.; Nambara, E. Role of basal aba in plant growth and development. *Genes (Basel)*. **2021**, *12*, doi:10.3390/GENES12121936.
67. Xu, Z.J.; Nakajima, M.; Suzuki, Y.; Yamaguchi, I. Cloning and characterization of the abscisic acid-specific glucosyltransferase gene from adzuki bean seedlings. *Plant Physiol.* **2002**, *129*, 1285–1295, doi:10.1104/pp.001784.

68. Zou, J.; Abrams, G.D.; Barton, D.L.; Taylor, D.C.; Pomeroy, M.K.; Abrams, S.R. Induction of lipid and oleosin biosynthesis by (+)-abscisic acid and its metabolites in microspore-derived embryos of *Brassica napus* L. cv reston: Biological responses in the presence of 8'-hydroxyabscisic acid. *Plant Physiol.* **1995**, *108*, 563–571, doi:10.1104/pp.108.2.563.
69. Kepka, M.; Benson, C.L.; Gonugunta, V.K.; Nelson, K.M.; Christmann, A.; Grill, E.; Abrams, S.R. Action of natural abscisic acid precursors and catabolites on abscisic acid receptor complexes. *Plant Physiol.* **2011**, *157*, 2108–2119, doi:10.1104/pp.111.182584.
70. Rodriguez, P.L. Abscisic Acid Catabolism Generates Phaseic Acid, a Molecule Able to Activate a Subset of ABA Receptors. *Mol. Plant* **2016**, *9*, 1448–1450, doi:10.1016/j.molp.2016.09.009.
71. Hou, S.T.; Jiang, S.X.; Zaharia, L.I.; Han, X.; Benson, C.L.; Slinn, J.; Abrams, S.R. Phaseic acid, an endogenous and reversible inhibitor of glutamate receptors in mouse brain. *J. Biol. Chem.* **2016**, *291*, 27007–27022, doi:10.1074/jbc.M116.756429.
72. Lück, M.; Bergs, F.; Jupke, A. Solvent accessibility limitation by plant matrix compounds in extraction of rutin from *Solanum lycopersicum*. *Sep. Sci. Plus* **2020**, *3*, 63–71, doi:10.1002/sscp.201900074.
73. Jones, W.P.; Kinghorn, A.D. Extraction of plant secondary metabolites. *Methods Mol. Biol.* **2012**, *864*, 341–366, doi:10.1007/978-1-61779-624-1_13.
74. Tabart, J.; Kevers, C.; Sipel, A.; Pincemail, J.; Defraigne, J.O.; Dommes, J. Optimisation of extraction of phenolics and antioxidants from black currant leaves and buds and of stability during storage. *Food Chem.* **2007**, *105*, 1268–1275, doi:10.1016/j.foodchem.2007.03.005.
75. Bosco, R.; Caser, M.; Vanara, F.; Scariot, V. Development of a rapid LC-DAD/FLD method for the simultaneous determination of auxins and abscisic acid in plant extracts. *J. Agric. Food Chem.* **2013**, *61*, 10940–10947,

doi:10.1021/jf4034305.

76. Chiwocha, S.D.S.; Abrams, S.R.; Ambrose, S.J.; Cutler, A.J.; Loewen, M.; Ross, A.R.S.; Kermode, A.R. A method for profiling classes of plant hormones and their metabolites using liquid chromatography-electrospray ionization tandem mass spectrometry: An analysis of hormone regulation of thermodormancy of lettuce (*Lactuca sativa* L.) seeds. *Plant J.* **2003**, *35*, 405–417, doi:10.1046/j.1365-313X.2003.01800.x.
77. Santiago da Silva, C.M.; Habermann, G.; Marchi, M.R.R.; Zocolo, G.J. The role of matrix effects on the quantification of abscisic acid and its metabolites in the leaves of *Bauhinia variegata* L. using liquid chromatography combined with tandem mass spectrometry. *Brazilian J. Plant Physiol.* **2012**, *24*, 223–232, doi:10.1590/S1677-04202012000300009.
78. Lai, W.T.; Khong, N.M.H.; Lim, S.S.; Hee, Y.Y.; Sim, B.I.; Lau, K.Y.; Lai, O.M. A review: Modified agricultural by-products for the development and fortification of food products and nutraceuticals. *Trends Food Sci. Technol.* **2017**, *59*, 148–160, doi:10.1016/j.tifs.2016.11.014.
79. Jovanovic, A.; Petrovic, P.; Đordjevic, V.; Zdunic, G.; Savikin, K.; Bugarski, B. Polyphenols extraction from plant sources. *Lek. sirovine* **2017**, *37*, 45–49, doi:10.5937/leksir1737045j.
80. Maisto, M.; Piccolo, V.; Novellino, E.; Schiano, E.; Iannuzzo, F.; Ciampaglia, R.; Summa, V.; Tenore, G.C. Optimization of Phlorizin Extraction from Annurca Apple Tree Leaves Using Response Surface Methodology. *Antioxidants* **2022**, *11*, 1–15, doi:10.3390/antiox11101933.
81. Cavalcanti, V.P.; Aazza, S.; Bertolucci, S.K.V.; Rocha, J.P.M.; Coelho, A.D.; Oliveira, A.J.M.; Mendes, L.C.; Pereira, M.M.A.; Morais, L.C.; Forim, M.R.; et al. Solvent mixture optimization in the extraction of bioactive compounds and antioxidant activities from garlic (*Allium sativum* l.). *Molecules* **2021**, *26*, doi:10.3390/molecules26196026.

82. Antony, A.; Farid, M. Effect of Temperatures on Polyphenols during Extraction. *Appl. Sci.* **2022**, *12*, doi:10.3390/app12042107.
83. Zhou, Y.; Wu, D.; Cai, P.; Cheng, G.; Huang, C.; Pan, Y. Special effect of ionic liquids on the extraction of flavonoid glycosides from *Chrysanthemum morifolium* Ramat by microwave assistance. *Molecules* **2015**, *20*, 7683–7699, doi:10.3390/molecules20057683.
84. Kim, H.K.; Verpoorte, R. Sample preparation for plant metabolomics. *Phytochem. Anal.* **2010**, *21*, 4–13, doi:10.1002/pca.1188.
85. Michiels, J.A.; Kevers, C.; Pincemail, J.; Defraigne, J.O.; Dommès, J. Extraction conditions can greatly influence antioxidant capacity assays in plant food matrices. *Food Chem.* **2012**, *130*, 986–993, doi:10.1016/j.foodchem.2011.07.117.
86. Annunziata, G.; Maisto, M.; Schisano, C.; Ciampaglia, R.; Daliu, P.; Narciso, V.; Tenore, G.C.; Novellino, E. Colon bioaccessibility and antioxidant activity of white, green and black tea polyphenols extract after in vitro simulated gastrointestinal digestion. *Nutrients* **2018**, *10*, doi:10.3390/nu10111711.
87. Maisto, M.; Annunziata, G.; Schiano, E.; Piccolo, V.; Iannuzzo, F.; Santangelo, R.; Ciampaglia, R.; Tenore, G.C.; Novellino, E.; Grieco, P. Potential Functional Snacks: Date Fruit Bars Supplemented by Different Species of *Lactobacillus* spp. *Foods* **2021**, *10*, 1760, doi:10.3390/foods10081760.
88. Carlo Tenore, G.; Caruso, D.; Buonomo, G.; D'avino, M.; Ciampaglia, R.; Maisto, M.; Schisano, C.; Bocchino, B.; Novellino, E. Lactofermented annurca apple puree as a functional food indicated for the control of plasma lipid and oxidative amine levels: Results from a randomised clinical trial. *Nutrients* **2019**, *11*, doi:10.3390/nu11010122.
89. ICH Official web site : ICH Available online: <https://www.ich.org/> (accessed

- on Feb 17, 2022).
90. Moon, J.K.; Shibamoto, T. Antioxidant assays for plant and food components. *J. Agric. Food Chem.* **2009**, *57*, 1655–1666, doi:10.1021/jf803537k.
 91. Babbar, N.; Oberoi, H.S.; Uppal, D.S.; Patil, R.T. Total phenolic content and antioxidant capacity of extracts obtained from six important fruit residues. *Food Res. Int.* **2011**, *44*, 391–396, doi:10.1016/j.foodres.2010.10.001.
 92. Benzie, I.F.F.; Strain, J.J. The ferric reducing ability of plasma (FRAP) as a measure of “antioxidant power”: The FRAP assay. *Anal. Biochem.* **1996**, doi:10.1006/abio.1996.0292.
 93. Surveswaran, S.; Cai, Y.Z.; Corke, H.; Sun, M. Systematic evaluation of natural phenolic antioxidants from 133 Indian medicinal plants. *Food Chem.* **2007**, doi:10.1016/j.foodchem.2006.06.033.
 94. Schisano, C.; Narciso, V.; Maisto, M.; Annunziata, G.; Grieco, P.; Sommella, E.M.; Tenore, G.C.; Novellino, E. In vitro effects of protein fractions from Controne beans (*Phaseolus vulgaris* L. ecotype Controne) on intestinal permeability, ACE and α -amylase activities. *Eur. Food Res. Technol.* **2019**, *245*, 2311–2322, doi:10.1007/s00217-019-03338-5.
 95. Poongunran, J.; Perera, H.K.I.; Jayasinghe, L.; Fernando, I.T.; Sivakanesan, R.; Araya, H.; Fujimoto, Y. Bioassay-guided fractionation and identification of α -amylase inhibitors from *Syzygium cumini* leaves. *Pharm. Biol.* **2017**, *55*, 206–211, doi:10.1080/13880209.2016.1257031.
 96. Justino, A.B.; Franco, R.R.; Silva, H.C.G.; Saraiva, A.L.; Sousa, R.M.F.; Espindola, F.S. B procyanidins of *Annona crassiflora* fruit peel inhibited glycation, lipid peroxidation and protein-bound carbonyls, with protective effects on glycated catalase. *Sci. Rep.* **2019**, *9*, 1–15, doi:10.1038/s41598-019-55779-3.
 97. Hong, Y.; Wang, Z.; Barrow, C.J.; Dunshea, F.R.; Suleria, H.A.R. High-throughput screening and characterization of phenolic compounds in stone

- fruits waste by lc-esi-qtof-ms/ms and their potential antioxidant activities. *Antioxidants* **2021**, *10*, 1–22, doi:10.3390/antiox10020234.
98. Sheng, F.; Hu, B.; Jin, Q.; Wang, J.; Wu, C.; Luo, Z. The analysis of phenolic compounds in walnut husk and pellicle by uplc-q-orbitrap hrms and hplc. *Molecules* **2021**, *26*, 1–18, doi:10.3390/molecules26103013.
99. Anton, D.; Bender, I.; Kaart, T.; Roasto, M.; Heinonen, M.; Luik, A.; Püssa, T. Changes in Polyphenols Contents and Antioxidant Capacities of Organically and Conventionally Cultivated Tomato (*Solanum lycopersicum* L.) Fruits during Ripening. *Int. J. Anal. Chem.* **2017**, *2017*, 6–10, doi:10.1155/2017/2367453.
100. Fathoni, A.; Saepudin, E.; Cahyana, A.H.; Rahayu, D.U.C.; Haib, J. Identification of nonvolatile compounds in clove (*Syzygium aromaticum*) from Manado. *AIP Conf. Proc.* **2017**, *1862*, doi:10.1063/1.4991183.
101. Ncube, E.N.; Mhlongo, M.I.; Piater, L.A.; Steenkamp, P.A.; Dubery, I.A.; Madala, N.E. Analyses of chlorogenic acids and related cinnamic acid derivatives from *Nicotiana tabacum* tissues with the aid of UPLC-QTOF-MS/MS based on the in-source collision-induced dissociation method. *Chem. Cent. J.* **2014**, *8*, 1–10, doi:10.1186/s13065-014-0066-z.
102. Yuzuak, S.; Ballington, J.; Xie, D.Y. HPLC-qTOF-MS/MS-based profiling of flavan-3-ols and dimeric proanthocyanidins in berries of two muscadine grape hybrids FLH 13-11 and FLH 17-66. *Metabolites* **2018**, *8*, doi:10.3390/metabo8040057.
103. Rue, E.A.; Rush, M.D.; van Breemen, R.B. Procyanidins: a comprehensive review encompassing structure elucidation via mass spectrometry. *Phytochem. Rev.* **2018**, *17*, 1–16, doi:10.1007/s11101-017-9507-3.
104. Rockenbach, I.I.; Jungfer, E.; Ritter, C.; Santiago-Schübel, B.; Thiele, B.; Fett, R.; Galensa, R. Characterization of flavan-3-ols in seeds of grape pomace by CE, HPLC-DAD-MS n and LC-ESI-FTICR-MS. *Food Res. Int.* **2012**, *48*,

- 848–855, doi:10.1016/j.foodres.2012.07.001.
105. Barros, L.; Dueñas, M.; Pinela, J.; Carvalho, A.M.; Buelga, C.S.; Ferreira, I.C.F.R. Characterization and Quantification of Phenolic Compounds in Four Tomato (*Lycopersicon esculentum* L.) Farmers' Varieties in Northeastern Portugal Homegardens. *Plant Foods Hum. Nutr.* **2012**, *67*, 229–234, doi:10.1007/s11130-012-0307-z.
 106. Li, Y.; Liu, Y.; Liu, R.; Liu, S.; Zhang, X.; Wang, Z.; Zhang, J.; Lu, J. HPLC-LTQ-orbitrap MSn profiling method to comprehensively characterize multiple chemical constituents in xiao-er-qing-jie granules. *Anal. Methods* **2015**, *7*, 7511–7526, doi:10.1039/c5ay00420a.
 107. Sinosaki, N.B.M.; Tonin, A.P.P.; Ribeiro, M.A.S.; Polisel, C.B.; Roberto, S.B.; da Silveira, R.; Visentainer, J. V.; Santos, O.O.; Meurer, E.C. Structural study of phenolic acids by triple quadrupole mass spectrometry with electrospray ionization in negative mode and H/D isotopic exchange. *J. Braz. Chem. Soc.* **2020**, *31*, 402–408, doi:10.21577/0103-5053.20190197.
 108. Nikolai Kuhnert, Rakesh Jaiswal, Marius Febi Matei, T.S. and; Deshpande, S. How to distinguish between feruloyl quinic acids and isoferuloyl quinic acids by liquid chromatography/ tandem mass spectrometry. *RAPID Commun. MASS Spectrom.* **2010**, *24*, 1575–1582.
 109. Grieman, M.M.; Greaves, J.; Saltzman, E.S. A method for analysis of vanillic acid in polar ice cores. *Clim. Past* **2015**, *11*, 227–232, doi:10.5194/cp-11-227-2015.
 110. Jaiswal, R.; Kuhnert, N. How to identify and discriminate between the methyl quinates of chlorogenic acids by liquid chromatography-tandem mass spectrometry. *J. Mass Spectrom.* **2011**, *46*, 269–281, doi:10.1002/jms.1889.
 111. Elsadig Karar, M.G.; Kuhnert, N. UPLC-ESI-Q-TOF-MS/MS Characterization of Phenolics from *Crataegus monogyna* and *Crataegus laevigata* (Hawthorn) Leaves, Fruits and their Herbal Derived Drops

- (Crataegutt Tropfen). *J. Chem. Biol. Ther.* **2016**, *01*, doi:10.4172/2572-0406.1000102.
112. Sun, J.; Liang, F.; Bin, Y.; Li, P.; Duan, C. Screening non-colored phenolics in red wines using liquid chromatography/ultraviolet and mass spectrometry/mass spectrometry libraries. *Molecules* **2007**, *12*, 679–693, doi:10.3390/12030679.
113. Said, R. Ben; Hamed, A.I.; Mahalel, U.A.; Al-Ayed, A.S.; Kowalczyk, M.; Moldoch, J.; Oleszek, W.; Stochmal, A. Tentative characterization of polyphenolic compounds in the male flowers of *Phoenix dactylifera* by liquid chromatography coupled with mass spectrometry and DFT. *Int. J. Mol. Sci.* **2017**, *18*, 1–18, doi:10.3390/ijms18030512.
114. De Beer, D.; Schulze, A.E.; Joubert, E.; Villiers, A.; Malherbe, C.J.; Stander, M.A. Food ingredient extracts of *Cyclopia subternata* (Honeybush): Variation in phenolic composition and antioxidant capacity. *Molecules* **2012**, *17*, 14602–14624, doi:10.3390/molecules171214602.
115. De Souza Mesquita, L.M.; e Paiva Caria, C.R.; Santos, P.S.; Ruy, C.C.; Da Silva Lima, N.; Taketa Moreira, D.K.; Da Rocha, C.Q.; Murador, D.C.; De Rosso, V.V.; Gambero, A.; et al. Modulatory effect of polyphenolic compounds from the mangrove tree *Rhizophora mangle* L. On non-alcoholic fatty liver disease and insulin resistance in high-fat diet obese mice. *Molecules* **2018**, *23*, doi:10.3390/molecules23092114.
116. Li, Z.H.; Guo, H.; Xu, W. Bin; Ge, J.; Li, X.; Alimu, M.; He, D.J. Rapid Identification of Flavonoid Constituents Directly from PTP1B Inhibitive Extract of Raspberry (*Rubus idaeus* L.) Leaves by HPLC-ESI-QTOF-MS-MS. *J. Chromatogr. Sci.* **2016**, *54*, 805–810, doi:10.1093/chromsci/bmw016.
117. Fabre, N.; Rustan, I.; de Hoffmann, E.; Quetin-Leclercq, J. Determination of flavone, flavonol, and flavanone aglycones by negative ion liquid chromatography electrospray ion trap mass spectrometry. *J. Am. Soc. Mass*

- Spectrom.* **2001**, *12*, 707–15, doi:10.1016/S1044-0305(01)00226-4.
118. Kumar, S.; Singh, A.; Kumar, B. Identification and characterization of phenolics and terpenoids from ethanolic extracts of *Phyllanthus* species by HPLC-ESI-QTOF-MS/MS. *J. Pharm. Anal.* **2017**, *7*, 214–222, doi:10.1016/j.jpha.2017.01.005.
119. Kang, J.; Price, W.E.; Ashton, J.; Tapsell, L.C.; Johnson, S. Identification and characterization of phenolic compounds in hydromethanolic extracts of sorghum wholegrains by LC-ESI-MSn. *Food Chem.* **2016**, *211*, 215–226, doi:10.1016/j.foodchem.2016.05.052.
120. Zhang, Y.; Xiong, H.; Xu, X.; Xue, X.; Liu, M.; Xu, S.; Liu, H.; Gao, Y.; Zhang, H.; Li, X. Compounds identification in semen cuscuteae by ultra-high-performance liquid chromatography (uplcs) coupled to electrospray ionization mass spectrometry. *Molecules* **2018**, *23*, doi:10.3390/molecules23051199.
121. Koolen, H.H.F.; da Silva, F.M.A.; Gozzo, F.C.; de Souza, A.Q.L.; de Souza, A.D.L. Antioxidant, antimicrobial activities and characterization of phenolic compounds from buriti (*Mauritia flexuosa* L. f.) by UPLC-ESI-MS/MS. *Food Res. Int.* **2013**, *51*, 467–473, doi:10.1016/j.foodres.2013.01.039.
122. Masike, K.; Mhlongo, M.I.; Mudau, S.P.; Nobela, O.; Ncube, E.N.; Tugizimana, F.; George, M.J.; Madala, N.E. Highlighting mass spectrometric fragmentation differences and similarities between hydroxycinnamoyl-quinic acids and hydroxycinnamoyl-isocitric acids. *Chem. Cent. J.* **2017**, *11*, 1–7, doi:10.1186/s13065-017-0262-8.
123. Bittner, K.; Rzeppa, S.; Humpf, H. Distribution and Quantification of Flavan-3-ols and Procyanidins with Low Degree of Polymerization in Nuts, Cereals, and Legumes. **2013**.
124. Quideau, S.; Deffieux, D.; Douat-Casassus, C.; Pouységu, L. Plant polyphenols: Chemical properties, biological activities, and synthesis. *Angew. Chemie - Int. Ed.* **2011**, *50*, 586–621, doi:10.1002/anie.201000044.

125. Yang, J.; Liu, R.H.; Halim, L. Antioxidant and antiproliferative activities of common edible nut seeds. *LWT - Food Sci. Technol.* **2009**, *42*, 1–8, doi:10.1016/j.lwt.2008.07.007.
126. Guo, C.; Bi, J.; Li, X.; Lyu, J.; Zhou, M.; Wu, X. Antioxidant profile of thinned young and ripe fruits of Chinese peach and nectarine varieties. *Int. J. Food Prop.* **2020**, *23*, 1272–1286, doi:10.1080/10942912.2020.1797782.
127. Ramsay, R.R.; Tipton, K.F. molecules Assessment of Enzyme Inhibition: A Review with Examples from the Development of Monoamine Oxidase and Cholinesterase Inhibitory Drugs., doi:10.3390/molecules22071192.
128. Kelley, D.E. Sugars and starch in the nutritional management of diabetes mellitus. *Am. J. Clin. Nutr.* **2003**, *78*, 858–864, doi:10.1093/ajcn/78.4.858s.
129. Sun, L.; Miao, M. Dietary polyphenols modulate starch digestion and glycaemic level: a review. *Crit. Rev. Food Sci. Nutr.* **2020**, *60*, 541–555, doi:10.1080/10408398.2018.1544883.
130. Sun, L.; Warren, F.J.; Gidley, M.J. Natural products for glycaemic control: Polyphenols as inhibitors of alpha-amylase. *Trends Food Sci. Technol.* **2019**, *91*, 262–273, doi:10.1016/j.tifs.2019.07.009.
131. Perrone, A.; Giovino, A.; Benny, J.; Martinelli, F. Advanced Glycation End Products (AGEs): Biochemistry, Signaling, Analytical Methods, and Epigenetic Effects. *Oxid. Med. Cell. Longev.* **2020**, *2020*, doi:10.1155/2020/3818196.
132. Moldogazieva, N.T.; Mokhosoev, I.M.; Mel'nikova, T.I.; Porozov, Y.B.; Terentiev, A.A. Review Article Oxidative Stress and Advanced Lipoxidation and Glycation End Products (ALEs and AGEs) in Aging and Age-Related Diseases. **2019**, doi:10.1155/2019/3085756.
133. Singh Jaggi, A.; Parkash Singh, V.; Bali, A.; Singh, N. Advanced Glycation End Products and Diabetic Complications. *Korean J Physiol Pharmacol* **2014**, *18*, 1–14, doi:10.4196/kjpp.2014.18.1.1.

134. González, I.; Morales, M.A.; Rojas, A. Polyphenols and AGEs/RAGE axis. Trends and challenges. *Food Res. Int.* **2020**, *129*, 108843, doi:10.1016/j.foodres.2019.108843.
135. Yeh, W.J.; Hsia, S.M.; Lee, W.H.; Wu, C.H. Polyphenols with antiglycation activity and mechanisms of action: A review of recent findings. *J. Food Drug Anal.* **2017**, *25*, 84–92, doi:10.1016/j.jfda.2016.10.017.
136. Spagnuolo, L.; Posta, S. Della; Fanali, C.; Dugo, L.; De Gara, L.; Gugliucci, A. Antioxidant and Antiglycation Effects of Polyphenol Compounds Extracted from Hazelnut Skin on Advanced Glycation End-Products (AGEs) Formation. **2021**, doi:10.3390/antiox.
137. Schiano, E.; Maisto, M.; Piccolo, V.; Novellino, E.; Annunziata, G.; Ciampaglia, R.; Montesano, C.; Croce, M.; Caruso, G.; Iannuzzo, F.; et al. Beneficial Contribution to Glucose Homeostasis by an Agro-Food Waste Product Rich in Abscisic Acid: Results from a Randomized Controlled Trial. **2022**, doi:10.3390/foods11172637.
138. Ameri, P.; Bruzzone, S.; Mannino, E.; Sociali, G.; Andraghetti, G.; Salis, A.; Ponta, M.L.; Briatore, L.; Adami, G.F.; Ferraiolo, A.; et al. Impaired increase of plasma abscisic acid in response to oral glucose load in type 2 diabetes and in gestational diabetes. *PLoS One* **2015**, *10*, doi:10.1371/JOURNAL.PONE.0115992.
139. Atkinson, F.S.; Villar, A.; Mul, A.; Zangara, A.; Risco, E.; Smidt, C.R.; Hontecillas, R.; Leber, A.; Bassaganya-riera, J. Responses in Healthy Adults. **2006**, 1–11.
140. Guri, A.J.; Hontecillas, R.; Si, H.; Liu, D.; Bassaganya-Riera, J. Dietary abscisic acid ameliorates glucose tolerance and obesity-related inflammation in db/db mice fed high-fat diets. *Clin. Nutr.* **2007**, *26*, 107–116, doi:10.1016/j.clnu.2006.07.008.
141. Egbuna, C.; Awuchi, C.G.; Kushwaha, G.; Rudrapal, M.; Patrick-

- Iwuanyanwu, K.C.; Singh, O.; Odoh, U.E.; Khan, J.; Jeevanandam, J.; Kumarasamy, S.; et al. Bioactive Compounds Effective Against Type 2 Diabetes Mellitus: A Systematic Review. *Curr. Top. Med. Chem.* **2021**, *21*, 1067–1095, doi:10.2174/1568026621666210509161059.
142. Iannuzzo, F.; Piccolo, V.; Novellino, E.; Schiano, E.; Salviati, E.; Summa, V.; Campiglia, P.; Tenore, G.C.; Maisto, M. A Food-Grade Method for Enhancing the Levels of Low Molecular Weight Proanthocyanidins with Potentially High Intestinal Bioavailability. *Int. J. Mol. Sci.* **2022**, *23*, 13557, doi:10.3390/ijms232113557.
143. Rein, M.J.; Renouf, M.; Cruz-Hernandez, C.; Actis-Goretta, L.; Thakkar, S.K.; da Silva Pinto, M. Bioavailability of bioactive food compounds: A challenging journey to bioefficacy. *Br. J. Clin. Pharmacol.* **2013**, *75*, 588–602, doi:10.1111/j.1365-2125.2012.04425.x.
144. Arif, M.A.; Alseekh, S.; Harb, J.; Fernie, A.; Frank, W. Abscisic acid, cold and salt stimulate conserved metabolic regulation in the moss *Physcomitrella patens*. *Plant Biol.* **2018**, *20*, 1014–1022, doi:10.1111/plb.12871.
145. Fang, Q.; Jiang, T.; Xu, L.; Liu, H.; Mao, H.; Wang, X.; Jiao, B.; Duan, Y.; Wang, Q.; Dong, Q.; et al. A salt-stress-regulator from the Poplar R2R3 MYB family integrates the regulation of lateral root emergence and ABA signaling to mediate salt stress tolerance in *Arabidopsis*. *Plant Physiol. Biochem.* **2017**, *114*, 100–110, doi:10.1016/j.plaphy.2017.02.018.
146. Del, G.; El, Á.; Lagunillas, T.; Algodón, E.; Totorá, F.L.A.; B, F.C. Exercise and the Institute of Medicine Recommendations for Nutrition. **2012**, *111*, 1979.
147. European Medicines Agency (EMA) Status of EMEA Scientific Guidelines and European Pharmacopoeia Monographs and Chapters in the Regulatory Framework Applicable to Medicinal Products. *Emea/42371/2008* **2008**, 2–4.
148. Pereira, M.N.; Matos, B.N.; Gratieri, T.; Cunha-Filho, M.; Gelfuso, G.M.

- Development and validation of a simple chromatographic method for simultaneous determination of clindamycin phosphate and rifampicin in skin permeation studies. *J. Pharm. Biomed. Anal.* **2018**, *159*, 331–340, doi:10.1016/j.jpba.2018.07.007.
149. Xiong, D.M.; Liu, Z.; Chen, H.; Xue, J.T.; Yang, Y.; Chen, C.; Ye, L.M. Profiling the dynamics of abscisic acid and ABA-glucose ester after using the glucosyltransferase UGT71C5 to mediate abscisic acid homeostasis in *Arabidopsis thaliana* by HPLC-ESI-MS/MS. *J. Pharm. Anal.* **2014**, *4*, 190–196, doi:10.1016/j.jpha.2014.01.004.
150. Ancillotti, C.; Ulaszewska, M.; Mattivi, F.; Del Bubba, M. Untargeted Metabolomics Analytical Strategy Based on Liquid Chromatography/Electrospray Ionization Linear Ion Trap Quadrupole/Orbitrap Mass Spectrometry for Discovering New Polyphenol Metabolites in Human Biofluids after Acute Ingestion of *Vaccinium myrti*. *J. Am. Soc. Mass Spectrom.* **2019**, *30*, 381–402, doi:10.1007/s13361-018-2111-y.
151. Hoang, Q.T.M.; Nguyen, V.K.; Oberacher, H.; Fuchs, D.; Hernandez-Vargas, E.A.; Borucki, K.; Waldburg, N.; Wippermann, J.; Schreiber, J.; Bruder, D.; et al. Serum Concentration of the Phytohormone Abscisic Acid Is Associated With Immune-Regulatory Mediators and Is a Potential Biomarker of Disease Severity in Chronic Obstructive Pulmonary Disease. *Front. Med.* **2021**, *8*, 1–14, doi:10.3389/fmed.2021.676058.
152. Pem, D.; Jeewon, R. Fruit and vegetable intake: Benefits and progress of nutrition education interventions-narrative review article. *Iran. J. Public Health* **2015**, *44*, 1309–1321.
153. Zocchi, E.; Hontecillas, R.; Leber, A.; Einerhand, A.; Carbo, A.; Bruzzone, S.; Tubau-Juni, N.; Philipson, N.; Zoccoli-Rodriguez, V.; Sturla, L.; et al. Abscisic Acid: A Novel Nutraceutical for Glycemic Control. *Front. Nutr.*

- 2017**, *4*, 1–13, doi:10.3389/fnut.2017.00024.
154. Doumas, M.; Imprialos, K.; Stavropoulos, K.; Athyros, V.G. Pharmacological Management of Type 2 Diabetes Complications. *Curr. Vasc. Pharmacol.* **2020**, *18*, 101–103, doi:10.2174/157016111802200101155519.
155. Schiano, E.; Piccolo, V.; Novellino, E.; Maisto, M.; Iannuzzo, F.; Summa, V.; Tenore, G.C. Thinned Nectarines, an Agro-Food Waste with Antidiabetic Potential: HPLC-HESI-MS/MS Phenolic Characterization and In Vitro Evaluation of Their Beneficial Activities. *Foods* **2022**, *11*, 1010, doi:10.3390/FOODS11071010.
156. Gavin, J.R.; Alberti, K.G.M.M.; Davidson, M.B.; DeFronzo, R.A.; Drash, A.; Gabbe, S.G.; Genuth, S.; Harris, M.I.; Kahn, R.; Keen, H.; et al. Report of the expert committee on the diagnosis and classification of diabetes mellitus. *Diabetes Care* **1998**, *21*, doi:10.2337/diacare.21.1.s5.
157. Calvert, M.; Blazeby, J.; Altman, D.G.; Revicki, D.A.; Moher, D.; Brundage, M.D. *Reporting of Patient-Reported Outcomes in Randomized Trials The CONSORT PRO Extension*; 2013; Vol. 309;.
158. Bonora, E.; Formentini, G.; Calcaterra, F.; Lombardi, S.; Marini, F.; Zenari, L.; Saggiani, F.; Poli, M.; Perbellini, S.; Raffaelli, A.; et al. HOMA-estimated insulin resistance is an independent predictor of cardiovascular disease in type 2 diabetic subjects: Prospective data from the Verona Diabetes Complications Study. *Diabetes Care* **2002**, *25*, 1135–1141, doi:10.2337/diacare.25.7.1135.
159. Sanchez-Perez, A. Abscisic acid, a promising therapeutic molecule to prevent Alzheimer's and neurodegenerative diseases. *Neural Regen. Res.* **2020**, *15*, 1035–1036, doi:10.4103/1673-5374.270307.
160. Baliño, P.; Gómez-Cadenas, A.; López-Malo, D.; Romero, F.J.; Muriach, M. Is There A Role for Abscisic Acid, A Proven Anti-Inflammatory Agent, in the Treatment of Ischemic Retinopathies? **2019**, doi:10.3390/antiox8040104.
161. Sordillo, L.M.; Russo, M.A.; Roma, D.; Shaikh, I.S.R.; Zocchi, E.;

- Hontecillas, R.; Leber, A.; Einerhand, A.; Carbo, A.; Bruzzone, S.; et al. Abscisic Acid: A Novel Nutraceutical for Glycemic Control. *Artic. 24 I Front. Nutr* **2017**, *4*, 24, doi:10.3389/fnut.2017.00024.
162. Sakthivel, P.; Sharma, N.; Klahn, P.; Gereke, M.; Bruder, D. Abscisic Acid: A Phytohormone and Mammalian Cytokine as Novel Pharmacon with Potential for Future Development into Clinical Applications. *Curr. Med. Chem.* **2016**, *23*, 1549–1570, doi:10.2174/0929867323666160405113129.
163. Tenore, G.C.; Carotenuto, A.; Caruso, D.; Buonomo, G.; D’Avino, M.; Brancaccio, D.; Ciampaglia, R.; Maisto, M.; Schisano, C.; Novellino, E. A nutraceutical formulation based on Annurca apple polyphenolic extract is effective on intestinal cholesterol absorption: A randomised, placebo-controlled, crossover study. *PharmaNutrition* **2018**, *6*, 85–94, doi:10.1016/j.phanu.2018.05.001.
164. Schiano, E.; Annunziata, G.; Ciampaglia, R.; Iannuzzo, F.; Maisto, M.; Tenore, G.C.; Novellino, E. Bioactive Compounds for the Management of Hypertriglyceridemia: Evidence From Clinical Trials and Putative Action Targets. *Front. Nutr.* **2020**, *7*, doi:10.3389/fnut.2020.586178.
165. Georgopoulos, A.; Margolis, S.; Bachorik, P.; Kwiterovich, P. Angeliki Georgopoulos, Simeon Margolis, Paul Bachorik, and Peter O. Kwiterovich. *Metabolism.* **1988**, *37*, 866–871.
166. Maisto, M.; Schiano, E.; Novellino, E.; Piccolo, V.; Iannuzzo, F.; Salviati, E.; Summa, V.; Annunziata, G.; Tenore, G.C. Application of a Rapid and Simple Technological Process to Increase Levels and Bioaccessibility of Free Phenolic Compounds in Annurca Apple Nutraceutical Product. **2022**.
167. Blesia, V.; Patel, V.B.; Al-Obaidi, H.; Renshaw, D.; Zariwala, M.G. Excessive Iron Induces Oxidative Stress Promoting Cellular Perturbations and Insulin Secretory Dysfunction in MIN6 Beta Cells. *cells* **2021**, *10*, 1441, doi:<https://doi.org/10.3390/cells10051141>.

168. Ježek, P.; Hlavatá, L. Mitochondria in homeostasis of reactive oxygen species in cell, tissues, and organism. *Int. J. Biochem. Cell Biol.* **2005**, *37*, 2478–2503, doi:10.1016/j.biocel.2005.05.013.
169. Lorinczova, H.T.; Begum, G.; Temouri, L.; Renshaw, D.; Zariwala, M.G. Co-Administration of Iron and Bioavailable Curcumin Reduces Levels of Systemic Markers of Inflammation and Oxidative Stress in a Placebo-Controlled Randomised Study. *Nutrients* **2022**, *14*, doi:10.3390/nu14030712.
170. Fairweather-Tait, S.J. Iron nutrition in the UK: getting the balance right. *Proc. Nutr. Soc.* **2004**, *63*, 519–528, doi:10.1079/pns2004394.
171. Gerber, P.A.; Rutter, G.A. The Role of Oxidative Stress and Hypoxia in Pancreatic Beta-Cell Dysfunction in Diabetes Mellitus. *Antioxidants Redox Signal.* **2017**, *26*, 501–518, doi:10.1089/ars.2016.6755.
172. Lenzen, S.; Drinkgern, J.; Tiedge, M. Low antioxidant enzyme gene expression in pancreatic islets compared with various other mouse tissues. *Free Radic. Biol. Med.* **1996**, *20*, 463–466, doi:10.1016/0891-5849(96)02051-5.
173. McCord, J.M. The evolution of free radicals and oxidative stress. *Am. J. Med.* **2000**, *108*, 652–659, doi:10.1016/S0002-9343(00)00412-5.
174. Hansen, J.B.; Moen, I.W.; Mandrup-Poulsen, T. Iron: The hard player in diabetes pathophysiology. *Acta Physiol.* **2014**, *210*, 717–732, doi:10.1111/APHA.12256.
175. Ayala, A.; Muñoz, M.F.; Argüelles, S. Lipid peroxidation: Production, metabolism, and signaling mechanisms of malondialdehyde and 4-hydroxy-2-nonenal. *Oxid. Med. Cell. Longev.* **2014**, *2014*, doi:10.1155/2014/360438.
176. Eguchi, N.; Vaziri, N.D.; Dafoe, D.C.; Ichii, H. The role of oxidative stress in pancreatic β cell dysfunction in diabetes. *Int. J. Mol. Sci.* **2021**, *22*, 1–18, doi:10.3390/ijms22041509.
177. Muthukrishnan, L. Nanonutraceuticals — Challenges and Novel Nano - based

- Carriers for Effective Delivery and Enhanced Bioavailability. *Food Bioprocess Technol.* **2022**, doi:10.1007/s11947-022-02807-2.
178. Zariwala, M.G.; Farnaud, S.; Merchant, Z.; Somavarapu, S.; Renshaw, D. Ascorbyl palmitate/DSPE-PEG nanocarriers for oral iron delivery: Preparation, characterisation and in vitro evaluation. *Colloids Surfaces B Biointerfaces* **2014**, *115*, 86–92, doi:10.1016/j.colsurfb.2013.11.028.
179. Lee, J.H.; Yeo, Y. Controlled drug release from pharmaceutical nanocarriers. *Chem. Eng. Sci.* **2015**, *125*, 75–84, doi:10.1016/J.CES.2014.08.046.
180. Kwon, G.S.; Okano, T. Polymeric micelles as new drug carriers. *Adv. Drug Deliv. Rev.* **1996**, *21*, 107–116, doi:10.1016/S0169-409X(96)00401-2.
181. Mursaleen, L.; Noble, B.; Somavarapu, S.; Zariwala, M.G. Micellar nanocarriers of hydroxytyrosol are protective against parkinson's related oxidative stress in an in vitro hcmec/d3-sh-sy5y co-culture system. *Antioxidants* **2021**, *10*, doi:10.3390/antiox10060887.
182. Cha, E.J.; Kim, J.E.; Ahn, C.H. Stabilized polymeric micelles by electrostatic interactions for drug delivery system. *Eur. J. Pharm. Sci.* **2009**, *38*, 341–346, doi:10.1016/j.ejps.2009.08.006.
183. Pela Zupanč, S.; Kocbek, P.; Gulrez Zariwala, M.; Renshaw, D.; Gul, M.O.; Elsaid, Z.; Taylor, K.M.G.; Somavarapu, S. Design and Development of Novel Mitochondrial Targeted Nanocarriers, DQAsomes for Curcumin Inhalation. **2014**, doi:10.1021/mp500003q.
184. Bajpai, A.K.; Shukla, S.K.; Bhanu, S.; Kankane, S. Responsive polymers in controlled drug delivery. *Prog. Polym. Sci.* **2008**, *33*, 1088–1118, doi:10.1016/j.progpolymsci.2008.07.005.
185. Pupo, E.; Padrón, A.; Santana, E.; Sotolongo, J.; Quintana, D.; Dueñas, S.; Duarte, C.; De La Rosa, M.C.; Hardy, E. Preparation of plasmid DNA-containing liposomes using a high-pressure homogenization-extrusion technique. *J. Control. Release* **2005**, *104*, 379–396,

- doi:10.1016/j.jconrel.2005.02.001.
186. Johnson, D.; Shepherd, R.M.; Gill, D.; Gorman, T.; Smith, D.M.; Dunne, M.J. Intracellular Calcium Ions by GKA50 , a Glucokinase. *Diabetes* **2007**, *56*, doi:10.2337/db07-0026.D.J.
 187. Mursaleen, L.; Ho, S.; Chan, Y.; Noble, B.; Somavarapu, S.; Zariwala, M.G. Curcumin and N-Acetylcysteine Nanocarriers Alone or Combined with Deferoxamine Target the Mitochondria and Protect against Neurotoxicity and Oxidative Stress in a Co-Culture Model of Parkinson ' s Disease. **2023**.
 188. Wolfe, K.L.; Rui, H.L. Cellular antioxidant activity (CAA) assay for assessing antioxidants, foods, and dietary supplements. *J. Agric. Food Chem.* **2007**, *55*, 8896–8907, doi:10.1021/jf0715166.
 189. Mursaleen, L.; Noble, B.; Ho, S.; Chan, Y.; Somavarapu, S.; Zariwala, M.G. N -Acetylcysteine Nanocarriers Protect against Oxidative Stress in a Cellular Model of Parkinson ' s Disease. **2020**, 1–21.
 190. Riemer, J.; Hoepken, H.; Czerwinska, H.; Robinson, S.R.; Dringen, R. Colorimetric ferrozine-based assay for the quantitation of iron in cultured cells. **2004**, *331*, 370–375, doi:10.1016/j.ab.2004.03.049.
 191. Scott Panter, S. Release of iron from hemoglobin. *Methods Enzymol.* **1994**, *231*, 502–514, doi:10.1016/0076-6879(94)31034-3.
 192. Rorsman, P.; Eliasson, L.; Renström, E.; Gromada, J.; Barg, S.; Göpel, S. The Cell Physiology of Biphasic Insulin Secretion. **2023**, *15*, 1–6.
 193. Moribe, K.; Limwikrant, W.; Higashi, K.; Yamamoto, K. Drug Nanoparticle Formulation Using Ascorbic Acid Derivatives. **2011**, *2011*, doi:10.1155/2011/138929.
 194. Shaaban, M.A.; Dawod, A.E.A.; Nasr, M.A. Role of iron in diabetes mellitus and its complications. 11–16, doi:10.4103/1110-2098.178938.
 195. Foundation, A.L. *Diabetologia*. **1993**, 1139–1145.
 196. Ma, Z.A.; Zhao, Z.; Turk, J. Mitochondrial Dysfunction and β -Cell Failure in

- Type 2 Diabetes Mellitus. **2012**, *2012*, doi:10.1155/2012/703538.
197. Kim, U.H. Roles of cADPR and NAADP in pancreatic beta cell signaling. *Cell Calcium* **2022**, *103*, 719–729, doi:10.1016/j.ceca.2022.102562.
198. Lenzen, S. Oxidative stress: the vulnerable β -cell. **2008**, 343–347, doi:10.1042/BST0360343.
199. Cooksey, R.C.; Jouihan, H.A.; Ajioka, R.S.; Hazel, M.W.; Jones, D.L.; Kushner, J.P.; Clain, D.A.M.C. Insulin Secretory Capacity in Mouse Models of Hemochromatosis. **2004**, *145*, 5305–5312, doi:10.1210/en.2004-0392.
200. Aregbesola, A.; Voutilainen, S.; Virtanen, J.K.; Mursu, J.; Tuomainen, T. Body iron stores and the risk of type 2 diabetes in middle-aged men. **2013**, 247–253, doi:10.1530/EJE-13-0145.